DEVELOPMENT OF FUNCTIONAL ORGANICS MATERIALS FOR HIGH EFFICIENT DYE SENSITIZED SOLAR CELL: A CHALLENGE FOR SUSTAINABLE ALTERNATIVE ENERGY

YAOWARAT SURAKHOT

A THESIS SUBMITTED IN PARTIAL FULFILLMENT OF THE
REQUIREMENTS FOR THE DEGREE OF DOCTOR OF
PHILOSOPHY
MAJOR IN CHEMISTRY
FACULTY OF SCIENCE
UBON RATCHATHANI UNIVERSITY
ACADEMIC YEAR 2015

UBON RATCHATHANI UNIVERSITY

THESIS APPROVAL

DOCTOR OF PHILOSOPHY

MAJOR IN CHEMISTRY FACULTY OF SCIENCE

TITLE DEVELOPMENT OF FUNCTIONAL ORGANICS MATERIALS FOR HIGH EFFICIENT DYE SENSITIZED SOLAR CELL: A CHALLENGE FOR SUSTAINABLE ALTERNATIVE ENERGY

AUTHOR MISS YAOWARAT SURAKHOT

EXAMINATION COMMITTEE

DR. SUPAWADEE NAMUANGRUK	CHAIRPERSON
ASSOC. PROF. DR. SIRIPORN JUNGSUTTIWONG	MEMBER
ASST. PROF. DR. TINNAGON KEAWIN	MEMBER

ADVISOR Siriporn Jungsuttiwong
....
(ASSOC. PROF. DR. SIRIPORN JUNGSUTTIWONG)

....
(ASSOC. PROF. DR. UTITH INPRASIT)
DEAN, FACULTY OF SCIENCE

A. Pongrat
....
(ASSOC. PROF. DR. ARIYAPORN PONGRAT)
VICE PRESIDENT
FOR ACADEMIC AFFAIRS

ACADEMIC YEAR 2015

ACKNOWLEDGEMENTS

I wish to express my admiration and appreciation to Assoc.Prof.Dr. Siriporn Jungsuttiwong, my advisor and Asst.Prof.Dr. Tinnagon Keawin for excellent suggestions, supervision, and understanding throughout my study. I wish to acknowledge my coadvisor Dr. Supawadee Namuangruk for constructive comments and suggestion. I would also like to thank the many people who contributed their time, instrumentation, and advice to my project. In particular, Prof.Dr. Vinich Promarak, Asst.Prof.Dr Taweesak Sudyoadsuk and Dr Narid Prachumrak for experimental data. I wish to acknowledge Thailand Graduate Institute of Science and Technology (TGIST), National science and technology development agency Thailand (NSTDA) and Ubon Ratchathani University for financial support. Gratitude is expressed to all my teachers for showing me a different line in life, as a Chemistry graduate student.

My sincere thankful is also express to the Department of Chemistry and Excellent Center for Innovation in Chemistry, Faculty of Science, Ubon Ratchathani University for providing a wonderful academic environment during the course work. My appreciation is extended to all the staff of the Department of Chemistry. Furthermore, I feel thankful to my sisters, brothers here in Computational and Theoretical Chemistry Ubon Ratchathani University and Center for Organic Electronic and Alternative Energy.

Most of all, I feel appreciate and grateful to my beloved family for their inculcation and encouragement that found me to be a fortitude person.

Yaowarat Surakhot
Reseacher

บทคัดย่อ

เรื่อง : การพัฒนาวัสดุสารอินทรีย์สำหรับเซลล์แสงอาทิตย์ชนิดสีย้อมไวแสงที่มีประสิทธิภาพสูง: ความท้าทายสำหรับการพัฒนาพลังงานทางเลือกที่ยั่งยืน
ผู้วิจัย : เยาวรัตน์ สุระโคตร
ชื่อปริญญา : ปรัชญาดุษฎีบัณฑิต
สาขาวิชา : เคมี
อาจารย์ที่ปรึกษา : รองศาสตราจารย์ ดร. ศิริพร จึงสุทธิวงษ์
คำสำคัญ : เดนซิตี้ฟังก์ชันแนล, เซลล์แสงอาทิตย์ชนิดสีย้อมไวแสง, หมู่ให้อิเล็กตรอนที่มีขนาดใหญ่, หมู่รับอิเล็กตรอนเพิ่มเติม, ตำแหน่งการแทนที่ของหมู่ยึดจับ

งานวิจัยนี้ทำการศึกษาสมบัติทางโครงสร้างและพลังงานของโมเลกุลสีย้อมไวแสง โดยใช้ระเบียบวิธีที่ใช้ใช้การศึกษาสมบัติทางโครงสร้างที่สภาวะพื้น คือทฤษฎีเดนซิตี้ฟังก์ชันแนล (DFT) ที่ระดับ B3LYP/6-31G (d,p) นำโครงสร้างที่เสถียรทำการคำนวณพลังงานการกระตุ้น (E_g) การดูดกลืนแสงสูงสุด (λ_{max}) และค่าความแรงออสซิลเลเตอร์ (*f*) โดยใช้วิธีไทม์ดีเพนเด้นต์-เด้นซิตี้ฟังก์ชันแนล (TDDFT) ในผลของสารตัวทำละลายโดยใช้สารละลายไดคลอโรมีเทน (CH_2Cl_2) นอกเหนือจากนั้นได้ทำการศึกษาการยึดจับของโมเลกุลสีย้อมบนพื้นผิวของไทเทเนียมไดออกไซด์ (101) เพื่อศึกษาพลังงานการยึดจับ และได้ทำการศึกษาการสมบัติทางแสงและการฉีดอิเล็กตรอน โดยใช้วิธี TDDFT โมเลกุลสีย้อมประเภท D-π-A เป็นโครงสร้างพื้นฐานของสีย้อมไวแสงอินทรีย์ ที่ถูกออกแบบให้มีสมบัติการส่งผ่านอิเล็กภายในโมเลกุล อย่างไรก็ตามการเพิ่มความยาวคอนจูเกตระหว่างหมู่ให้อิเล็กตรอนและหมู่รับอิเล็กตรอนก็เป็นอีกหนึ่งวิธีการที่ทำให้มีการดูดกลืนแสงของโมเลกุลสีย้อมที่สูงและกว้างในช่วงวิสิเบล หนึ่งวิธีในการออกแบบโครงสร้างของโมเลกุลสีย้อมคือการเพิ่มหมู่ให้อิเล็กตรอน D-D-π-A ไม่เพียงแต่ส่งผลให้มีความสามารถในการให้อิเล็กตรอนเพิ่มขึ้น สามรถป้องกันการเกิดการซ้อนทับกันของโมเลกุลสีย้อม อย่างไรก็ตามการเพิ่มหมู่ให้อิเล็กตรอนที่มีขนาดใหญ่ สามารถไปลดจำนวนการยึดจับของโมเลกุลสีย้อมบนพื้นผิวของไทเทเนียมไดออกไซด์ได้ นอกเหนือจากนั้นการเพิ่มความยาวคอนจูเกตระหว่างหมู่ให้อิเล็กตรอนและหมู่รับอิเล็กตรอน และการเพิ่มหมู่ให้อิเล็กตรอนเพิ่มเติมเป็นระบบ D-π-A-π-A และ D-A-π-A พบว่า ช่วยเพิ่มความสามารถในการเก็บเกี่ยวแสงของโมเลกุลสีย้อม และการศึกษาผลของตำแหน่งการแทนที่ของหมู่ยึดจับในอนุพันธ์อินโดล จากผลการศึกษาพบว่าความแตกต่างของตำแหน่งของการแทนที่ของหมู่ยึดจับในหมู่อินโดลส่งผลต่อสมบัติทางแสงของโมเลกุลสีย้อม จากผลการศึกษาสามารถสรุปได้ว่า ผลการคำนวณมีความสอดคล้องกับผลการทดลอง การคำนวณโดยระเบียบวิธีทางเคมีควอนตัมสามารถทำนายสมบัติเชิงโมเลกุลของโมเลกุลที่ใช้เป็นสีย้อมไวแสงในเซลล์แสงอาทิตย์ชนิดสีย้อมไวแสงได้

ABSTRACT

TITLE : DEVELOPMENT OF FUNCTIONAL ORGANICS MATERIALS FOR HIGH EFFICIENT DYE SENSITIZED SOLAR CELL: A CHALLENGE FOR SUSTAINABLE ALTERNATIVE ENERGY
AUTHOR : YAOWARAT SURAKHOT
DEGREE : DOCTOR OF PHILOSOPHY
MAJOR : CHEMISTRY
ADVISOR : ASSOC.PROF.SIRIPORN JUNGSUTTIWONG, Ph.D.
KEYWORDS : DENSITY FUCNTIOANAL THEORY, DYE-SENSITIZED SOLAR CELL, BULKY DONOR EFFECT, AUXILIARY ACCEPTOR, SUBSTITUTION POSITION OF ANCHORING GROUP

In this research, the structure and energetic properties of sensitizer for dye-sensitized solar cells were investigated, the ground-state structure of all molecules were fully optimized using density functional theory (DFT) method. Optimized structures were then be used to calculate excitation energy (E_g), maximum absorption wavelength (λ_{max}), and oscillator strength (*f*) in dichloromethane solvent (CH_2Cl_2), by applying Time-Dependent Density Functional Theory (TDDFT). Furthermore, the adsorption complexes of dyes on the TiO_2 anatase (101) surface were carried out by means of the periodic calculation. The optical properties and electron-injection characteristics from dyes to the TiO_2 surface are then computed by TDDFT method. The D-π-A structural system is the basis of metal-free dyes owing to its effective photoinduced intramolecular charge transfer properties. Moreover, in order to possess broad and intense spectral absorption in the visible light region, one strategy for optimizing dye structure is to introduce more π-conjugation linker between the donor and acceptor, Another strategy is to incorporate a donor-donor moiety into the framework, D-D-π-A structural system, resulting in stronger electron-donating ability but also greater steric hindrance, which can prevent unfavorable dye aggregation. However, more bulky of the donor moiety could reduce the number density of the adsorbed dye on the TiO_2 surface. In addition, increase conjugated bridge between the donor and acceptor units and auxiliary acceptor to form a D-π-A-π-A and D-A-π-A frameworks owing to the expended conjugation. It was found that a system can improve light harvesting efficiency. Furthermore, we also study in the effect of substitution position of anchoring groups on indole derivatives. It was found that the effect of substitution position of anchoring groups on indole ring affected to the absorption properties of dyes molecule. In conclusion, it has been shown that these computational tools described above can provide the detailed characterizations which are in agreement with experimental efficiency and therefore can be of valuable help in further design of novel organic sensitizer for higher efficiency of photovoltaic device.

CONTENTS

PAGE

ACKNOWLEDGEMENTS I

THAI ABSTRACT II

ENGLISH ABSTRACT III

CONTENTS V

LIST OF TABLES VII

LIST OF FIGURES X

LIST OF ABBREVIATIONS XVI

CHAPTER 1 INTRODUCTION

1.1 Dye-sensitized solar cells (DSCs) 1

1.2 Molecular properties 3

1.3 Koopmans's theorem 5

1.4 Computation chemistry 6

1.5 Objectives of this research 18

CHAPTER 2 LITERATURE REVIEWS

2.1 Donor-π-acceptor frameworks 21

2.2 Auxiliary acceptor 26

2.3 Indole dyes 29

CHAPTER 3 THE NUMBER DENSITY EFFECT OF N-SUBSTITUTED DYES ON THE TiO_2 SURFACE IN DYE SENSITIZED SOLAR CELLS

3.1 Computational details 33

3.2 Results and discussion 34

3.3 Conclusion 46

CHAPTER 4 THE EFFECT OF BULKY-DONOR TO CHARGE RECOMBINATION AND CHARGE SEPARATION

4.1 Computational details 50

4.2 Results and discussion 51

4.3 Conclusion 66

CONTENTS

PAGE

CHAPTER 5 THE EFFECT OF AUXILIARY ACCEPTOR ON DYE SENSITIZED SOLAR CELLS
5.1 Computational details 68
5.2 Results and discussion 69
5.3 Conclusion 91
CHAPTER 6 THE EFFECT OF ACCEPTOR POSITION ON INDOLE MOEITY
6.1 Computational details 94
6.2 Results and discussion 95
6.3 Conclusion 106
CHAPTER 7 CONCLUSION 108
REFERENCES 111
CURRICULUM VITAE 122

LIST OF TABLES

TABLE		PAGE
3.1	The selected important inter-ring distances (*r*, Å) and dihedral angle (ϕ, °) calculated by B3LYP/6-31G(d,p) calculations	35
3.2	The energies and percentage composition of frontier molecular orbitals of organic sensitizers	36
3.3	The distance of charge transfer upon excitation (D_{CT}), dipole moment (μ) electronic properties, maximum absorption wavelength and oscillator strength (*f*) obtained by TDDFT at the CAM- B3LYP/6-31G (d,p) in CH_2Cl_2 solvent (C-PCM model)	38
3.4	Molecular volume, Box size, and projected area of **D2TC** and **D3TC**	42
3.5	The selected bond length (Å) and adsorption energy (E_{ads}) of dye-TiO_2 calculated by PBE/DNP in $DMol^3$	43
4.1	Calculated TDDFT (CAM-B3LYP) excitation energies for the lowest transition (eV, nm), oscillator strengths (*f*), composition in terms of molecular orbital contributions and experimental absorption maxima	51
4.2	Calculated TDDFT (CAM-B3LYP) excitation energies for the lowest transition (eV, nm), oscillator strengths (*f*), composition in terms of molecular orbital contributions and experimental absorption maxima	54
4.3	Wavelength (λ_{max}) for ICT spectra of **CCTA** using TDDFT method during DFTB dynamics	57
4.4	Photovoltaic parameters of DSCs with carbazole dye and N719 sensitizers	61

LIST OF TABLES (CONTINUED)

TABLE		PAGE
4.5	The electronic properties, absorption wavelength and oscillator strength (f) obtained by TD-ωB97XD/6-31G(d) on DFTB geometry	62
5.1	The selected important inter-ring distances (r, Å) and dihedral angles (ϕ, °) calculated by B3LYP/6-31G(d,p) calculations	70
5.2	The energies and percentage composition of frontier molecular orbitals	72
5.3	Calculated TDDFT (CAM-B3LYP) excitation energies for the lowest transition (eV, nm), oscillator strengths (f), composition in terms of molecular orbital contributions and experimental absorption maxima	74
5.4	The electronic properties, absorption wavelength and oscillator strength (f) obtained by TDDFT at the CAM-B3LYP/6-31G (d)	77
5.5	The selected bond length (Å) and adsorption energy (kcal/mol) of dye-TiO_2 calculated by PBE/DNP in $DMol^3$	79
5.6	The selected important inter-ring distances (r, Å) and dihedral angles (ϕ, °) calculated by B3LYP/6-31G(d,p) calculations	83
5.7	The energies and percentage composition of frontier molecular orbitals of dyes	85
5.8	Calculated TDDFT (CAM-B3LYP) excitation energies for the lowest transition (eV, nm), oscillator strengths (f), composition in terms of molecular orbital contributions and experimental absorption maxima	87
5.9	The selected bond length (Å) and adsorption energy (kcal/mol) of dye-TiO_2 calculated by PBE/DNP in $DMol^3$	88

LIST OF TABLES (CONTINUED)

TABLE		PAGE
5.10	The electronic properties of the TiO_2-dye complexes calculated by TD-CAM-B3LYP/6-31G(d,p) level of theory	91
6.1	Selected important inter-ring distances (Å) and dihedral angles (°) calculated by B3LYP/6-31G(d,p) calculations	96
6.2	The energies and percentage composition of frontier molecular orbitals of organic sensitizers	98
6.3	The electronic properties, absorption wavelength and oscillator strength (f) obtained by TDDFT at the CAM-B3LYP/6-31G (d,p) in CH_2Cl_2 solvent (C-PCM model)	101
6.4	The selected bond length (Å) and adsorption energy (kcal/mol) of dye-TiO_2 calculated by PBE/DNP in DMol^3	102
6.5	The electronic properties, absorption wavelength and oscillator strength (f) obtained by TDDFT at the CAM-B3LYP/6-31G (d,p) in gas phase	104

LIST OF FIGURES

FIGURE		PAGE
1.1	Schematic overview of a dye-sensitized solar cell	2
1.2	Simple energy level diagram for DSCs	2
1.3	Summary of electronic energy levels. Both n → π * and π → π* transition are represented	3
1.4	Potential energy diagrams with vertical transition	4
1.5	Frozen orbital approximation	6
1.6	Molecular structures of target molecules in the effect of donor	19
1.7	Molecular structures of target molecules in the effect of linker part	20
1.8	Molecular structures of target molecules in the effect of difference acceptor position series	20
2.1	The chemical structures of **JK-5** and **JK-6**	22
2.2	The chemical structures of **JK24** and **JK-25**	22
2.3	The chemical structures of **MK-2** and **MK-5**	23
2.4	The chemical structures of **TA-St-CA**	23
2.5	FMO of **CFT1A, CFT2A,** and **CFT1PA** adsorbed on $(TiO_2)_{38}$ surfaces by B3LYP/6-31G(d,p)	24
2.6	The chemical structures of **JD4**	24
2.7	The chemical structures of **1N-PSP**	25
2.8	(a) HOMO-1, (b) LUMO +12, and (c) LUMO +21 of the $(TiO_2)_{38}$-**UB1** System	25
2.9	Chemical structures of sensitizers **LS-1, LS-4** and **LS-5**	26
2.10	Chemical structures of D-A-π-A sensitizers (**WS-1** to **WS-4**) and reference dye **LS-1**	27
2.11	Chemical structures of **ID7-ID9** and reference dye	27
2.12	Molecular structures of isoindigo dyes (**ID1–ID6**)	28
2.13	Structures of the indoloquinoxaline-based dyes	29

LIST OF FIGURES (CONTINUED)

FIGURE		PAGE
2.14	Structures of the **D1**, **D2** and **D3** dyes	30
3.1	Sketch map of the synthesized **D1TC**, **D2TC** and **D3TC** sensitizers	33
3.2	Optimized structures of **D1TC** and **D2TC** by DFT/B3LYP/6-31G(d,p)	35
3.3	HOMO (left) LUMO (middle) and charge density difference (right) between the excited and ground states of the dyes. The green and red colors indicate a decrease and increase of charge density	37
3.4	ρ-/ρ+ (green/red) isocontour surfaces of (a) **D1TC**, (b) **D2TC**, and (c) **D3TC**, computed at the TD-CAM-B3LYP/6-31G(d,p) level	38
3.5	Molecular orbital energy level diagram of the dyes, TiO_2 conduction band, and redox potential of I^-/I_3^- electrolyte	39
3.6	Absorption spectra of **D1TC**, **D2TC** and **D3TC** calculated by TDCAM-B3LYP/6-31G(d,p) level in CH_2Cl_2 solvent (C-PCM model)	40
3.7	Molecular widths of **D2CT** and **D3TC** calculated by PBE/DNP on DMol^3	42
3.8	Molecular volume and projected area of **D2TC** and **D3TC**	43
3.9	Absorption spectra of **D2TC@TiO$_2$** and **D3TC@TiO$_2$** calculated by TD-CAM-B3LYP/6-31G(d) level in gas phase	45
3.10	MOs relevant to the transition from S_0 to S_1 of organic sensitizer adsorbed on the $(TiO_2)_{38}$ in gas phase calculated by TD-CAM-B3LYP/6-31G(d) on DMol^3 geometry. (a) **D2TC@TiO$_2$** (b) **D3TC@TiO$_2$**	46

LIST OF FIGURES (CONTINUED)

FIGURE **PAGE**

4.1 The recombination processes in DSCs 48

4.2 Chemical structures of the synthesized **CarFTPC**, **CarFT2C**, **CarFP2C** and **CarFT3C** dyes 50

4.3 Absorption spectra of **CarFTPC**, **CarFP2C**, **CaeFT2C** and **CarFT3C** calculatet by TD-CAM-B3LYP /6-31G (d,p) level in CH_2Cl_2 solvent (C-PCM model) 51

4.4 LHE of **CarFTPC**, **CarFP2C**, **CarFT2C** and **CarFT3C** calculated by TD-CAM-B3LYP /6-31G (d,p) level in CH_2Cl_2 solvent (C-PCM model) 52

4.5 Chemical structure of the synthesized **CarCarFuC**, **CarCarTFuC**, **CarCarT2FuC** and **CarCarT3C** dyes 53

4.6 Absorption spectra of **CarCarFuC**, **CarCTFuC**, **CarCarT2C** and **CarCarT3C** calculated by TD-CAM-B3LYP /6-31G (d,p) level in CH_2Cl_2 solvent (C-PCM model) 54

4.7 LHE of **CarCarFuC**, **CarCarTFuC**, **CarCarT2C** and **CarCarT3C** calculated by TD-CAM-B3LYP/6-31G (d,p) level in CH_2Cl_2 solvent (C-PCM model) 55

4.8 Chemical structure of the synthesized **CCTA** and **CFTA** dyes 56

4.9 HOMO-LUMO plots of **CCTA** and **CFTA** 57

4.10 Absorption spectra of **CCTA** during DFTB dynamics 58

4.11 Optimized bidentate bridging mode of **CCTA** and **CFTA** on the $(TiO)_{38}$. Molecular dynamics simulation of S_0 using DFTB at 298 K, dt = 0.7254 fs with NVT and NVE ensemble 59

4.12 The possible π-π aggregation phenomena in **CFTA-TiO$_2$** (a) compared with **CCTA-TiO$_2$** (b) 60

LIST OF FIGURES (CONTINUED)

FIGURE		PAGE
4.13	Absorption spectra of **CFTA-TiO_2** and **CCTA-TiO_2** calculated by TD-ω-B97XD/6-31G(d) level in gas phase	62
4.14	MOs relevant to the transition from S_0 to S_1 of (a) **CFTA** (b) **CCTA** organic sensitizer adsorbed on the $(TiO_2)_{38}$ in gas phase calculated by TD-ωB97XD/6-31G(d) on DFTB geometry	63
4.15	Observed distribution of electronic couplings (in meV) for charge recombination V_{CR} and charge separation V_{CS} in **CCTA-TiO_2** (a,b) and **CFTA-TiO_2** (c,d). Distributions are presented over geometries sample from NVE molecular dynamics simulations	65
5.1	Sketch map of TPA-dyes with/without sets isoindigo as auxiliary acceptor (**TTPC**, **TT2C**, **TIDP** and **TIDT**)	69
5.2	The molecular orbital surface at the ground state and first excited state when transition occurs	71
5.3	Molecular orbital energy level diagrams of the dyes, TiO_2 conduction band, and redox couple of I^-/I_3^- electrolyte	72
5.4	Absorption spectra of **TTPC**, **TT2C**, **TIDP** and **TIDT** calculated by TD-CAM-B3LYP /6-31G (d,p) level in CH_2Cl_2 solvent (C-PCM model)	73
5.5	LHE of **TTPC**, **TT2C**, **TIDP** and **TIDT** calculated by TD-CAM-B3LYP /6-31G (d,p) level in CH_2Cl_2 solvent (C-PCM model)	75
5.6	Frontier molecular orbitals of organic sensitizer adsorbed on the $(TiO_2)_{38}$ in gas phase calculated by CAM-B3LYP/6-31G(d) on $DMol^3$ geometry	78
5.7	Conjugation units affect dyes orientation on the surface of TiO_2	80

LIST OF FIGURES (CONTINUED)

FIGURE **PAGE**

5.8 Optimization geometry dyes on the surface of TiO_2 calculated by PBE/DNP in $DMol^3$ 80

5.9 Sketch map of the indoline series (**Indo**, **IndoEDOT**, **IndoBT**, and **IndoBTD**) 81

5.10 Optimized structures of Indo, **Indo**, **IndoEDOT**, **IndoBT**, and **IndoBTD** by DFT/B3LYP/6-31G(d,p) 82

5.11 The molecular orbital surface at the ground state and first excited state when transition occurs 83

5.12 Molecular orbital energy level diagram of the dyes, TiO_2 conduction band, and redox couple of I^-/I_3^- electrolyte 85

5.13 Absorption spectra of **Indo**, **IndoEDOT**, **IndoBT**, and **IndoBTD** calculated by TD-CAM-B3LYP /6-31G (d,p) level in CH_2Cl_2 solvent (C-PCM model) 86

5.14 MOs relevant to the transition from S_0 to S_1 of organic sensitizer adsorbed on the $(TiO_2)_{38}$ in gas phase calculated by TD-CAM-B3LYP/6-31G(d) on $DMol^3$ geometry 89

6.1 Sketch map of the synthesized **IND1**, **IND6**, **IND3**, and **IND4** sensitizer 95

6.2 Optimized structures of **IND1**, **IND6**, **IND3** and **IND4** by DFT/B3LYP/6-31G(d,p) 96

6.3 The molecular orbital surfaces **I IND1**, **IND6**, **IND3** and **IND4** molecules 97

6.4 Molecular orbital energy level diagram of the dyes, TiO_2 conduction band, and redox couple of I^-/I_3^- electrolyte 99

LIST OF FIGURES (CONTINUED)

FIGURE **PAGE**

6.5 Absorption spectra of **IND1**, **IND6**, **IND3** and **IND4** calculated by TD-CAM-B3LYP /6-31G (d,p) level in CH_2Cl_2 solvent 100

6.6 Absorption spectra of sensitizer adsorbed on the $(TiO_2)_{38}$ in gas phase calculated by CAM-B3LYP/6-31G(d,p) on $DMol^3$ geometry 103

6.7 Alignment of the ground and excited state energy levels for the dye-TiO_2 complexes and the frontier molecular orbital of dyes adsorbed on the $(TiO_2)_{38}$. Purple dashed and light blue dashed lines indicate the edge of the experimental conduction band of TiO_2 and the calculated HOMO energy levels of the dye-TiO_2 105

LIST OF ABBREVIATIONS

ABBREVIATIONS	FULL WORD
Å	Augstrom
λ_{abs}	Absorption wavelength
B3LYP	Becke's three parameter hybrid functional and Lee-Yang-Parr gradient-corrected correlation functional
r	Bond distance
CAM-B3LYP	Coulomb-attenuating method of B3LYP
CB	Conduction band
CPCM	Conductor-like Polarizable Continuum Model
DSCs	Dye-sensitized solar cells
D-π-A	Donor-π-acceptor
D-D-π-A	Donor-donor-π-acceptor
D-A-π-A	Donor-acceptor-π-acceptor
D-π-A-π-A	Donor-π-acceptor-π–acceptor
DFT	Density functional theory
°	Degree of angle
Φ	Dihedral angle
DFT	Density functional theory
E_g	Lowest excitation energy
Δ_{H-L}	HOMO-LUMO gap
GGA	Generalized Gradient Approximation
GTO	Gaussian type orbital
HF	Hartree Fock
HOMO	Highest occupied molecular orbital
LUMO	Lowest unoccupied molecular orbital
I^-/I_3^-	Iodide / triiodide redox couple

LIST OF ABBREVIATIONS (CONTINUED)

ABBREVIATIONS	**FULL WORD**
J_{sc}	The photocurrent density measured at short circuit
KS	Kohn sham
LDA	Local Density Approximation
LHE	Light harvesting efficiency
nm	Nanometer
PCM	Polarizable continuum model
Ru	Ruthenium
STO	Slater type orbital
TDDFT	Time dependent density functional theory
TiO_2	Titanium dioxide
V_{oc}	The open circuit photo-voltage
η	Conversion efficiency
Ψ	Wave function
E	Energy
$\hat{H}$	Hamiltonian operator
ρ	Electron density
T	Kinetic energy
ν	Exchange-correlation potential
f	Oscillator strengths
λ_{max}	Wavelength maxima

CHAPTER 1

INTRODUCTION

1.1 Dye-sensitized solar cells (DSCs)

Dye-sensitized solar cells (DSCs) are one of the most promising alternatives to compete with the traditional silicon solar cell because organic dye molecules in DSCs show distinguished advantages such as their high optical absorption extinction coefficient, adjustable spectral wavelength response, low cost materials, and their environmental friendly [1-2]. A schematic of the interior of DSCs showing the principle of how the device operates is shown in Figure 1.1. The typical basic configuration is as follows: The mesoporous oxide layer composed of a network of TiO_2 nanoparticles that have been sintered together to establish electronic conduction. The mesoporous layer is deposited on a transparent conducting oxide (TCO) on a glass or plastic substrate. The most commonly used substrate is glass coated with fluorine-doped tin oxide (FTO). Attached to the surface of the nanocrystalline film is a monolayer of the charge-transfer dye. Photoexcitation of the latter results in the injection of an electron into the conduction band of TiO_2, leaving the dye in its oxidized state. The dye is restored to its ground state by electron transfer from the electrolyte, usually an organic solvent containing the iodide/triiodide redox system. The regeneration of the sensitizer by iodide intercepts the recapture of the conduction band electron by the oxidized dye. The basic electron transfer processes in DSCs are shown in Figure 1.1. Reaction 1 is direct the exited electron from ground state. Besides the desired pathway of the electron transfer processes (processes 2, 3, 4, and 5) shown in Figure 1.2.

In general the molecular structure of an organic dye for DSCs has been designed and synthesized based on following properties: (i) matching of oxidation potentials of the ground and exited states for a dye, which are usually replaced by the highest occupied molecular orbital (HOMO) and the lowest unoccupied molecular orbital (LUMO), with the energy levels of I^-/I_3^- redox potential and E_{CB} of the TiO_2

electrode, respectively; (ii) a donor-linkage-acceptor (D-π-A) system required for a wide range absorption extending to the near-infrared [3].

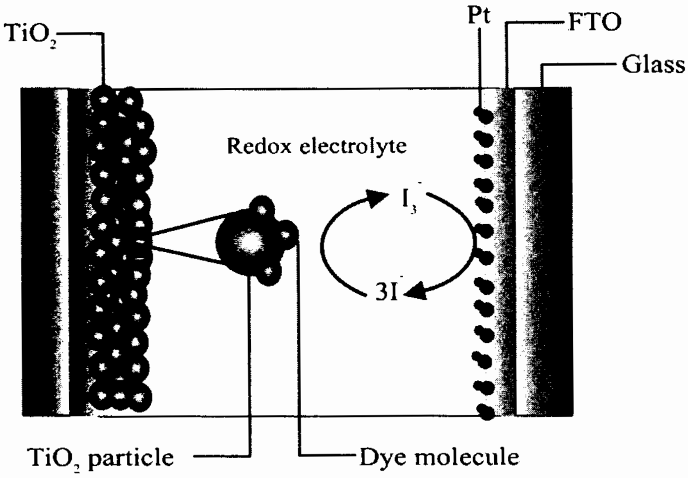

Figure 1.1 Schematic overview of a dye-sensitized solar cell

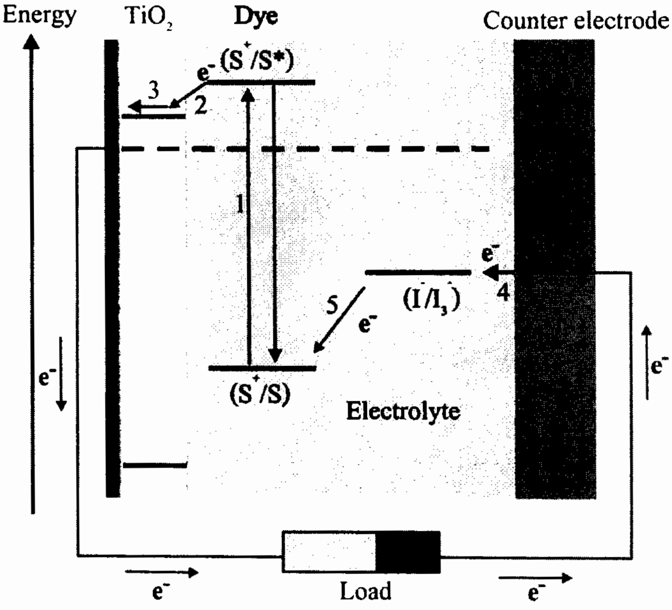

Figure 1.2 Simple energy level diagram for DSCs

1.2 Molecular properties

1.2.1 UV-Visible Absorption Spectra

Molecular absorption in the ultraviolet (UV) and the visible region of the spectrum is dependent on the electronic structure of the molecules. Absorption of energy is quantized, resulting in the elevation of electronics from orbital in the ground state to the higher energy orbital an excited state. The absorption characteristics of organic molecules in the UV region depend on the electronic transitions that can occur and the effect of the atomic environment on the transitions. The relative ease with which the various transitions can occur is summarized in Figure 1.3. Although the energy changes are not shown in scale, it is readily seen, for example, that an $n \rightarrow \pi^*$ transition requires less energy than $\pi \rightarrow \pi^*$ or $\sigma \rightarrow \sigma^*$ transition.

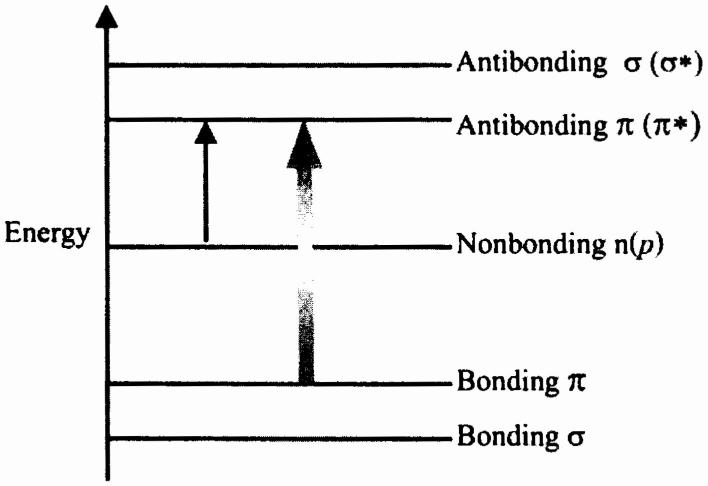

Figure 1.3 Summary of electronic energy levels. Both $n \rightarrow \pi^*$ and $\pi \rightarrow \pi^*$ transition are represented

As conjugation is increased in a molecule more delocalization (stability) of the π electrons results. The effect of this delocalization is to decrease the π* molecular orbital. The result is a decrease in transition energy from $\pi \rightarrow \pi^*$ and thus a red shift or bathochromic shift. The molar absorptivity will increase in this case and better quantitative analysis will be achieved. The molar absorptivity will increase as well depending on the number of the double bonds. Spectroscopists use the terms defined in the table on the right when describing shifts in absorption. Thus, extending conjugation generally results in bathochromic and hyperchromic shifts in absorption [4].

1.2.2 Franck-Condon principle

According to the Born-Oppenheimer approximation, the motions of electrons are much rapid than those of the nuclei (i.e. the molecular vibrations). The time when the electron excited to the excited state takes about 10^{-15} s, which is very quick compare to the characteristic time for molecular vibration (10^{-10}-10^{-12} s). These observed are the basic of Franck-Condon principle: an electron transition occurs without changing in the position of nuclei and environment. The result of state is called a *Franck-Condon state* and the transition is called vertical transition, as shown in Figure 1.4

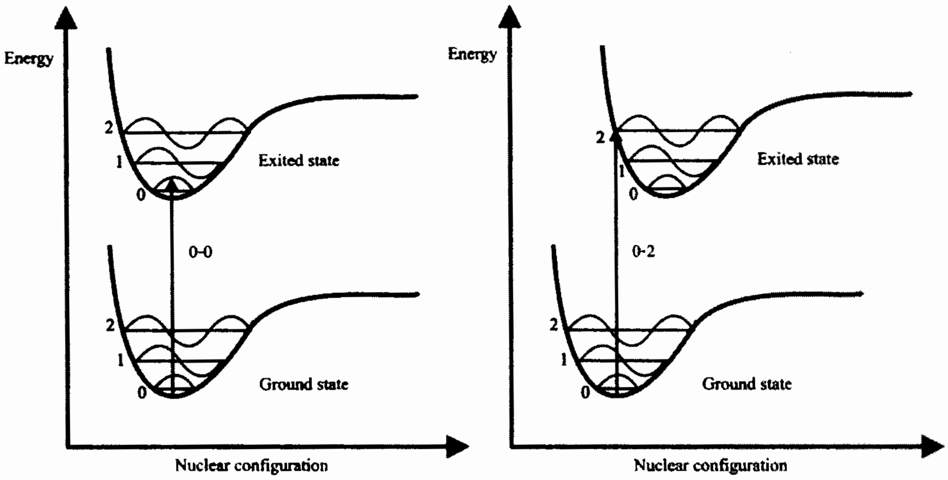

Figure 1.4 Potential energy diagrams with vertical transition

As shown, the potential energy curve as a function of the nuclear configuration (in a diatomic molecule) is represented by a Morse function. At room temperature, most of molecules vibrate in the low level of the ground state. Thus, the electronic transition is also 0-0 transition (at least). On the other hand, at high temperature (assumed with high energy), the electronic transition can be 0-1, 0-2, 0-3 or arbitrary state depending on vibration energy [5].

1.3 Koopmans's theorem

Given an N-electron Hartree-Fock single determinant $|^{N}\Psi_0\rangle$ with occupied and virtual spin orbital energies ε_a and ε_r, then the ionization potential to produce an $(N - 1)$-electron single determinant $|^{N-1}\Psi_a\rangle$ with identical spin orbitals, obtained by removing an electron from spin orbital χ_a , and the electron affinity to produce an $(N + 1)$-electron single determinant $|^{N+1}\Psi^r\rangle$ with identical spin orbitals, obtained by adding an electron to spin orbital χ_r , are just-ε_a and -ε_r , respectively. Koopmans' theorem thus gives us a way of calculating approximate ionization potentials and electron affinities. This "frozen orbital" approximation assumes that the spin orbitals in the $(N \pm 1)$-electron states, i.e., the positive and negative ions if $|^{N}\Psi_0\rangle$ is a neutral species, are identical with those of the N-electron state. This approximation neglects relaxation of the spin orbitals in the $(N \pm 1)$-electron states, i.e., the spin orbitals of $|^{N}\Psi_0\rangle$ are not the optimum spin orbitals for $|^{N-1}\Psi_a\rangle$ or $|^{N+1}\Psi^r\rangle$. Optimizing the spin orbitals of the $(N \pm 1)$-electron single determinants by performing a separate Hartree-Fock calculation on these states would lower the energies $^{N-1}E_a$ and $^{N+1}E^r$ and thus the neglect of relaxation in Koopmans' theorem calculations tends to produce too positive an ionization potential and too negative an electron affinity. In addition, of course, the approximation of a single determinant wave function leads to errors, and the correlation effects, which one obtains in going beyond the Hartree-Fock approximation, will produce further corrections to Koopmans' theorem results. In particular, correlation energies are largest for the system with the highest number of electrons. Therefore, correlation effects tend to cancel the relaxation error for ionization potentials, but add to the relaxation error for electro affinities. In general, Koopmans' ionization potentials are reasonable first approximations to experimental ionization potentials and we shall be discussing a number of such calculations later in this chapter. Koopmans' electron affinities are unfortunately often bad. Many neutral molecules will add an electron to form a stable negative ion. Hartree-Fock calculations on neutral molecules, however, almost always give positive orbital energies for all the virtual orbitals. Electron affinities are considerably more difficult to calculate than ionization potentials.

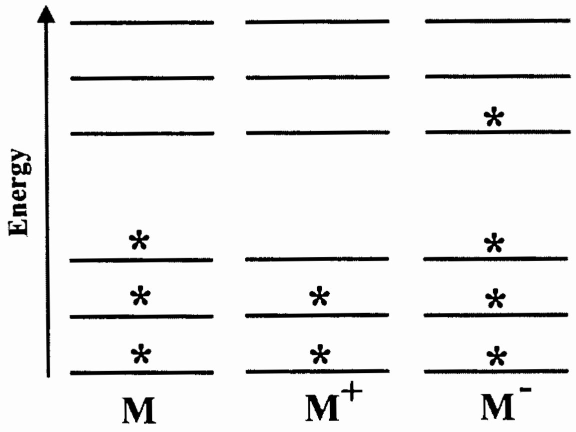

Figure 1.5 Frozen orbital approximation

1.4 Computation chemistry

1.4.1 The Hatree-Fock Theory [6-8]

Hamiltonian operator for many-electron system, the quantum chemical methods is based on finding solution to the Schrodinger wave equation on molecular orbital theory.

$$H\Psi = E\Psi \tag{1.1}$$

Where H is Hamiltonian operator which gives the kinetic and potential energies of the system The Hamiltonian operator for many electrons system can be written.

$$\hat{H} = -\sum_{i=1}^{n}\frac{1}{2}\nabla_i^2 - \sum_{A=1}^{K}\frac{1}{2M}\nabla_A^2 - \sum_{i=1}^{n}\sum_{A=1}^{K}\frac{Z_A}{r_{iA}} + \sum_{i=1}^{n}\sum_{j<i}^{n}\frac{Z_A}{r_{ij}} + \sum_{A=1}^{K}\sum_{B<A}^{K}\frac{Z_A Z_B}{R_{AB}} \tag{1.2}$$

In Equation 1.2, the first and second term represent the kinetic energies of electron and nucleus, respectively. The third term is the electron–nucleus attraction. The forth term corresponds to the electron-electron repulsion and the fifth the nuclear-nuclear repulsion.

1.4.2 Born-Oppenheimer approximation

The Born-Oppenheimer approximation is central to quantum chemistry. Since nuclei are much heavier than the electron one can treat electrons as if they are moving in the field of fixed nuclei. In other words, for any give atom configuration the electron are always located in the energetically lowest possible configuration. Another way to explain this approximation is that since the moment of the electrons is rapid compared to the moment of the nuclei, the see the change of the locations of the nuclei as an adiabatic change in the system. With these approximations the total energy of the system is,

$$E_{total} = \sum_i \frac{1}{2} m_i \dot{\vec{r}}_i^{\,2} + \sum_i \sum_{j>i} \frac{Z_i Z_j}{|r_i - r_j|} + E_{elec}\,(\{\vec{r}_i^{\,2}\}) \tag{1.3}$$

Where $\dot{\vec{r}}_i$ is the position, $\vec{r}_i$ is the velocity, m_i the mass and Z_i the change of i: th ion. The first term describes the classical kinetic energy of the ions and the second term is Coulombic interaction of the ions. The index of summation at second term is $i > j$ to count each ion-ion interaction only once and to exclude seft-interaction. The third term is the total energy of the electron gas in current ion configuration.

1.4.3 Density functional theory [9-10]

All the ab initio methods started from the Hartree-Fock (HF) approximation in the HF equation. Currently, these methods are widely used by quantum chemistry. However, we found that for higher accuracy calculations it also requires higher computing cast with large basic sets. So that, an alternative to the HF methods that is also popular among quantum chemists is density functional theory (DFT). Main reason for population of DFT is that it has the electron correlation and less computational demand. Moreover, it can be used to calculate on molecules of 100 or more atoms.

The basic idea of DFT is that the energy of an electronic system can be written in terms of the electron probability density (ρ) and the electronic energy (E) can also be a functional of the electron density and is denoted $E[\rho]$.

1.4.4 Kohn-Sham orbitals and equations

In 1920s Fermi and Thomas developed the approximate models such as the Thomas-Fermi method. However, Hohenberg and Kohn proved that the ground-state energy and all other ground-state electronic properties can be determined by the electron density. Kohn and Sham (1965) considered system in which pared electron are described by the same spatial one-electron orbitals and they showed that the exact ground-state electronic energy (*E*) and *n* electron system can be written as

$$E=[\rho]\frac{h^2}{2m_e}\sum\int\psi_i^*(r_1)\nabla_1^2\psi_1(r_1)dr_1-j_0\sum_{I=1}^{n}\frac{z_I}{r_{I1}}\rho(r_1)dr_1+\frac{1}{2}j_0\int\frac{\rho(r_1)\rho(r_2)}{r_{12}}dr_1dr_2+E_{xc}[\rho] \quad (1.4)$$

Where the one-electron spatial orbitals ψ_i (i=1, 2,..., n) are the Kohn-Sham orbitals. The exact ground-state electron density is given by

$$\rho(r)=\sum_{i=1}^{n}\left|\psi_i(r)\right|^2 \quad (1.5)$$

We can write in the easy form as

$$E_{DFT}=T[\rho]+E_{ne}[\rho]+J[\rho]+E_{XC}[\rho] \quad (1.6)$$

Where the sum is over all the occupied Kohn-Sham (KS) orbitals; ρ is known once these orbitals have been computed. The first term on the right in equation 1.6 represents the kinetic energy of the electron; the second term represents the electron nucleus attraction; the third term represents the Coulomb interaction between the total charge distribution at r_1 and r_2; the last term is the exchange-correlation energy of the system, which is also s functional of the density and takes into account all non-classical electron-electron interactions of the four terms, E_{xc} is the one we do not know how to obtain exactly. Although the Hohenberg-Kohn theorem tells us that *E* and therefore E_{xc} must be functional of the electron density, we do not know the latter's exact analytical form and so are forced to use approximate expressions. For the n-electron orbitals have the form.

$$\left\{-\frac{\hbar^2}{2m_e}\nabla_1^2 - j_0\sum_{I=1}^{n}\frac{Z_I}{r_{I1}} + j_0\int\frac{\rho(r_2)}{r_{12}}dr_2 + V_{XC}(r_1)\right\}\psi_i(r_1) = \varepsilon_i\psi_i(r_1) \tag{1.7}$$

Where ε_i is the KS orbital energies and the exchange-correlation potential, V_{xc} is the functional derivative of the exchange-correlation energy:

$$V_{XC}[\rho] = \frac{\delta E_{XC}[\rho]}{\delta_\rho} \tag{1.8}$$

E_{xc} is the sum of the exchange energy and the correlation energy, $E_{xc} = E_x + E_c$. Each of the parts can be treated under the density functional models. If E_{xc} is known, then V_{xc} can be computed. The significance of the KS orbitals is that they allow the density (ρ) to be computed from equation 1.5. The KS equations are solved in a self-consistent fashion. Initially, we guess the electron density (ρ), typically by using a superposition of atomic densities. By using some approximate form for the functional $E_{xc}[\rho]$, we next compute V_{xc} as a function of r. The set of KS equations is then solved to obtain an initial set of KS orbitals. This set of KS orbitals is then used to compute an improved density from equation 1.8 and exchange-correlation energy have converged to within some tolerance.

1.4.5 Functional

The important key in DFT is to find the exchange and correlation functional E_{xc} that gives the accurate calculated result. The various functions were proposed and obtained from experiments and high-level ab initio calculations.

1.4.5.1 Local density approximation

The generation of approximations for E_{xc} has lead to large and still expanding field of research. Thomas and Fermi studied the Homogeneous electron gas in early 1920's the orbital of system are, plane waves. If the electron interaction is approximate by the classical Hatree potential the total energy functional can be readily computed. Under these condition the dependence of kinetic and exchange energy on the density of electron gas can be extracted and expressed in term of local functions of the density. This suggests that inhomogeneous system we might approximate the function as an integral over a local function of the charge density. Using the kinetic and exchange energy densities of the non-interacting homogeneous electron gas this leads to;

$$T[\rho(r)] = 2.87\int \rho^{5/3}(r)dr$$

$$E_X[\rho] = 0.74\int \rho^{4/3}(r)dr \tag{1.9}$$

These results are highly suggestive of a representation for E_{xc} in an inhomogeneous system. The local exchange correlation energy per electron might be approximate as a simple function of the local charge density. That is, approximation of the form;

$$E_{XC}^{LDA}[\rho(r)] = \int \in_{XC}(\rho(r))\rho(r)dr \tag{1.10}$$

Within the LDA $\in_{XC}$ is a function of only the local value of the density. It can be separate into exchange and correlation contribution;

$$\in_{XC}(\rho) = \in_X(\rho) + \in_C(\rho) \tag{1.11}$$

The Dirac form can be used for

$$\in_X(\rho) = -C\rho^{1/3} \tag{1.12}$$

Where for generality a free constant, C, has been introduced rather than that determined for the homogeneous electron gas. This function is form much more widely applicable than is implied from its derivation and can be established from scaling arguments. The functional form for the correlation energy is unknown and has been simulated for the homogeneous electron gas in numerical quantum Monte Carlo calculations which yield essentially exact result. The resultant exchange correlation energy has been fitted by a number of analytic forms all of which yield similar results in practice and are collectively referred to as LDA functional.

1.4.5.2 Gradient corrected or generalized gradient approximation

The local density approximation can be considered to be the zeroth order approximation to the semi-classical expansion of the density matrix in term of density and its derivatives. A natural progression beyond the LDA is that gradient expansion approximation in which first order gradient terms is the expression are include. In the generalized gradient approximation (GGA) a function a functional from is adopted which ensure the normalization condition and that the exchange hole is negative definite. This lead to an energy functional that depends on both the density and its gradient but retains the analytic properties of the exchange correlation hole inherent in the LDA. An approach to improving the LDA, so call generalized gradient approximation (GGA), is to include gradient correlations by making E_{xc} a functional of the density and its gradient:

$$E_{XC}^{GGA}\left[\rho(r)\right]=\int \in_{XC}\left(\rho(r)\right)\rho(r)dr+\int F_{XC}\left[\rho(r)\left|\nabla\right|\rho(r)\right]d \tag{1.13}$$

Where F_{XC} is a correction chosen to satisfy one or several known limits for F_{XC}. Clearly, there is no unique recipe for F_{XC}, and several functional is currently a currently a very active area of research and although incremental improvements are likely, it is far from clear whether the research will be successful in providing the substantial increase in accuracy that is desired.

1.4.5.3 Hybrid functional

There is an exact connection between the non-interacting density functional system and the fully interacting much body system via integration of the work done in gradually turning on the electron-electron interaction. The adiabatic connection approach allow the eact functional to be formally written as

$$\mathrm{E}_{XC}\left[\rho\right]=\frac{1}{2}\int d\vec{r}d\vec{r}'\int_{\lambda=0}^{1}d\lambda\frac{\lambda e^{2}}{\left|\vec{r}-\vec{r}'\right|}\left[<\rho(\vec{r})\rho(\vec{r}')>_{\rho,\lambda}-\rho(\vec{r})\delta(\vec{r}-\vec{r}')\right] \tag{1.14}$$

Where the expectation value $<\ldots>_{\rho,\lambda}$ is the density-density correlation functional and is computed at density $\rho(r)$ for a system described by effective potential;

$$V_{eff} = V_{en} + \sum_{i \neq j} \frac{\lambda e^2}{|\vec{r} - \vec{r}'|} \tag{1.15}$$

Thus the exact energy could be computed if one knew the variation of density correlation function with the coupling constant, λ . The LDA recover by replacing the pair correlation function with that for the homogeneous electron gas. The adiabatic integration approach suggests a difference approximation for the exchange- correlation functional. At $\lambda = 0$ the non-interacting system corresponds identically to Hartree-Fock ansatz, while the LDA and GGA functional are constructed to be excellent approximations for the fully interacting homogeneous electron gas that is, a system with $\lambda = 0$ It is therefore not unreasonable to approximate the integral over the coupling constant as a weighted sum of the end point that is, we might set:

$$E_{XC} \approx aE_{Fock} + aE_{EX}^{GGA} \tag{1.16}$$

With the coefficients are to be determined by reference to a system for which the exact result is known. Becke adopted this approach in the definition of a functional with coefficients determined by a fit to the observe atomization energies, ionization potential, proton affinities and total atomic energies for a number of small molecules. Hybrid functional of this type is now very widely used in chemical applications with the B3LYP functional being the most notable. Computed binding energies, geometries and frequencies are systematically more reliable than the best GGA functional. A Becke style three- parameter functional may be defined via the following expression:

$$E_{XC}^{B3LYP} = (1-a)E_X^{LSD} + aE_{XC}^{\lambda=0} + bE_X^{B88} + cE_C^{LYP} + (1-c)E_C^{LSD} \tag{1.17}$$

Here, the parameter C_0 allows any admixture of Hartree-Fock and LDA local exchange to be used. In addition, Becke's gradient correction to LDA exchange is also included, scaled by the parameter c_X. Similarly, the VWN3 local correlation functional is used and it used, and it may be optionally corrected by the LYP correction via the parameter the parameter c_C. In B3LYP functional, the parameters values are those specified by Becke, which he determined by fitting to the atomization energies, ionization potential, proton affinities and first row atomic energies in the G1 molecule set: $c_0 = 0.20$, $c_X = 0.72$ and $c_C = 0.81$. Note that Beck used the Perdew-Wang 1991 correlation functional in his original work rather than VWN3 and LYP. The fact that the same coefficients work well with different functional reflects the underlying physical justification for using such a mixture of Hartree-Fock and DFT exchange first pointed out by Becke.

1.4.6 Basis Sets

Each molecular orbital (one electron function) is expressed as a linear combination of n basis functions. The individual orbital Ψ_i molecular or atomic depending on the investigated system, are expanded in term of set of basis function, centered on the nucleus or nuclei.

$$\Psi_i = \sum_{v} c_{iv}\varphi_v \tag{1.18}$$

Where the orbital expansion coefficient, are optimized during the calculation. The set of basis function available for an expansion is called the basis set. These basis function can be slater type orbital (STO) function which similar to the orbital obtained by analytical solution of Schrödinger equation for hydrogen atom. However, a more efficient computational of two electron integrals is achieved with Gaussian type orbital (GTO) function, It is therefore more common to use called contracted Gaussian function, in which several primitive GTO functions are combined in a fixed, predefined linear combination.

The smallest possible basis set representation is termed a minimal or single zeta basis set and comprises only the number of functions required to accommodate all the electrons of the atoms of the system. Doubling the number of functions, a double zeta basis set, provides a more flexible description since there are two sets of functions for each occupied shell of the atoms. So-called split-valence basis sets, where the description is split into an inner component describing the core electrons with one level of representation, e.g. minimal basis, and an outer component describing the valence electrons with another level of representations.

The choice of basis set is very important for the quality of the computational results. A sufficient flexible and balanced basis set must be used to obtain accuracy results, but accuracy and computational cost has to be weighed against each order. The trade-off becomes increasingly important to consider when large systems are investigated.

1.4.6.1 Minimal basis sets

Minimal basis sets contain the minimum number of basis function need for each atom. Minimal basis sets use fixed-size atomic type orbitals. The STO-3G basis is minimal basis set. It uses three Gaussian primitive per basis function, which accounts for the “3G” in its name. STO stands for “Slater type orbital”, and the STO-3G basis set approximates slater orbitals with Gaussian function.

1.4.6.2 Split-valence basis sets

The description of the valence electrons can be significantly improved over that in the minimal STO-3G basis set, if more than one basis function is used per valence electron. Basis sets of this type are called "split valence" basis sets as the description of valence orbitals are split into two (or more) basis functions. A related term is “double zeta” in reminiscence of the greek symbol used for the orbital exponents of STOs. The term "double zeta" (DZ) does not imply, however, whether two basis sets are used for all of the orbitals or only for the valence space. One very economical, small split valence basis set is the 3-21G basis set. The nonvalence electrons are described by single basis functions composed of a contraction of three Gaussians. Each valence electron is described by two basis functions. The first of these basis functions is composed of two Gaussian primitives while the second consists of a single uncontracted Gaussian primitive.

1.4.6.3 Polarization functions

Split valence basis sets allow orbital to change size, but not change the shape. Polarized basis sets remove limitation by adding orbitals with angular momentum beyond what is required for the ground state to description of each atom. To further increase the flexibility of the orbital description, double zeta basis sets are frequently augmented with basis functions of higher angular momentum. A typical first step consists of the addition of a set of d-type functions to the basis sets of those atoms, which have occupied s- and p-shells in their electronic ground states. For hydrogen, this corresponds to the addition of a set of p-type functions. Two different notations exist to specify the addition of polarization functions. The first notation adds one asterisk to the basis set to specify addition of polarization functions to non-hydrogen atoms, while two asterisks symbolize the addition of polarization functions to all atoms (including hydrogen). The 6-31G** basis set10 is thus constructed from the split valence 6-31G basis set through addition of one set of d-functions to all non-hydrogen atoms and one set of p-functions to all hydrogen atoms. In the second (preferable) notation the polarization functions are specified through their angular quantum number explicitly. The 6-31G** basis set would then be termed "6-31G(d,p)". This latter notation is much more flexible as multiple sets of polarization functions can be specified much more easily.

1.4.6.4 Diffuse basis functions

The theoretical description of negatively charged species is particularly challenging for *ab initio* MO theory. This is due to the fact that the excess negative charge spreads outward to a much larger degree than is typically the case for uncharged or positively charged molecules. The description of such a diffuse charge distribution is not very well possible with the typical split valence basis sets discussed before. Addition of very diffuse basis functions (with correspondingly small orbital exponents) cures this problem to certain extends as it allows the description of electron density relatively far from the nucleus. Diffuse basis functions are typically added as an additional set of uncontracted Gaussian functions of the same angular momentum as the valence electrons

1.4.7 Time depėndent density functional theory [11-15]

In general introduction to TDDFT is given before deriving the working equations of TDDFT linear response theory for the calculation of excitation energies. Subsequently, we present route to computing excited state nuclear gradients within TDDFT linear response theory, the popular extended Lagrangian ansatz and the implicit differentiation method.

1.4.7.1 Time-Dependent Kohn-Sham Theory

According to the Runge-Gross theorem there is a one to one correspondence between the time-dependent external potential, υ_{ext} (r, t), and the time-dependent electron density, ρ(r, t) for a fixed initial state. This can be seen as a generalization of the usual Hohenberg-Kohn theorem electronic ground states. Similar to the static case, one can cast the many-electron problem into the Kohn-Sham non-interacting electrons form assuming non-interacting υ-representability. The latter assumption means that the density of the interacting system can be reproduced by the non-interacting potential υ_S, i.e.

$$\rho(\mathrm{r},t)=\sum_{i}^{\mathrm{occ}}\left|\phi_i(\mathrm{r},t)\right|^2 \tag{1.19}$$

Where the orbitals satisfy ϕ_i(r, t) the time-dependent Kohn-Sham equations

$$i\frac{\partial}{\partial t}\phi_i(\mathrm{r},t)=\left(-\frac{\nabla^2}{2}+\upsilon_S[\rho](\mathrm{r},t)\right)\phi_i(\mathrm{r},t) \tag{1.20}$$

$$\upsilon_S[\rho](\mathrm{r},t)=\upsilon_{\mathrm{ext}}(\mathrm{r},t)+\int dr'\frac{\rho\left[r',t\right]}{\left|r-r'\right|}+\upsilon_{\mathrm{ext}}[\rho](\mathrm{r},t) \tag{1.21}$$

With defining the exchange-correlation potential υ_{ext} [ρ] (r, t). In the usual adiabatic approximation the exchange-correlation potential is taken to be simply the derivative of the static ground state exchange-correlation energy, E_{XC}, with respect to the density,

$$\upsilon_{\mathrm{ext}}[\rho](\mathrm{r},t)\approx\frac{\delta E_{XC}[\rho]}{\delta_{\rho}} \tag{1.22}$$

In the past few years, time dependent density functional theory (TDDFT) has been developed to calculate the properties on the excited state of molecules. TDDFTextends the basic ideas of ground state density functional theory (DFT) to the treatment of excitations and of more general time-dependent phenomena. Recently, it was important implemented in many quantum calculation programs such as Gaussian. TDDFT is a very popular tool in studying photochemistry due to its computation cost is not expensive. Furthermore, many research groups have reported the good agreement between TDDFT results with experiments.

1.5 Objectives of this research

The aim of this project is to develop high efficiency DSCs based on organic dyes using combined theoretical and experimental studies. The target dye molecules are shown in Figure 1.6. The theoretical part will do the calculation of dye molecules with varieties of donor groups, Linker and acceptor. The experimental part will do the synthesis of the obtained molecules and DSCs device fabrication and testing. To divide in to three sections, the first is effect of donor moiety (Figure 1.6), the second is difference linker (Figure 1.7) and series and the third is difference acceptor position series (Figure 1.8).

1.5.1 To study the structural and energetic properties of different donor dyes based on of organic dyes using the computational calculations.

1.5.2 To calculate the adsorption energies of organic using the DMol^3 program in Material Studio 5.5 software suite.

1.5.3 To improve and enhance the electronic and optical properties of target organic dye molecules using the combined theoretical and experimental studies.

1.5.4 To provide useful information such as calculated energy band gap, electronic transition and optical properties of organic dye-sensitizer to experimentalist for the molecular level of understanding.

1.5.5 To study mode of adsorption of dye molecule on TiO_2 surface which related to effect of electron injection from dye to external load and then related to power conversion efficiency of DSCs.

1.5.6 To develop and design new efficient dye solar cells (DSCs) based on D-π-A using the electronic and optical properties from our known target molecules.

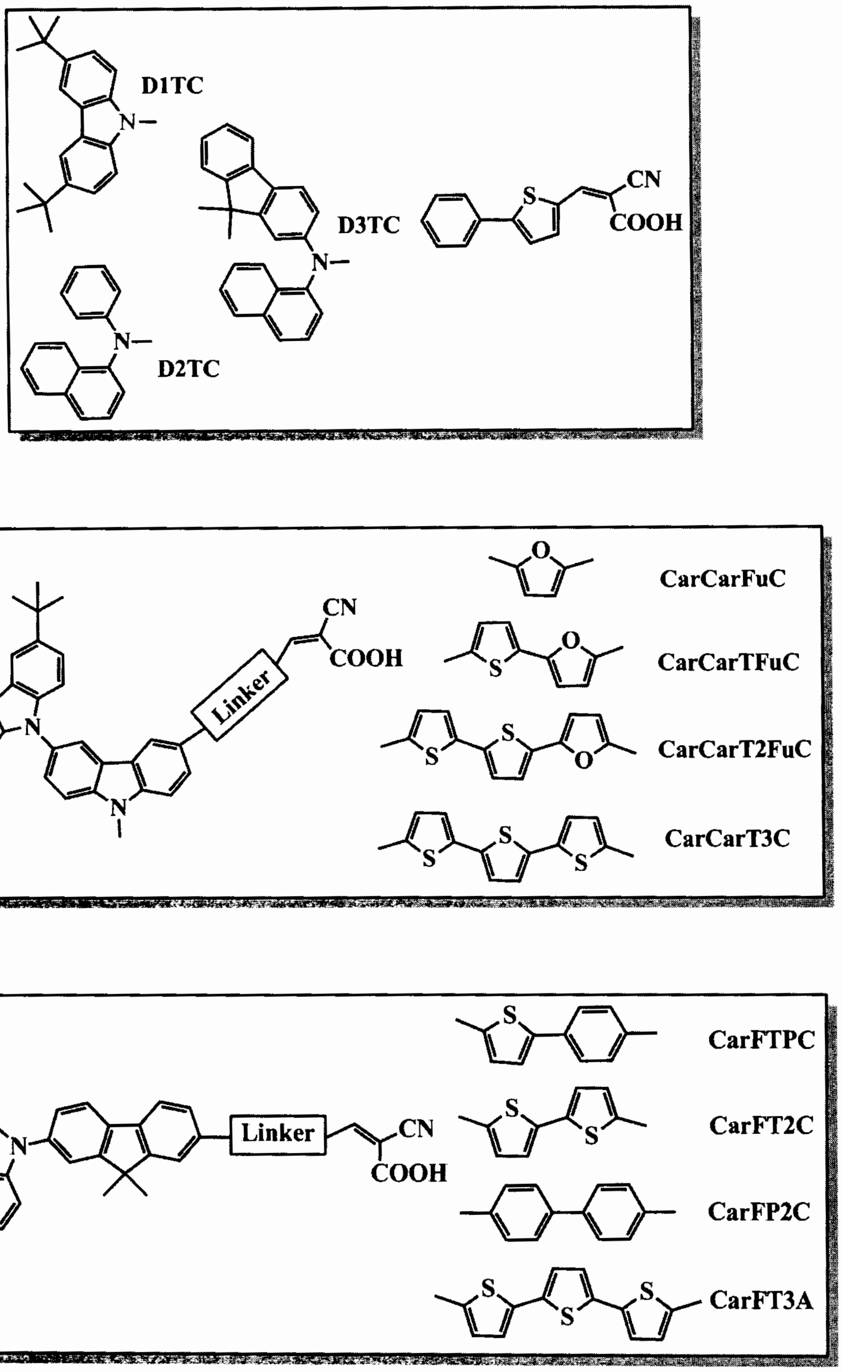

Figure 1.6 Molecular structures of target molecules in the effect of donor

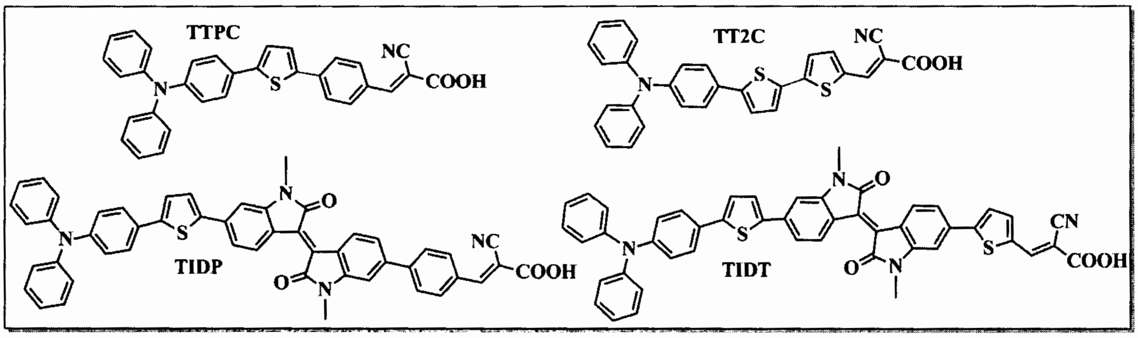

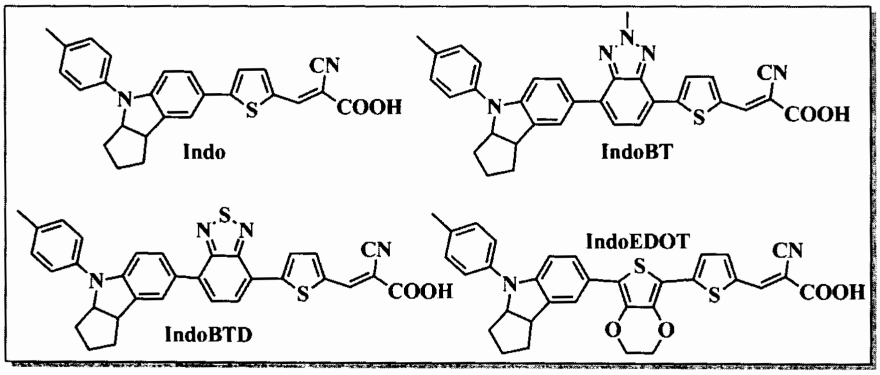

Figure 1.7 Molecular structures of target molecules in the effect of linker part

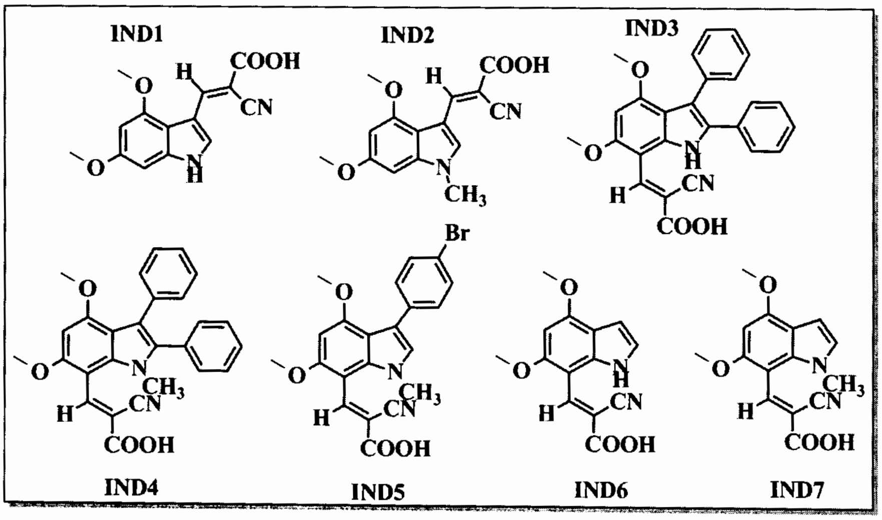

Figure 1.8 Molecular structures of target molecules in the effect of difference acceptor position series

CHAPTER 2

LITERATURE REVIEWS

Dye-sensitized solar cells (DSCs) have attracted great attention over the last 15 years owing to their prospect of high energy conversion efficiency and low production cost. The major factor for the low conversion efficiency of many organic dyes in the DSCs is due to the sharp and narrow absorption band of organic dyes. Therefore, the absorption spectra of organic dyes must be broadened and red-shifted for efficient solar-cell performance. DSCs have attracted much attention since the breakthrough made by Grätzel et al. in 1991 [1]. Several ruthenium-based sensitizers, such as N3, N719, and black dye have achieved remarkable conversion efficiency of 10-11% under standard global air mass [16]. However, ruthenium complex dyes are not suitable for cost-effective environmentally friendly photovoltaic systems, because ruthenium is a rare and expensive metal, which limits the potentially wide application of these complexes. Many scientists are paying a good deal of attention to organic dyes for use in DSCs due to their high extinction coefficient, facile molecular design, and no concern with the noble metal resource. [17]

2.1 Donor-π-acceptor frameworks

Sanghoon Kim and coworker synthesized the organic sensitizers that consist of the bis-dimethyl-fluoreneaniline moiety acting as electron donor and cyanoacrylic acid moiety acting as acceptor (**JK-5** and **JK-6**), the two functions being connected by conducting thiophene units and perform DFT/TDDFT calculations to provide a detailed characterization of the structural, electronic and optical properties of the two sensitizers. They found those two sensitizers shown a highly efficient, yielding 91% IPCE and 8.01% conversion efficiency respectively [16].

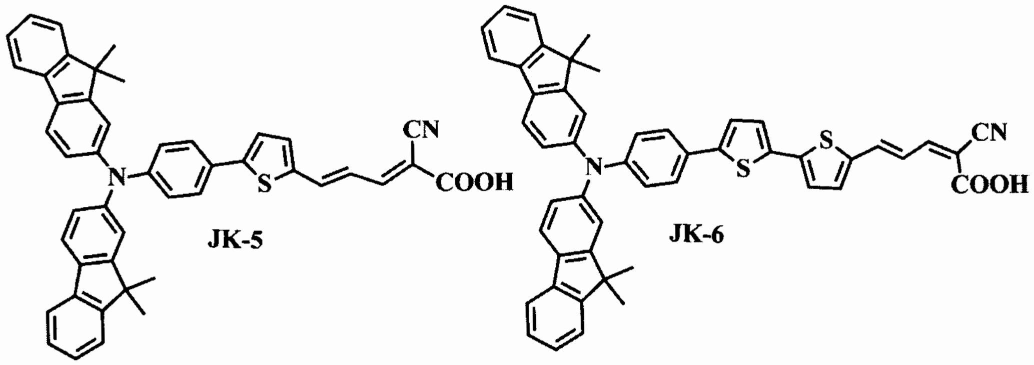

Figure 2.1 The chemical structures of JK-5 and JK-6

Duckhyun Kim and coworker synthesized novel organic dyes containing N-aryl carbazole bridged by thiophene units (**JK-24** and **JK-25**). They obtained a maximum solar energy to electricity conversion efficiency of 5.15% under AM1.5 irradiation with DSCs [18].

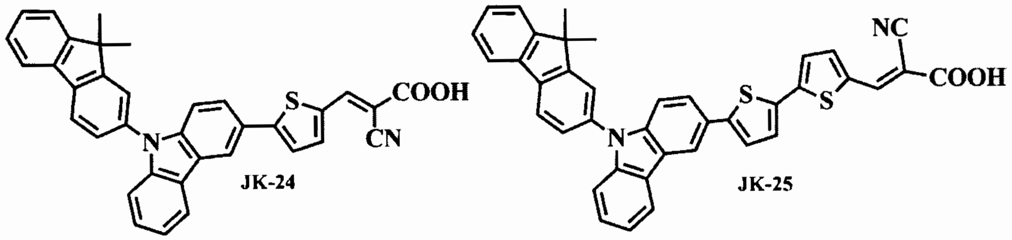

Figure 2.2 The chemical structures of JK24 and JK-25

Zhong-Sheng Wang and coworker synthesized carbazole derivative as an electron donor and a cyanoacrylic acid moiety as an electron acceptor and an anchoring group (**MK-2** and **MK-5**). They found that sensitizers shown a highly efficient, 8.3% of efficiency, which is comparable to 8.1% for the DSCs based on N719 under a comparable condition [19].

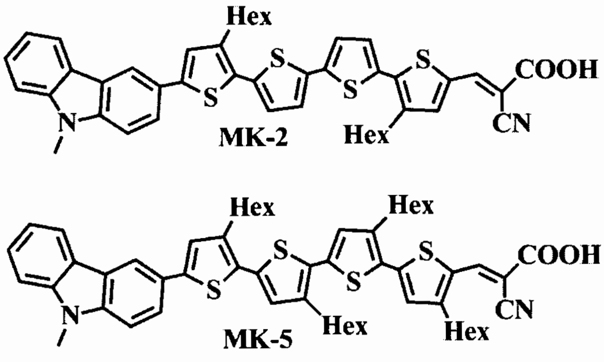

Figure 2.3 The chemical structures of MK-2 and MK-5

Cai-Rong Zhang and coworker was studied organic dye sensitizer TA-St-CA, which contains a π-conjugated oligo-phenylenevinylene unit with an electron donor-acceptor moiety using density functional theory (DFT), and the electronic absorption spectrum was investigated via time-dependent DFT (TDDFT). From the results features of electronic absorption spectra were assigned on account of the qualitative agreement between the experiment and the calculations [20].

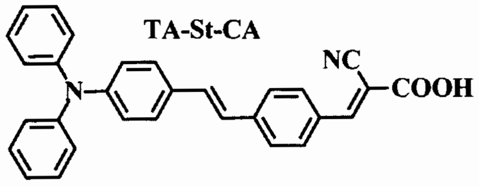

Figure 2.4 The chemical structures of TA-St-CA

Siripom Jungsuttiwong and coworker investigated the electron injection capability of carbazole base dyes, the adsorption of dyes on the TiO_2 anatase (101) was performed with DFT calculations using DMol^3 program, and they found that the calculated adsorption energies of these dyes on TiO_2 cluster were -14 kcal/mol, implying that these dyes strongly bind to TiO_2 surface. Moreover, the electronic HOMO and LUMO shapes of all dye-TiO_2 complexes exhibited injection mechanism of electron via ICT transition [21].

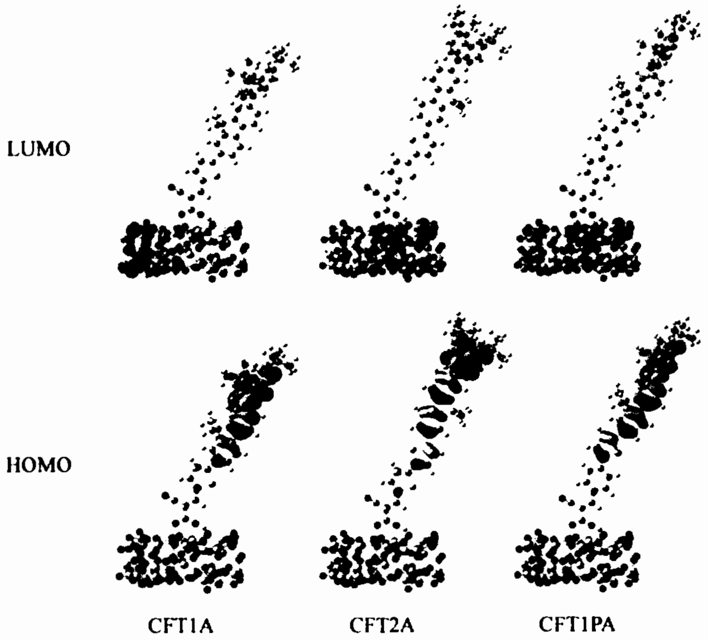

Figure 2.5 FMO of CFT1A, CFT2A, and CFT1PA adsorbed on $(TiO_2)_{38}$ surfaces by B3LYP/6-31G(d,p)

Eunji Lee and coworker were studied novel carbazole based organic dyes, **JD4**, photophysical characteristics and DSCs performances. They found that carbazole based organic dyes show high efficiency, 6.25% [22].

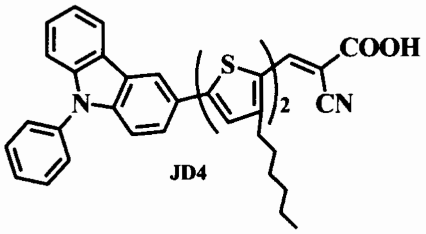

JD4

Figure 2.6 The chemical structures of JD4

Yuan Jay Chang and Tahsin J. Chow were synthesized organic dipolar compounds containing a donor (D), a bridge (B), and an acceptor (A), forming a D-B-A type. The best performance among these compounds was found in **1N-PSP**, which showed a maximal IPCE value of 82%, J_{sc} value of 16.81 mA·cm^{-2}, V_{oc} value of

0.74 V, and *FF* value of 0.57, that correspond to an overall conversion efficiency of 7.08% [23].

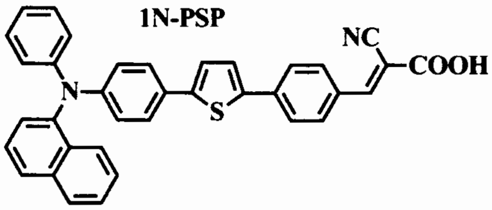

Figure 2.7 The chemical structures of 1N-PSP

Supawadee Namuangruk and coworker report newly designed D-D-π-A type dyes and studied the cluster model $(TiO_2)_{38}$-dye systems with the TD-CAM-B3LYP method and fully relaxed geometries that were optimized by the PBE/DNP method with $DMol^3$. They found that the potential of direct electron injection from the dye to TiO_2 in one step with electronic excitation for the present D-D-π-A dyes. The direct electron injection, inhibited aggregation, and high molar extinction coefficient may be the origin of the observed high efficiency. This type of D-D-π-A structure with direct electron injection would simplify the strategy for designing organic sensitizers [24].

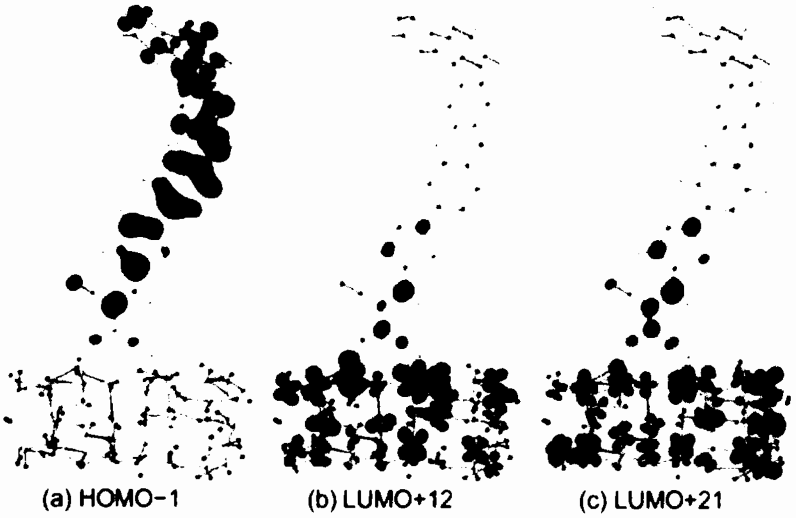

Figure 2.8 (a) HOMO-1, (b) LUMO +12, and (c) LUMO +21 of the $(TiO_2)_{38}$-UB1 System

2.2 Auxiliary acceptor

Wenqin Li and coworker designed and synthesized **LS-5** along with the same conjugated bridge and anchoring group, but TPA as electron donor, to systematically investigate the effect of electron donor on photovoltaic performances of DSCs. Remarkably, with respect to the reference dyes of **LS-1**, **LS-5** and **LS-4** (Figure 2.9). They found that the indoline containing dye shows a more negative oxidation potential and a bathochromic shift in absorption spectra than the TPA substituted dye, indicative of the more powerful electron-donating capability of the indoline unit. The indoline dye based dye-sensitized solar cell exhibited promising conversion efficiency of 6.05% [25].

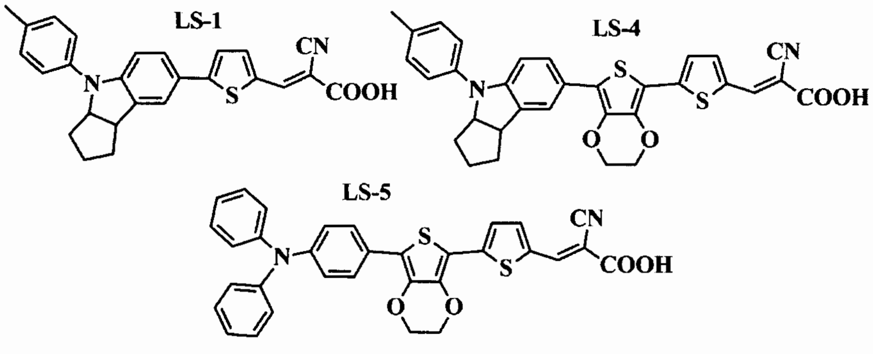

Figure 2.9 Chemical structures of sensitizers LS-1, LS-4 and LS-5

Weihong Zhu and coworker report a series of novel cyanoacetic acid derivatives with a novel specific donor-acceptor-π-bridge-acceptor (D-A-π-A) configuration to construct metal-free organic sensitizers coded as **WS-1** to **WS-4** (Figure 2.10). They found that the stability and spectral response of indoline dye-based DSCs are improved by the strong electron-withdrawing BTD unit in the conjugation bridge. The incident-photon-conversion efficiency of **WS-2** reaches nearly 850 nm with a power conversion efficiency as high as 8.7% in liquid electrolyte and 6.6% in ionic-liquid electrolyte [26].

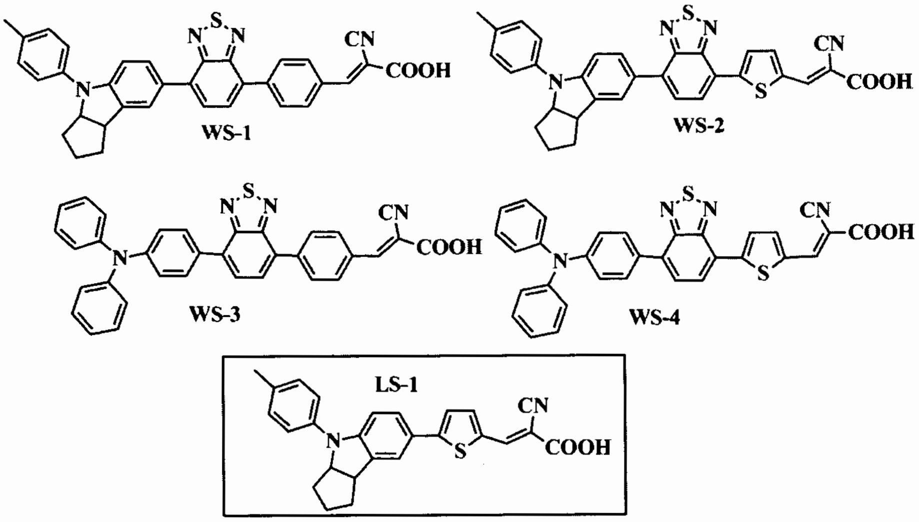

Figure 2.10 Chemical structures of D-A-π-A sensitizers (WS-1 to WS-4) and reference dye LS-1

Dan Wang and coworker study a series of isoindigo-based metal-free organic sensitizers have been synthesized and used in DSCs. Measurement data indicated that the fine-tuning of the donor or linker moiety could conveniently adjust the HOMO and LUMO energy levels. All DSCs sensitized by three new dyes displayed an efficient panchromatic spectra response with the improved light-harvesting capability in near-infrared region, in which a highest photovoltaic conversion efficiency of 5.56% [27].

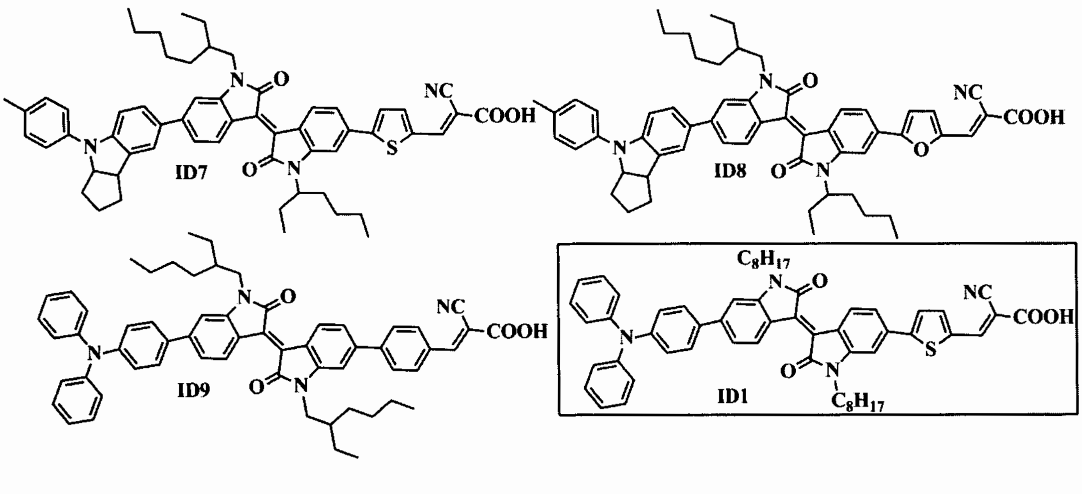

Figure 2.11 Chemical structures of ID7-ID9 and reference dye

Weijiang Ying and coworker designed and synthesized six new D-A-π-A organic sensitizers (**ID1-ID6** shown in Figure 2.12), in which triarylamine as the donor, isoindigo as an auxiliary electron withdrawing unit, thiophene, furan and benzene as the linker, and a cyanoacrylic acid moiety acting as the anchoring group. It was found that their absorption spectra were broad with long wavelength absorption maximum approximately at 589 nm and the absorption onset at 720 nm on the TiO_2 film. Electrochemical experiments indicate that the HOMO and LUMO energy levels can be conveniently tuned by alternating the donor moiety and the linker. All of these dyes performed as sensitizers for the DSCs test under AM 1.5 similar experimental conditions, and a maximum overall conversion efficiency of 5.98% is obtained for **ID6** [28].

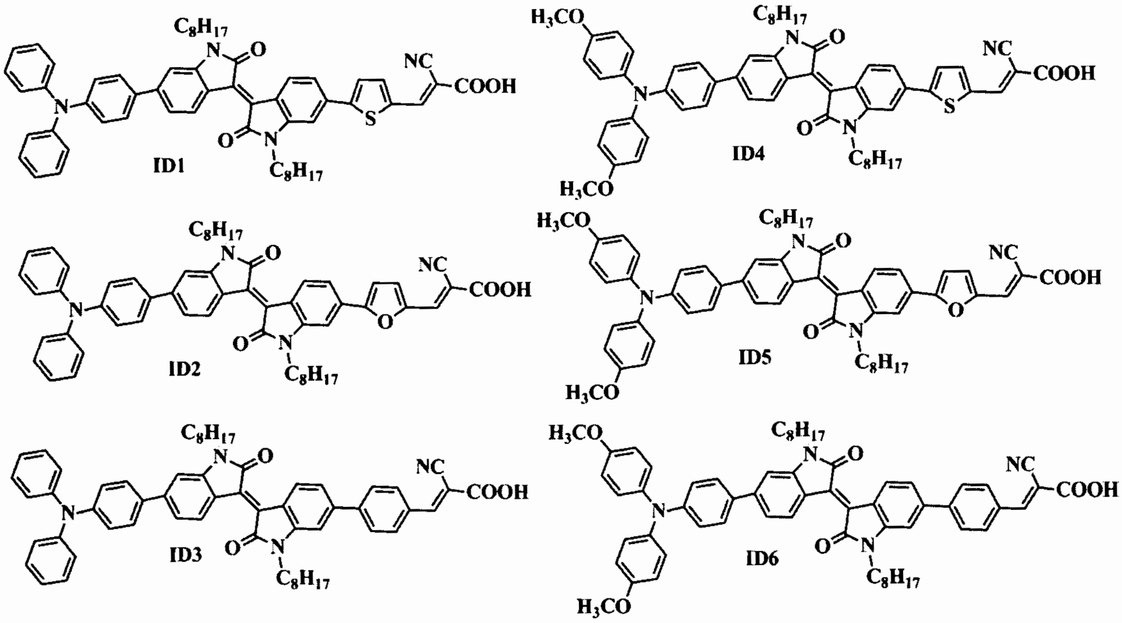

Figure 2.12 Molecular structures of isoindigo dyes (ID1–ID6)

2.3 Indole dyes

A. Venkateswararao and coworker synthesis and characterization of new organic dyes containing indolo[2,3-b]quinoxaline donor, cyanoacrylic acid acceptor and the conjugation pathway composed of phenyl or thiophene fragments. The structures of the dyes are shown in Figure 2.13.We found that the optical and photovoltaic properties are mainly dependent on the nature of the π-linker. The nature of the linker plays a significant role on the absorption and electrochemical properties of the dyes. A dye containing bithiophene linker (**8d**) exhibited the red-shifted absorption with high molar extinction coefficient. However, the aggregation propensity of the planar structures of the compounds containing extended conjugation affected its light harvesting properties in the dye sensitized solar cells. Among the series a dye containing thiophene directly attached to the indoloquinoxaline unit (**5**) displayed the highest efficiency in DSCs [29].

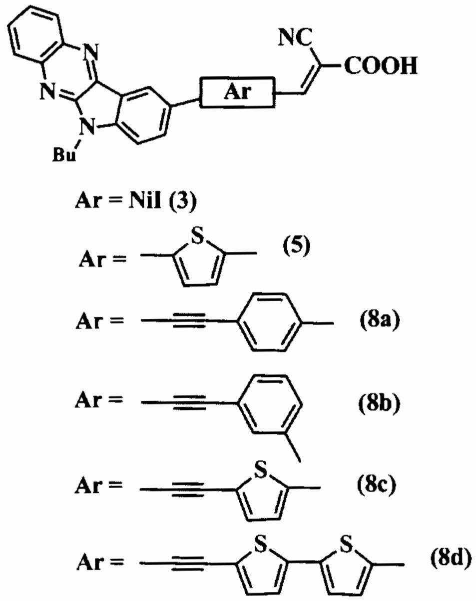

Figure 2.13 Structures of the indoloquinoxaline-based dyes

Dickson D. Babu and coworker synthesized three new sensitizers by following the simple synthetic protocols as shown in Figure 2.14. Three new Donor-π-Acceptor type dyes **D1-D3** carrying 3-(1-hexyl-1H-indol-3-yl)-2-(thiophen-2-yl) acrylonitrile as backbone with three different acceptor units. The study reveals that the dye carrying

4-aminobenzoic acid as an acceptor showed the highest photovoltaic efficiency among the three dyes [30].

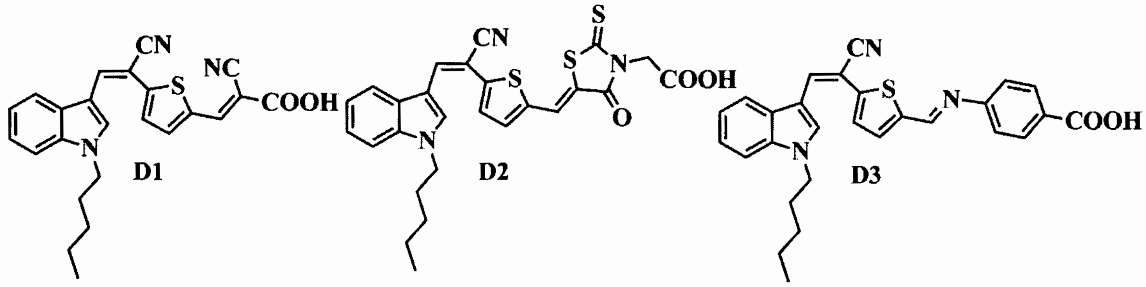

Figure 2.14 Structures of the D1, D2 and D3 dyes

CHAPTER 3

THE NUMBER DENSITY EFFECT OF N-SUBSTITUTED DYES ON THE TiO_2 SURFACE IN DYE SENSITIZED SOLAR CELLS

Dye-sensitized solar cells (DSCs) have attracted great attention over the last 15 years owing to their prospect of high energy conversion efficiency and low production cost [1]. The typical basic conjugation is as follows: the mesoporous oxide layer, which is composed of a network of TiO_2 nanoparticles that have been sintered together to establish electronic conduction, is deposited on a transparent conducting oxide (TCO), on a glass or plastic substrate. The most commonly used substrate is glass coated with fluorene-doped tin oxide (FTO). Attached to the surface of the nanocrystalline film is a monolayer of the charge transfer dye. Photoexcitation of the charge-transfer dye results in the injection of an electron into the conduction band of TiO_2, leaving the dye in its oxidized state. The dye is restored to its ground state by electron transfer from the electrolyte, which is usually an organic solvent containing the iodide/triiodide redox system. The regeneration of the sensitizer by iodide, intercepts the recapture of the conduction-band-electron by the oxidized dye [3]. There are mainly three kinds of dyes commonly used in DSCs, including ruthenium dyes [31], porphyrin dyes [32-36] and metal free organic dyes [37-40]. Compared with the other two dye types, the metal-free organic D-π-A dyes have received a great deal of attention due to their low cost, relatively simple synthetic procedure, ease of molecular modification and tailoring high molar extinction coefficients, and environmental friendliness.

However, organic dyes also have their own drawbacks, such as a narrower absorption spectrum, and a faster charge recombination. In this study, we are attempting to improve their solar-to-electrical-energy conversion efficiency in DSCs regarding charge recombination. There are two different improper recombination types in DSCs. One is the "inner-path recombination" consisting of the recombination of an electron injected into the semiconductor with the dye action before dye regeneration, which deteriorates the rate of electron injection, leading to a decrease of photocurrent and J_{sc} value. The other type of charge recombination in DSCs is "outer-path recombination", which occurs between the injected electrons in the semiconducting oxide electrode and the oxidized electrolyte. It strongly affects the theoretical potential difference between the oxide electrode and the electrolyte, resulting in a reduced $V_{oc.}$ One of the common strategies to suppress this improper recombination path, while also suppressing undesirable molecular aggregation, is to introduce a starburst-triarylamine derivative as a donor group in D-π-A dyes. An extra-bulky donor could prevent the electrolyte from approaching the surface of the semiconducting oxide electrode, therefore, J_{sc} and V_{oc} would be enhanced and finally provide better device performance [41-42]. However, one drawback of this dye design is that its bulky donor greatly reduces the number density of the adsorbed dyes on the oxide electrode surface, which decreases the absolute amount of injected electrons from the dyes to the electrode, resulting in poorer photocurrent generation in DSCs. Recently, various kinds of metal-free organic dyes have been developed as sensitizers in DSCs, and their efficiency has been improved gradually through molecular design. Many efficient organic dyes for DSCs containing triphenylamine [43-44], coumarin [45-46], indoline [17], fluorene [47], or carbazole [19] moieties have been developed, yielding efficiencies in the range of 4-9%. Among them, N-substituted derivative dyes are promising due to the high efficiency and good stability. In this study, molecular design concepts were introduced in order to additionally improve their solar-to-electrical-energy conversion efficiency in DSCs regarding electron injection efficiency. We are attempting to disclose the relationship between the performance, structures, and the number density of the adsorbed dye on the TiO_2 surface using combined theoretical and experimental investigations of the physical properties of dye sensitizers. The effect of different N-substituted electron donating [48-49] has been investigated. The calculated results are very helpful when designing and synthesising novel dye sensitizers with higher performance. The derivatives of N-substituted donor with D–π–A architecture in the present study, namely **D1TC**, **D2TC** and **D3TC** are theoretically investigated. These dyes compose of an electron-accepting cyanoacrylic acid group (A) and a π-conjugated bridge (π) of one thiophene moiety while there are different electrons donating moieties on the donor group (D). We aim to reveal the effects of the sensitizer donor on the performance of the photovoltaic devices affecting both the geometrical structures and the optical properties of the derivatives of N-substituted donor with a D-π-A structure. Therefore, the introductions of more electron donors on a simple D-π-A dye system are designed, as can be seen in Figure 3.1. The variations of the donor are categorized into two types: (i) carbazole substituted at N-position (ii) diphenylamine (DPA)-like substituted at N-position, one phenyl of DPA is replaced by naphthalene unit forming **D2TC** while in **D3TC**, two phenyl units of DPA are replaced by naphthalene and fluorene, respectively. Figure 3.1 shows the molecular structures of **D1TC**, **D2TC** and **D3TC** which are studied for the purpose of comparing the variation and architecture of the donor.

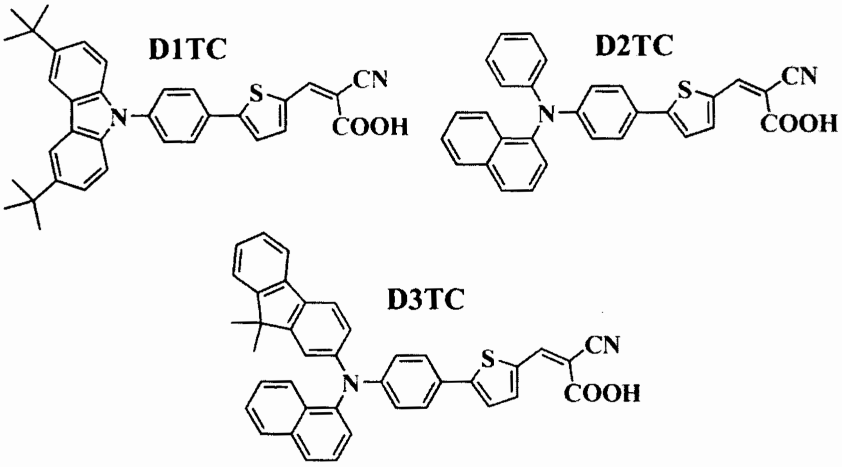

Figure 3.1 Sketch map of the synthesized D1TC, D2TC and D3TC sensitizers

3.1 Computational details

The ground-state structures of organic dye molecules are fully optimized using density functional theory (DFT) at the Becke3 (exchange) and the Lee–Yang–Parr (correlation) hybrid functional [50] with 6-31G(d,p) basis set [51]. The excitation energies and the electronic absorption spectra of organic dye molecules are investigated using time-dependent density functional theory (TDDFT) at the CAM-B3LYP functional [52], with the same basis set as in the ground-state calculations. The solvation effect is included by means of conductor-like polarizable continuum model (C-PCM). The solvent used in our calculations and experiment is dichloromethane (CH_2Cl_2). The absorption spectra of all organic sensitizers and the contribution of molecular orbitals in the electronic transitions are simulated using the GaussSum program version 3.0 [53]. The results are compared with the experimental data [54]. All calculations are performed using the Gaussian09 program package [55]. The electron-injection characteristics from **D2TC** and **D3TC** to the TiO_2 (101) anatase surface [56] are carried out. The dye@$(TiO_2)_{38}$ systems are fully optimized by the Perdew–Burke–Ernzerhof (PBE) functional with the double numerical polarization (DNP) basis set. The core electron is treated with DFT semicore pseudopotentials (DSPPs) by DMol^3 code in Materials Studio 5.5. The energy convergence tolerance is set to 2 x 10^{-5} Hartree, the maximum force 0.004 Hartree Å^{-1}, and the maximum displacement 0.005 Å. The optical properties of the relaxed complex are then computed with the TD-CAMB3LYP/6-31G(d) method. The adsorption energies (E_{ads}) of dyes on the $(TiO_2)_{38}$ clusters can be obtained using the following expression:

$$E_{ads} = E_{dye+TiO_2} - [E_{dye} + E_{TiO_2}]$$

where $E_{dye+TiO_2}$ is the total energy of the dye@$(TiO_2)_{38}$ system, and $E_{dye}$and E_{TiO_2} are the energies of the dye and $(TiO_2)_{38}$ cluster, respectively.

3.2 Results and discussion

3.2.1 Ground-state geometries of organic sensitizers

The optimized geometries obtained by density functional theory (DFT) B3LYP/6-31G(d,p) level of organic dye molecules are shown in Figure 3.2, and selected important inter-ring distance and dihedral angle parameters are listed in Table 1. The bond lengths of all the important inter-ring bonds are in the range of 1.40 to 1.46 Å. Due to the rigid structural arrangement of a carbazole donor, the dihedral angles between the donor unit (D) and the phenyl ring (Ph) is calculated to be 49.27° which is significantly larger than those of **D2TC** and **D3TC** (26.71° and 26.86°), with free rotation around the N-position of a DPA-like structure. Consequently, the twisted structure in the donor part of these dyes resulted in preventing dye aggregation [57-58]. In the acceptor part, the dihedral angles between the thiophene ring (T) and the cyanoacrylic acid anchoring are coplanar in the range of 0.64° to 1.08°. Therefore, the electron from the donor can efficiently delocalize to the acceptor moiety and as a result transfers to the conduction band (CB) of the semiconductor.

Table 3.1 The selected important inter-ring distances (r, Å) and dihedral angle (ϕ, °) calculated by B3LYP/6-31G(d,p) calculations

Dyes	**Dihedral angle (ϕ) and inter-ring distance (r)**		
	D - Ph	**Ph -T**	**T - CA**
D1TC	-49.27 (1.41)	23.75 (1.46)	-0.64 (1.42)
D2TC	-26.71 (1.40)	20.78 (1.45)	-1.05 (1.42)
D3TC	-26.86 (1.40)	21.02 (1.45)	1.08 (1.42)

D = Donor, Ph = Phenyl, T = Thiophene, CA = Cyanoacrylic acid

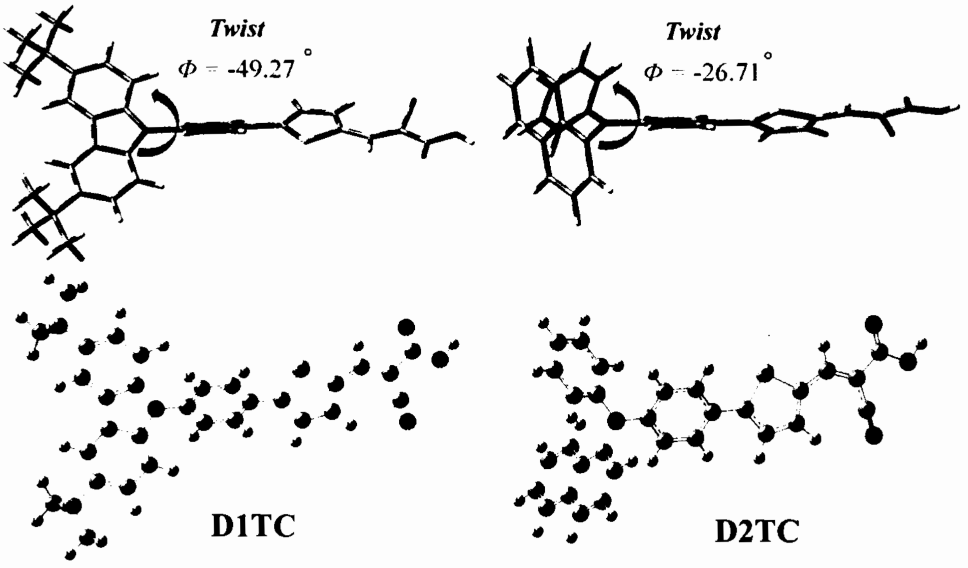

D1TC D2TC

Figure 3.2 Optimized structures of D1TC and D2TC by DFT/B3LYP/6-31G(d,p)

Table 3.2 The energies and percentage composition of frontier molecular orbitals of organic sensitizers

Dyes	Molecular orbitals	Orbitals energy (eV)	Percentage composition		
			Donor	Linker	Acceptor
D1TC	LUMO	-2.78	1	49	50
	HOMO	-5.38	81	17	2
D2TC	LUMO	-2.57	3	48	49
	HOMO	-5.27	52	41	7
D3TC	LUMO	-2.57	3	48	49
	HOMO	-5.14	63	32	5

3.3.2 Electronic structures of organic sensitizers

To gain insight into the electronic structures, frontier molecular orbitals are obtained to examine the highest occupied molecular orbital (HOMO) and the lowest unoccupied molecular orbital (LUMO) due to the relative ordering of the HOMO and LUMO which provides a reasonable qualitative indication of the charge transfer properties. The molecular orbitals of **D1TC**, **D2TC** and **D3TC** are depicted in Figure 3.3 and the density of state (DOS) are presented in Table 3.2. In organic sensitizers, the electron density on the HOMO is delocalized on donor group and the electron density on the LUMO is delocalized on acceptor group. The HOMO to LUMO transition corresponds to the intramolecular charge transfers (ICT) from the donor group to the acceptor group. The different electronic densities between the ground state and excited state (shown in Figure 3.3) are clearly assigned to the unambiguous character of excited state. Obviously, the decreasing electron density is primarily from the electron donor, whereas the increasing electron density is mainly on the acceptor group, which is indicative of the intramolecular charge transfer when transition occurs upon photoirradiation. This agrees well with the electronic structure analysis discussed above. Moreover, the HOMO of all dyes show that the electrons density of **D1TC** is predominantly located at the rigid carbazole moiety while **D2TC** and **D3TC**, the electron is located all over the donor moiety and contributed to the linker part. Therefore intramolecular charge transfer could be more efficient in **D2TC** and **D3TC** than in **D1TC** according to Marcus theory. The distance of charge transfer (D_{CT}, Å) and the transition dipole moment (μ, Debye) are calculated for a better understanding of the performance of the intramolecular charge transfer upon photoexcitation. The D_{CT} is the spatial distance between two barycenters of the density depletion ($\rho-$) and density enhancement ($\rho+$) distributions, while dye is under irradiation. The isosurface ($\rho-/\rho+$) of the dyes are illustrated in Figure 3.4, and the DCT and m values are listed in Table 3. As shown, the D_{CT} values (Å) are found to be in this order: **D1TC** (3.59) < **D2TC** (4.04) < **D3TC** (4.20). The m also give the same trend as **D1TC** (12.9) < **D2TC** (14.9) < **D3TC** (15.9). Based on the D_{CT} and m, **D3TC** is predicted to give the best DSC performance among these dyes.

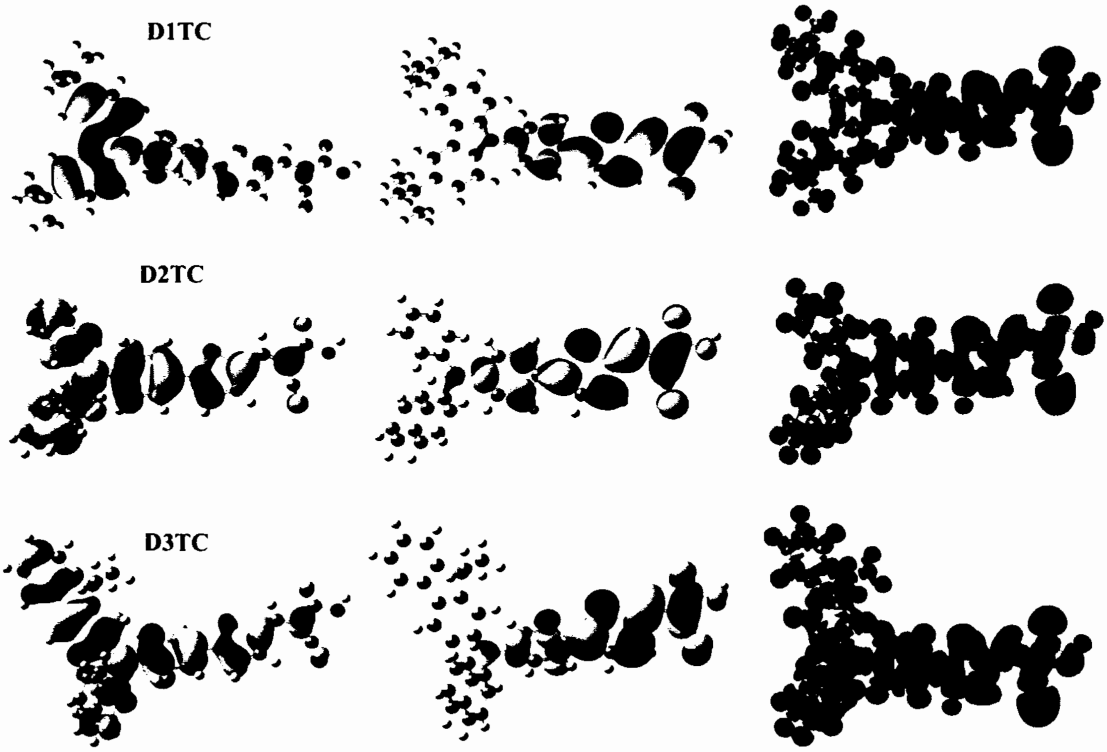

Figure 3.3 HOMO (left) LUMO (middle) and charge density difference (right) between the excited and ground states of the dyes. The green and red colors indicate a decrease and increase of charge density

Table 3.3 The distance of charge transfer upon excitation (D_{CT}), dipole moment (μ) electronic properties, maximum absorption wavelength and oscillator strength (*f*) obtained by TDDFT at the CAM- B3LYP/ 6-31G (d,p) in CH_2Cl_2 solvent (C-PCM model)

Dyes	D_{CT} (Å)/ μ (Debye)	Electronic transitions	λ_{max} (nm/eV)	*f*	Assignment; H=HOMO, L=LUMO, etc.	Expt. λ_{max} (nm/eV)
D1TC	3.59/12.9	$S_0 \rightarrow S_1$	397(3.12)	1.4218	(+0.53) H → L (+0.43) H-2 → L (-0.11) H → L+1	355(3.49)
D2TC	4.04/14.9	$S_0 \rightarrow S_1$	428(2.90)	1.4686	(+0.62) H → L (+0.21) H-1 → L (-0.17) H-1 → L (-0.10) H → L+2	436(2.84)
D3TC	4.20/15.6	$S_0 \rightarrow S_1$	434(2.85)	1.4867	(+0.60) H → L (+0.24) H-1 → L (-0.19) H-2 → L (-0.11) H → L+2	438(2.83)

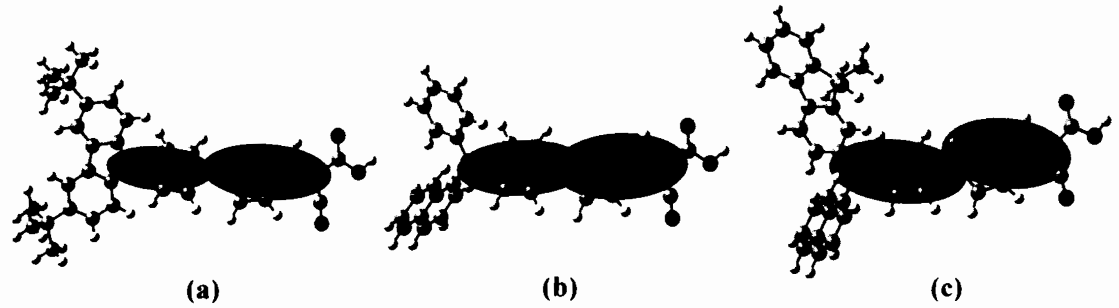

Figure 3.4 *$\rho-/\rho+$* **(green/red) isocontour surfaces of (a) D1TC, (b) D2TC, and (c) D3TC, computed at the TD-CAM-B3LYP/6-31G(d,p) level**

In addition, suitable energy levels of the HOMO and the LUMO orbitals of the organic dye are required to match the I^-/I_3^- redox potential and conduction band level of the TiO_2 semiconductor. The calculated molecular orbital energies of **D1TC**, **D2TC** and **D3TC** are computed by using B3LYP/6-31G(d,p) in CH_2Cl_2 as shown in Figure 3.5. For the LUMO levels, the results show that the replacement of carbazole with diphenylamine-like substituent raises the LUMO level from -2.80 (**D1TC**) to -2.69 eV (**D2TC** and **D3TC**). However, the LUMO levels of all dyes lie above the E_{CB} of TiO_2 leading to efficient injection of excited electrons into the semiconductor electrode. Compared with electrolyte redox potential, the HOMO levels of all dyes are below the I^-/I_3^- redox potential. These results show the accepting electron efficiency of the oxidized dye from the electrolyte system. The HOMO energy levels of **D1TC**, **D2TC**, and **D3TC** are calculated to be -5.37, -5.22, and -5.12 eV, respectively. As shown, the HOMO levels of D1TC–3 are systematically increased with increasing donor ability (**D3TC** < **D2TC** < **D1TC**) approaching the redox potential of the electrolyte system, which resulted in the energy gaps being in a sequence of **D3TC** (2.43) < **D2TC** (2.53 eV) < **D1TC** (2.57 eV). Therefore, **D3TC** with its narrow energy gap would be an efficient sensitizer to extend the absorption wavelengths of these organic dyes.

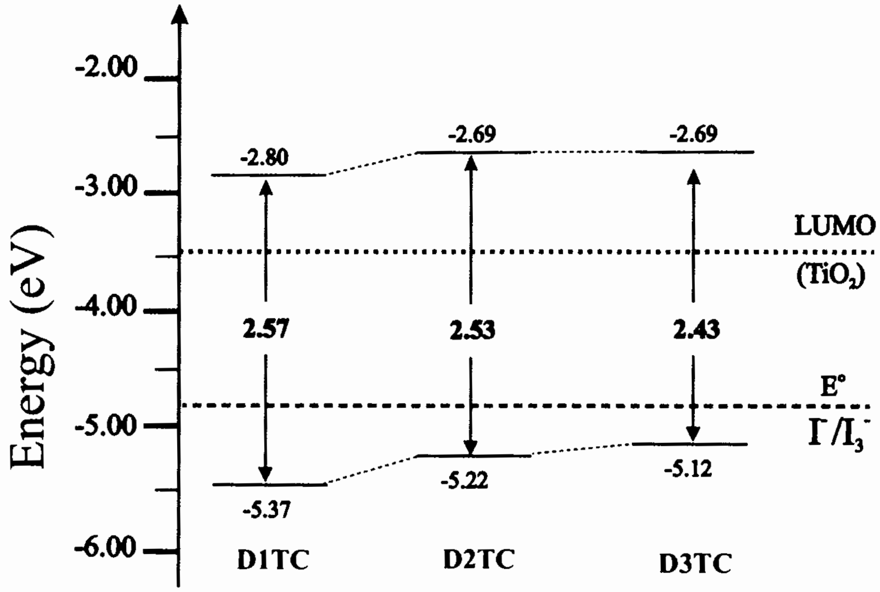

Figure 3.5 Molecular orbital energy level diagram of the dyes, TiO_2 conduction band, and redox potential of I^-/I_3^- electrolyte

3.2.3 Absorption spectra of organic sensitizers

The absorption spectra of these molecules have been studied by TD-CAM-B3LYP/6-31G(d,p) level in the CH_2Cl_2 solvent. Comparison of the theoretically calculated wavelength with experimental data has been performed. The corresponding simulated absorption spectra of **D1TC-D3TC** are shown in Figure 3.6. The electronic properties, oscillator strengths, conjugations of the orbitals, and the maximum wavelength in the solvent phase of all organic sensitizers are shown in Table 3.3. The strongest absorption peak with the largest oscillator strength arises from $S_0 \rightarrow S_1$ transition and corresponds to the intramolecular charge transfer transition, which is primarily contributed from the HOMO to the LUMO.

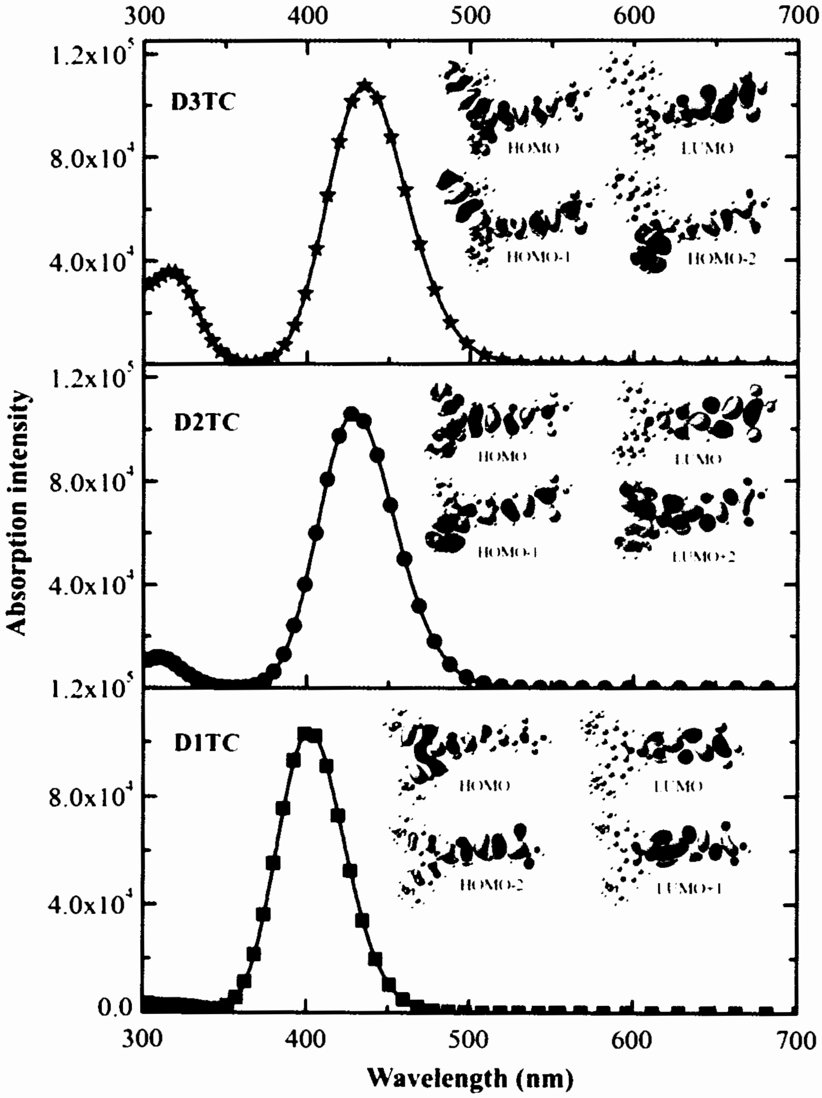

Figure 3.6 Absorption spectra of D1TC, D2TC and D3TC calculated by TDCAM-B3LYP/6-31G(d,p) level in CH_2Cl_2 solvent (C-PCM model)

It is found that the calculated data have similar tendencies with the experiment. The trend of maximum absorption wavelength is **D3TC** > **D2TC** > **D1TC** which exhibits red-shift and the absorption intensity increases with the increase of electron donating ability of donor groups. This tendency also confirms the D_{CT} prediction. These results indicate that **D1TC** exhibits obvious blue-shift due to the electrons from the rigid carbazole donor, connected at N-position with large twisted angle, hardly transferred to the anchoring group. Therefore, its conjugation length, and D_{CT} values are smallest in comparison to **D2TC** and **D3TC**. In the next section, the adsorption of the organic sensitizers on the TiO_2 cluster, of **D2TC** and **D3TC** will be compared and discussed.

3.2.4 Adsorption of organic sensitizers on the TiO_2 cluster

The TiO_2 film were modelled with a stoichiometric anatase (101) surface as the $(TiO_2)_{38}$ cluster, which is similar to that described by Nazeeruddin et al [59]. This model has been wildly used to study dye@TiO_2 adsorption and represents a reasonable choice between accuracy and computational convenience, and nicely reproduces the main electronic characteristics of TiO_2 nanoparticles. The HOMO, LUMO and HOMO–LUMO energy gap of the this cluster are calculated to be 27.98, 23.52, and 24.46 eV, respectively, while the lowest excitation is obtained as 3.75 eV which is reasonably higher than typical band gaps of TiO_2 nanoparticles of a few nm size of 3.2–3.3 eV. The TiO_2 conduction band edge was calculated at ca. -4 eV vs. vacuum, in good agreement with experimental values. In addition, this cluster size has been comparatively tested with a relatively larger $(TiO_2)_{82}$ cluster and the both clusters shows a similar conduction band structure, within 0.1 eV, to the corresponding periodic model. Therefore, this work we use the $(TiO_2)_{38}$ cluster for representing the TiO_2 surface for dye adsorption. The optimized structures of dye@$(TiO_2)_{38}$ adsorption complexes are shown in Figure 3.7. The intermolecular Ti–O bond distances and adsorption energies calculated by PBE/DNP are tabulated in Table 3.5. The bond distances between 5c-Ti and O atom of **D2TC** and **D3TC** are in range of 2.14-2.26 Å. The adsorption energy (E_{ads}) of **D2TC@TiO$_2$** and **D3TC@TiO$_2$** are calculated to be -15.89 and -19.54 kcal mol^{-1} respectively, indicating the strong interactions between the dyes and the TiO_2 cluster. The higher adsorption energy of **D3TC**, with a stronger electron donating group, can be related to the stronger electronic coupling strengths between the anchoring group of dye and the TiO_2 surface, which could corresponds to higher observed J_{sc}. However, we found that the adsorption energies did not correspond to observed J_{sc} as expected. The J_{sc} of 10.96 mA cm^{-2} for **D2TC** is significantly higher than 7.62 mA cm^{-2} for **D3TC**.

Table 3.4 Molecular volume, Box size, and projected area of D2TC and D3TC

Dyes	Molecular volume [a] (Å^3)	Box size a x b x c (Å^3)	Projected area a x b(Å^2)
D2TC	3311.80	10 x 20.40 x 21.20	180
D3TC	4614.18	10 x18 x 21.20	214

[a] Molecular volume is calculated by Connolly surface

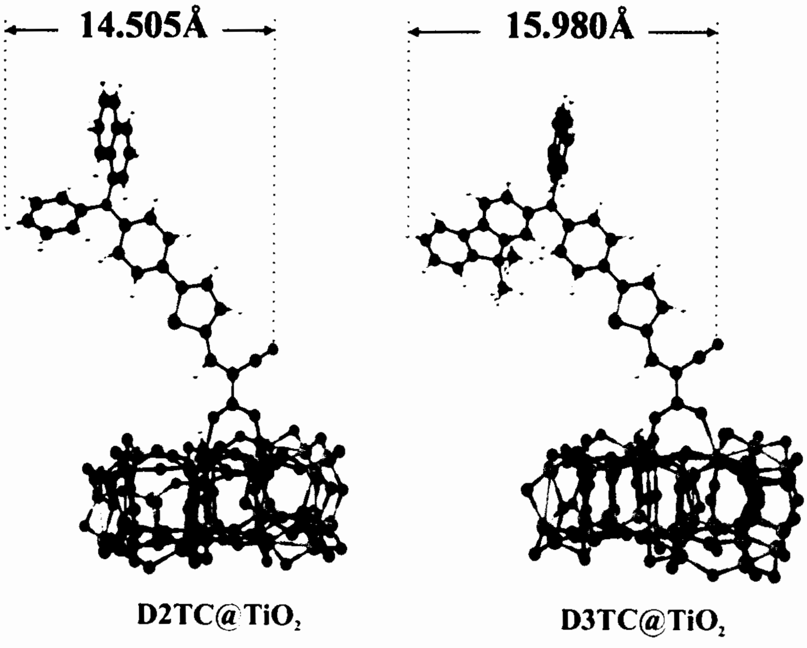

Figure 3.7 Molecular widths of D2TC and D3TC calculated by PBE/DNP on DMol^3

Table 3.5 The selected bond length (Å) and adsorption energy (E_{ads}) of dye-TiO_2 calculated by PBE/DNP in $DMol^3$

Complexes	Ti - O	Ti - O′	E_{ads} (kcal/mol)	J_{SC} (mA cm^{-2})	V_{OC} (V)	FF	Dye uptake (molecule cm^{-2})	(%)
D2TC@TiO_2	2.14	2.26	-15.89	10.96	0.77	0.645	4.55×10^{17}	5.45
D3TC@TiO_2	2.14	2.18	-19.54	7.62	0.76	0.674	1.38×10^{17}	3.91

These results can be rationalized by molecular volume and projected area (Figure 3.8), as well as molecular width (Figure 3.7). The molecular volume is calculated by a Connelly surface, which represents the molecular volume of the dye including its van der Waals volume. The projected area explains the area on the TiO_2 surface that is occupied by the adsorbed dye. These values of **D2TC** and **D3TC** are listed in Table 3.4. As shown, the molecular widths are calculated to be 14.505 Å and 15.980 Å (Figure 3.7), the molecular volumes are 1810.68 Å^{3}and 1937.13 Å^3 (Table 4), together with the measured projected area (dark area in Figure 9) of 180 Å^{2}and 214 Å^2, for **D2TC** and **D3TC** respectively, which correspond to the dye uptakes of 4.55×10^{17} and 1.38×10^{17} molecule per cm^2, see Table 3.4.

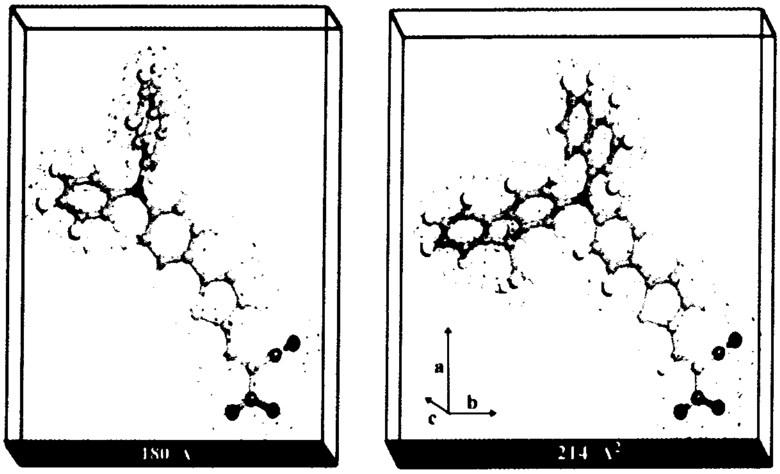

D2TC **D3TC**

Figure 3.8 Molecular volume and projected area of D2TC and D3TC

These results indicate that **D3TC** would cover a larger area on the TiO_2 surface due to the bulky of the donor moiety. Consequently, the number density of the adsorbed **D3TC** on the surface could be reduced leading to the lower dye uptake. Then the absolute amount of injected electrons from the dyes to the electrode per cm^2 is decreased, related to the lower observed J_{sc} value of 7.62 mA cm^{-2} compared to 10.96 mA cm^{-2} of **D2TC**. These findings highlight the poorer energy conversion efficiency of 3.91% in **D3TC** compared to the better performance of 5.45% in **D2TC** under simulated AM 1.5 irradiation (100 $mWcm^{-2}$), see Table 3.5.

3.2.5 Dye@TiO_2 adsorption and the electron injection mechanism

To study the electron injection mechanism of selected dyes at the interface of the dye@TiO_2 surface, the ten lowest vertical transitions are simulated using TD-CAM-B3LYP/6-31G(d). The calculated excitation energies for the peak having the highest oscillator strength are illustrated in Figure 3.9. The results show that the strongest transition in our dyes is characterized as a linear combination of some conjugurations. The Kohn-Sham orbitals, which are most relevant to these transitions, are shown in Figure 3.10 (a) and (b). There is a very similar trend between D2TC and **D3TC**, Therefore we only discuss **D3TC**. The highest oscillator strength of 1.5635 for **D3TC** is assigned as the linear combination of $0.17(H \rightarrow L + 25) + 0.14(H\text{-}1 \rightarrow L + 27) + 0.27(H\text{-}2 \rightarrow L + 38)$. These orbitals, together with TDDFT functional, show that the transition with large oscillator strength is characterized as the transition from the orbitals localized in the donor-π-spacer (D-π) unit to the orbitals delocalized over the acceptor (A) unit of dyes and the $(TiO_2)_{38}$ clusters.

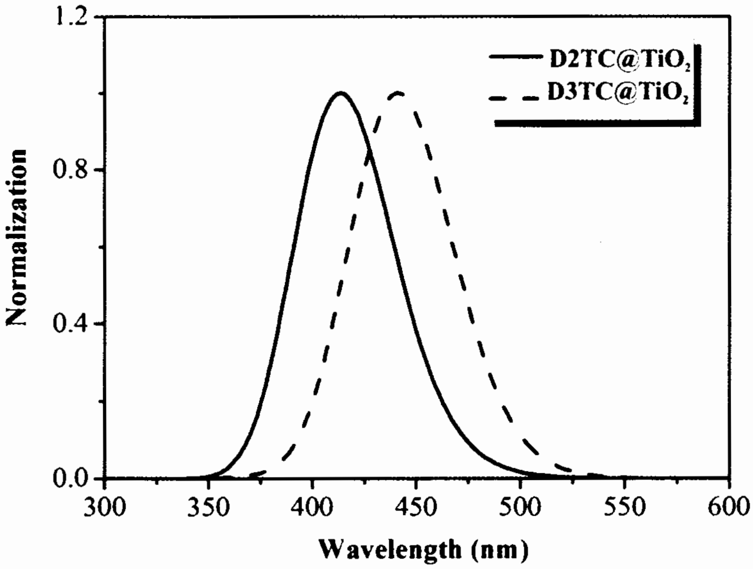

Figure 3.9 Absorption spectra of D2TC@TiO$_2$ and D3TC@TiO$_2$ calculated by TD-CAM-B3LYP/6-31G(d) level in gas phase

The former orbitals are similar to the HOMOs of dyes and the latter orbitals correspond to the interacting orbitals between the LUMOs of dyes and the conduction band of TiO$_2$. This means that the electron excitation of this system directly induces the electron injection from dye into TiO$_2$ surface. This is the origin of the high photoelectric conversion efficiency of this system. Note that the latter orbitals are firstly embedded in the conduction band of TiO$_2$ and then the injected electron is transferred to the conduction bands of TiO$_2$. These compositions of the electronic transitions for two dyes, as shown in Figure 3.10 (a) and (b), strongly indicated that when the intramolecular charge transfer is initially performed, electrons moved from the donor to the anchoring group via phenyl-thiophene bridging, then jumped onto the TiO$_2$ surface.

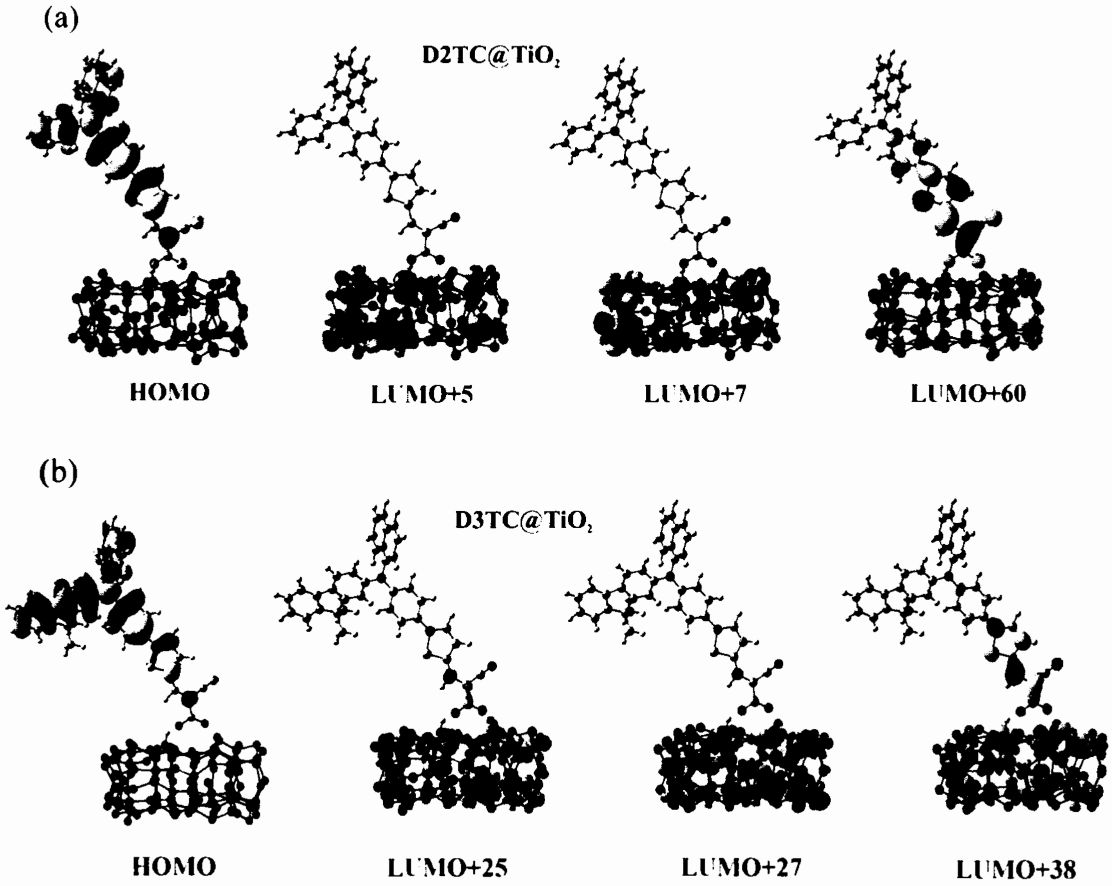

Figure 3.10 MOs relevant to the transition from S_0 to S_1 of organic sensitizer adsorbed on the $(TiO_2)_{38}$ in gas phase calculated by TD-CAM-B3LYP/6-31G(d) on DMol^3 geometry. (a) D2TC@TiO$_2$ (b) D3TC@TiO$_2$

3.3 Conclusions

In summary, **D1TC**, **D2TC** and **D3TC** have been studied for the purpose of comparison, based on the variation and architecture of the donor, N-substituted donors-π-acceptor type. These dyes are composed of cyanoacrylic acid anchoring group and phenyl-thiophene moiety as π-spacer. We have designed 3 different donors for variation, carbazole substituted at N-position forming **D1TC**, diphenylamine (DPA)-like substituted at N-position, one phenyl of DPA is replaced by naphthalene unit forming **D2TC**, while two phenyl units of DPA are replaced by naphthalene and fluorene forming **D3TC**, respectively. We found that **D3TC**, with the strongest electron donating ability, shows the most red shift in the UV absorption spectra and the highest performance charge transfer. Moreover, the calculated adsorption energy -19.54 kcal mol^{-1} for **D3TC@(TiO_2)$_{38}$** complex indicates the strongest interactions between the dyes and the TiO_2 surface, therefore **D3TC** is expected to be the most potential sensitizer. Nevertheless, **D2TC** has shown the best photovoltaic performance. This controversial issue has been solved by performing the molecular volume, projected area on the TiO_2 surface and molecular width to investigate the effect of N-substituted donors on the number density of the adsorbed dye on TiO_2 surface. It has been found that the more bulky donor moiety in **D3TC** reduces the number density of the adsorbed dye on the TiO_2 surface. The molecular width of **D2TC** and **D3TC** are calculated to be 14.505 Å and 15.980 Å together with the computed projected area of 180 and 214 Å^2 (Figure 3.8) which excellently agrees with the dye uptake of 4.55 x 10^{17} and 1.38x 10^{17} molecule per cm^2, respectively. The photovoltaic performance shows a poorer energy conversion efficiency of 3.91% in **D3TC** compared to the significantly better performance of 5.45% in **D2TC** under simulated AM 1.5 irradiation (100 mW cm^{-2}). In conclusion, it has been shown that these computational tools described above can provide detailed characterizations, which can qualitatively explain experimental efficiency and therefore can be of great valuable in further design of novel organic sensitizers for higher efficiency photovoltaic devices.

CHAPTER 4

THE EFFECT OF BULKY-DONOR TO CHARGE RECOMBINATION AND CHARGE SEPARATION

Organic dyes also have their own drawbacks, such as a narrower absorption spectrum, and a faster charge recombination. There are two different improper recombination types in DSCs. One is the "inner-path recombination" consisting of the recombination of an electron injected into the semiconductor with the dye action before dye regeneration, which deteriorates the rate of electron injection, leading to a decrease of photocurrent and J_{sc} value. The other type of charge recombination in DSCs is “outer-path recombination”, which occurs between the injected electrons in the semiconducting oxide electrode and the oxidized electrolyte. (Figure 4.1) It strongly affects the theoretical potential difference between the oxide electrode and the electrolyte, resulting in a reduced V_{oc} [60-61]

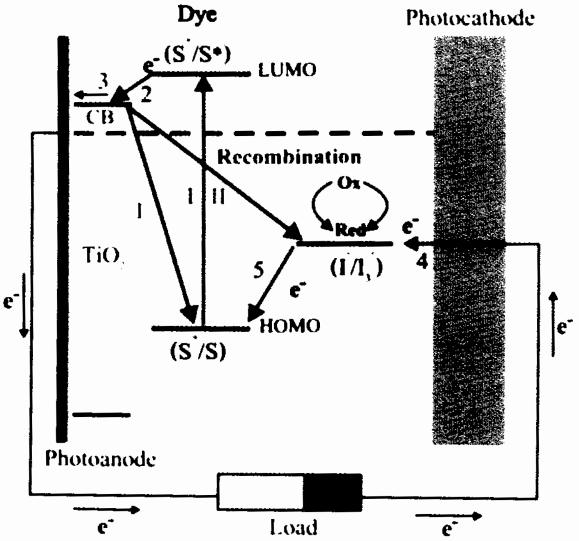

Figure 4.1 The recombination processes in DSCs

4.1 Computational details

The ground-state structures of dye molacules were performed using the density functional theory (DFT) and time-dependent DFT (TDDFT) for static (all series) and the density-functional tight-binding (DFTB) method for **CCTA** and **CFTA** molecular dynamics [62-63]. The vertical excitation energies and the electronic absorption spectra of molecule were investigated using time-dependent density functional theory (TDDFT) at B3LYP, PBE0, BHandHLYP, CAM-B3LYP, LC-ωPBE and ωB97X-D functions. We used these five different functionals in TDDFT within adiabatic approximation to evaluate the effect of different functional on predicting the absorption spectra for **CCTA** and **CFTA** series. The solvation effect was included by means of conductor-like polarizable continuum model (C-PCM) model. The solvent used in our calculations were CH_2Cl_2. The vertical excitation energies were performed using Gaussian09 program package. The optimized bidentate bridging modes of **CCTA** and **CFTA** on the $Ti_{18}O_{57}H_{42}$ surface are carries out [64]. The dye-TiO_2 systems are optimized by molecular dynamics simulation of S_0 using DFTB.

In this chapter, three series of dyes are investigated therefore the discussions are divided in to three section, first is carbazole-fluorene derivatives to form D-D-π-A system were investigated theoretically by means of quantum mechanical calculations based on the DFT [65]. The carbazole has strong absorption in the near UV region and a low redox potential. The electrochemical and spectroscopic properties of carbazole and its derivative have been extensively investigated. The 3, 6 positions of carbazole have been substituted with *tert*-butyl groups to prevent oxidative coupling reaction. In order to increase solubility property and prevent the recombination of electron from the semiconductor to the electrolyte, alkyl groups were introduced at the C-9 position of fluorene ring. The effects of increasing thiophene units for tuning the absorption spectra of the dyes were investigated. The effects of increasing different conjugation length for tuning the absorption spectra of the dyes (**CarFTPC**), (**CarFT2C**), (**CarFP2C**) and (**CarFT3C**) as shows in Figure 4.2 were investigate.

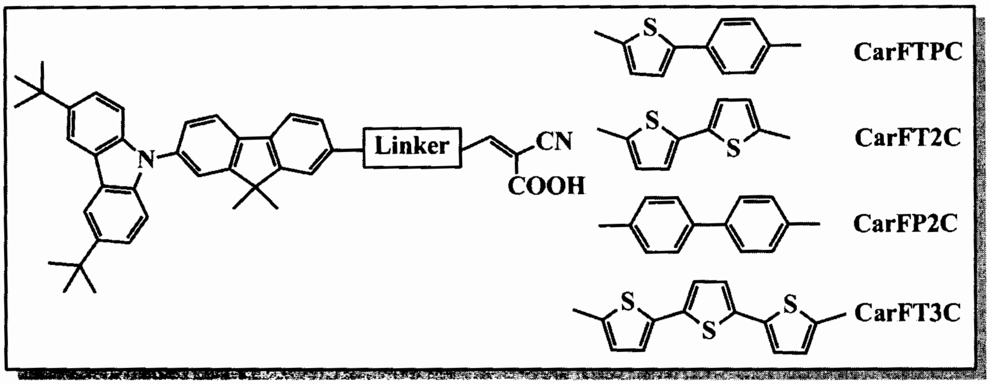

Figure 4.2 Chemical structures of the synthesized CarFTPC, CarFT2C, CarFP2C and CarFT3C dyes

4.2 Results and dicussion

4.2.1 Absorption spectra of carbazole-fluorene derivatives

To gain insight into the excited states giving rise to the absorption spectra of D-D-π-A organic dyes, TDDFT calculations were employed by TD-CAM-B3LYP/6-31G(d,p) level in CH_2Cl_2 solvent (C-PCM model). Comparison of the theoretically calculated wavelength with experimental data was performed. It is found that the calculated data have similar tendency with the experiment. The transition energies of electronic spectra, oscillator strength, configurations of the orbitals, and the calculated values of the absorption wavelength in the solvent phase of all organic dyes are shown in Table 4.1. It was found that, the λ_{max} of **CarFTPC**, **CarFP2C**, **CarFT2C** and **CarFT3C** are 413, 444, 472, and 487 nm, respectively. These results indicate that **CarFT3C** dye exhibits red-shifted compared to that of organic dyes.

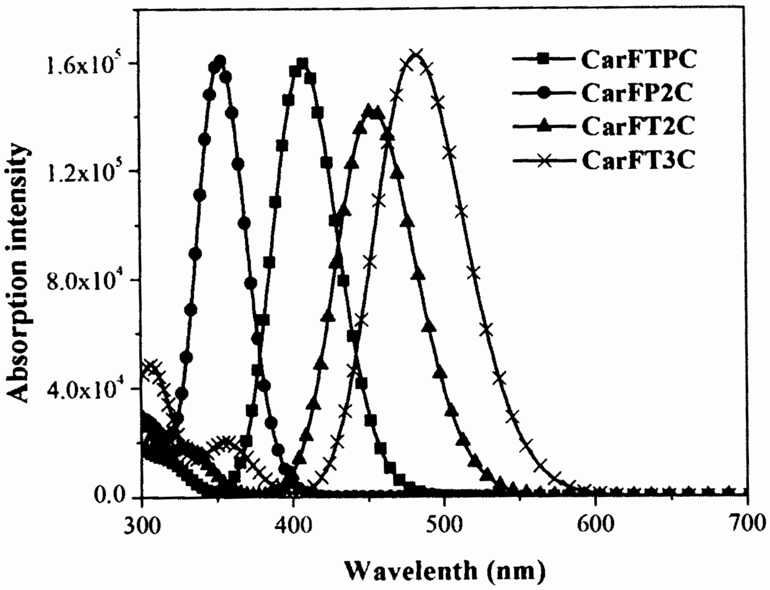

Figure 4.3 Absorption spectra of CarFTPC, CarFP2C, CaeFT2C and CarFT3C calculatet by TD-CAM-B3LYP /6-31G (d,p) level in CH_2Cl_2 solvent (C-PCM model)

Table 4.1 Calculated TDDFT (CAM-B3LYP) excitation energies for the lowest transition (eV, nm), oscillator strengths (*f*), composition in terms of molecular orbital contributions and experimental absorption maxima

Dyes	State	Composition	E (eV, nm)	*f*
CarFTPC	$S_0 \rightarrow S_1$	(-0.42) H→ L (0.48) H-1 → L (-0.18) H-3 → L	3.04, 407	2.2017
CarFP2C	$S_0 \rightarrow S_1$	(0.47) H→ L (0.34) H-1 → L	3.51, 352	2.2188
CarFT2C	$S_0 \rightarrow S_1$	(-0.46) H→ L (0.47) H-1 → L	2.73, 453	1.9595
CarFT3C	$S_0 \rightarrow S_1$	(0.53) H→ L (-0.36) H-1 → L	2.56, 482	2.2435

To estimate the photocurrent performance of these dyes, the light harvesting efficiency (LHE) needs to be as large as possible to maximize the photocurrent response. We were interested in how the π-spacer within the molecular structure affect J_{sc} values. To provides an approximation to J_{sc} following equation.

$$J_{sc} = \int \mathrm{LHE}(\lambda)\Phi_{\mathrm{inject}}\eta_{\mathrm{collect}}d\lambda$$

In this equation, LHE is the light-harvesting efficiency at a specific λ, Φ_{inject} is the electron injection efficiency, and η_{collect} is the electron collection efficiency, which is constant. According to above equation, to obtain a high value for J_{sc}, LHE and Φ_{inject} should both be as large as possible. The LHE can be calculated using this equation.

$$\mathrm{LHE} = 1-10^{-A} = 1-10^{-f}$$

where $A(f)$ is the absorption intensity (oscillator strength) of the dye, corresponding to λ_{max}.

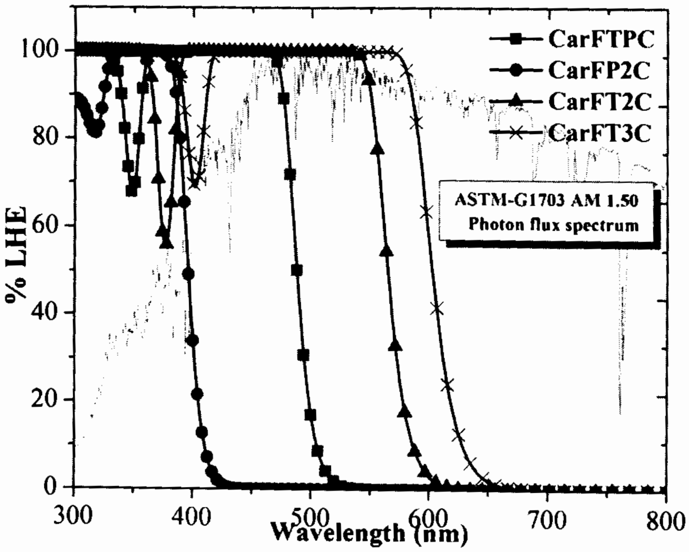

Figure 4.4 LHE of CarFTPC, CarFP2C, CarFT2C and CarFT3C calculated by TD-CAM-B3LYP /6-31G (d,p) level in CH_2Cl_2 solvent (C-PCM model)

The light harvesting efficiency (LHE) is the efficiency of dye in responding to light. The value of LHE of the dyes has to be as high as possible to maximize the photocurrent response. The LHE of **CarFTPC**, **CarFP2C**, **CarFT2C** and **CarFT3C** molecules are shown in Figure 4.3. The LHE of all dyes will give similar trend with absorption spectra. We can assume that the **CarFT3C** with three thiophene ring can improve light harvesting efficiency than other molecules.

For the second series is the conformation of target molecules as dye-sensitizers, a donor-donor-π-conjugate acceptor (D-D-π-A) organic material based on carbazole-carbazole as the donor group, with different linker unit and cyanoacrylic acid moiety as acceptor as show in Figure 4.5.

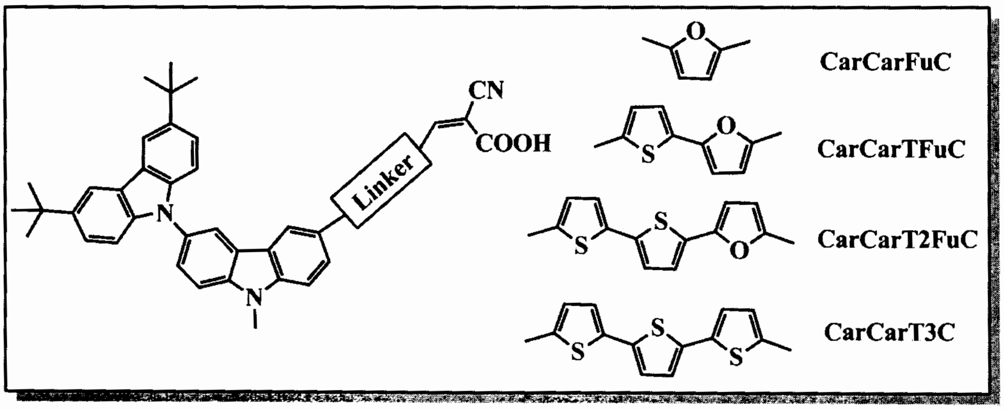

Figure 4.5 Chemical structure of the synthesized CarCarFuC, CarCarTFuC, CarCarT2FuC and CarCarT3C dyes

4.2.2 Absorption spectra of carbazole-carbazole derivatives

The absorption spectra of these molecules have been studied by TD-CAM-B3LYP/6-31G(d,p) level in CH_2Cl_2 solvent (C-PCM model). Comparison of the theoretically calculated wavelength with experimental data was performed. It is found that the calculated data have similar tendency with the experiment. The transition energies of electronic spectra, oscillator strength, configurations of the orbitals, and the calculated values of the absorption wavelength in the solvent phase of all organic dyes are shown in Table 4.2. It was found that, the λ_{max} of **CarCarFuC**,

CarCarTFuC, **CarCarT2C** and **CarCarT3C** are 413, 444, 472, and 487 nm, respectively. These results indicate that **CarCarT3C** dye exhibits red-shifted compared to that of organic dyes.

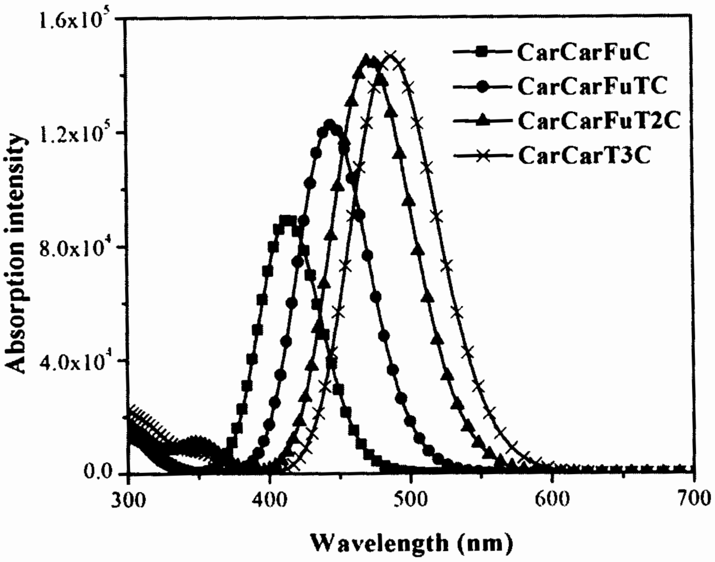

Figure 4.6 Absorption spectra of CarCarFuC, CarCTFuC, CarCarT2C and CarCarT3C calculated by TD-CAM-B3LYP /6-31G (d,p) level in CH_2Cl_2 solvent (C-PCM model)

Table 4.2 Calculated TDDFT (CAM-B3LYP) excitation energies for the lowest transition (eV, nm), oscillator strengths (*f*), composition in terms of molecular orbital contributions and experimental absorption maxima

Dyes	State	Composition	E (eV, nm)	*f*
CarCarFuC	$S_0 \rightarrow S_1$	(-0.38) H→ L (+0.54) H-1 → L	2.99, 413	1.2303
CarCarTFuC	$S_0 \rightarrow S_1$	(-0.45) H→ L (+0.46) H-1 → L	2.78, 444	1.6875
CarCarT2FuC	$S_0 \rightarrow S_1$	(-0.27) H→ L (+0.55) H-1 → L	2.62, 472	2.0006
CarCarT3C	$S_0 \rightarrow S_1$	(-0.28) H→ L (+0.55) H-1 → L	2.54, 487	2.0183

The light harvesting efficiency (LHE) is the efficiency of dye in responding to light. The value of LHE of the dyes has to be as high as possible to maximize the photocurrent response. The LHE of **CarCarFuC**, **CarCarTFuC**, **CarCarT2C** and **CarCarT3C** molecules are shown in Figure 4.6. The LHE of all dyes will give similar trend with absorption spectra. We can assume that **CarCarT3C** molecules can improve light harvesting efficiency than other dyes molecule.

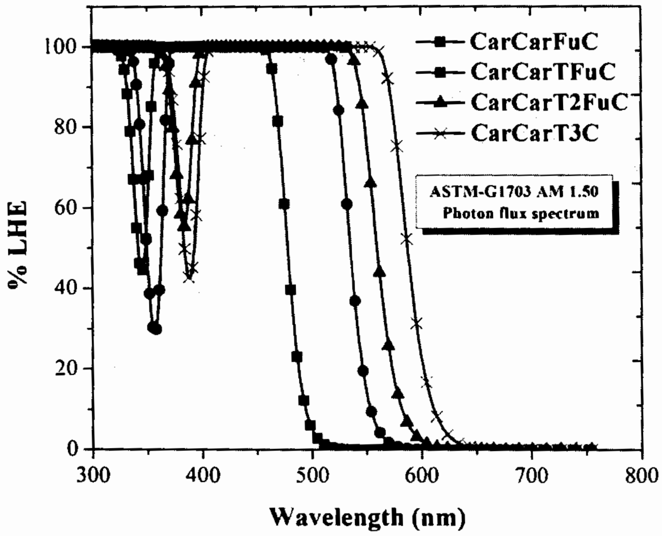

Figure 4.7 LHE of CarCarFuC, CarCarTFuC, CarCarT2C and CarCarT3C calculated by TD-CAM-B3LYP /6-31G (d,p) level in CH_2Cl_2 solvent (C-PCM model)

4.2.3 The effect of bulky-donor to charge recombination and charge separation in carbazole-cased sensitizer

Carbazole derivatives have interested in their excellent electron donating moiety in DSCs, which providing efficient charge-separation in a molecule [60-66-68], the bulky, nonplanar structure of the designed moiety may prove to be valid in solving the problem of the close π-π aggregation of the dye molecules [69]. Both 3,6-di-tert-butyl and N-dodecyl substituents assist the solubility of the dye, but they also form a hydrophobic blocking layer on the TiO_2 surface to suppress the approach of iodide/triiodide in the electrolyte to TiO_2 [70]. **CCTA** and **CFTA** (Figure

4.8) using Ndodecyl-3-(3,6-di tert-butylcarbazol-N-yl)carbazol-6-yl and 2-(3,6-di-tert butylcarbazol-N-yl)-9,9 bishexylfluoren-7-yl as donor moieties were synthesized [71].

The third series is theoretically prove that introducing carbazole as a donor group in D-π-A dyes can suppress the improper recombination, and also suppressing undesirable close π–π aggregation of the dye molecules. An extra-bulky donor could form a hydrophobic blocking layer on the TiO_2 surface to suppress the approach of iodide/triiodide in the electrolyte to TiO_2, consequently leading to an improvement of the open-circuit voltage (V_{oc}). In order to disclose the relationship among the performance, structures and the properties, the theoretical investigations of the physical properties of dye sensitizers are indispensable.

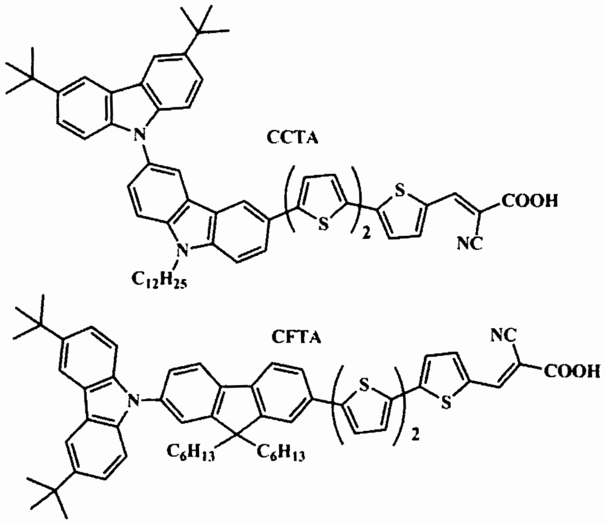

Figure 4.8 Chemical structure of the synthesized CCTA and CFTA dyes

4.2.3.1 Effect of various DFT functionals on absorption spectra

The calculated excitation energies of all analogues using B3LYP, PBE0, BHandHLYP, LC-ωPBE, CAM-B3LYP and ωB97XD functional in solvent phase are listed in Table 4.3. The amount of the Hartree-Fock exchange included in the applied functional increased in the order B3LYP (20% HF) < PBE0 (25%HF) < BHandHLYP (50%HF). The results showed that the maximal wavelength (λ_{max}) of ICT spectra was significantly red-shifted as the amount of the HF exchange decreased. For the long-range-corrected, LC-ωPBE function was significantly blue-shifted than CAM-B3LYP and ωB97XD functions. We also found that the maximal wavelength (λ_{max}) of ICT spectra is $S_0 \rightarrow S_1$ excitation which is significantly red-shifted as the amount of the HF exchange decreased for hybrid function. For the long-range-correction function, the long-range-corrected ωB97XD empirical dispersion provide the most stable and reliable results. The discrepancies between calculated and experimental excitation energies were found to be within 0.04 eV for **CCTA** and 0.08 eV for **CFTA** with ωB97XD function. The frontier molecular orbital results indicated that the intramolecular charge transfer (ICT) was occurred.

Table 4.3 Wavelength (λ_{max}) for ICT spectra of CCTA using TDDFT method during DFTB dynamics

B3LYP	PBE0	BHandHLYP	CAM-B3LYP	LC-ωPBE	ωB97X-D	Expt.
637 (1.94)	604 (2.05)	506 (2.45)	492 (2.52)	433 (2.86)	473 (2.62)	456 (2.71)

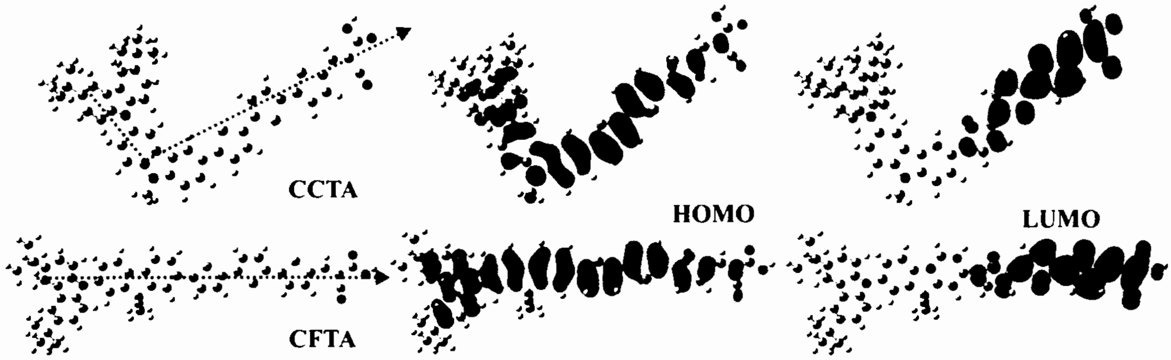

Figure 4.9 HOMO-LUMO plots of CCTA and CFTA

The optimized geometries obtained by density functional theory (DFT) B3LYP/6-31G(d,p) level of organic dye molecules are shown in Figure 4.9. They are composed of four moieties on the dye molecules; (i) "carbazole" group acting as secondary electron donor (ii) different primary electron donor groups of "carbazole" and “fluorene”, forming **CCTA** and **CFTA** dyes, respectively (iii) “thiophene” group acting as linker (iv) “Cyanoacylic acid” acting as electron acceptor. **CFTA** dye, with donor carbazole-fluorine moiety, performs a straight structure (linear). Replacing carbazole-fluorene by carbazole-carbazole donor resulted in V-shape conformation which can prevent the aggregation of dye molecule. The frontier molecular orbital properties were obtained to examine the HOMO and the LUMO due to the relative ordering of the HOMO and LUMO provides a reasonable qualitative indication of the charge transfer properties. The electron density on HOMO is delocalized on donor group and the electron density on LUMO is delocalized on acceptor group, the HOMO to LUMO transition that corresponding to ICT from donor group to acceptor group.

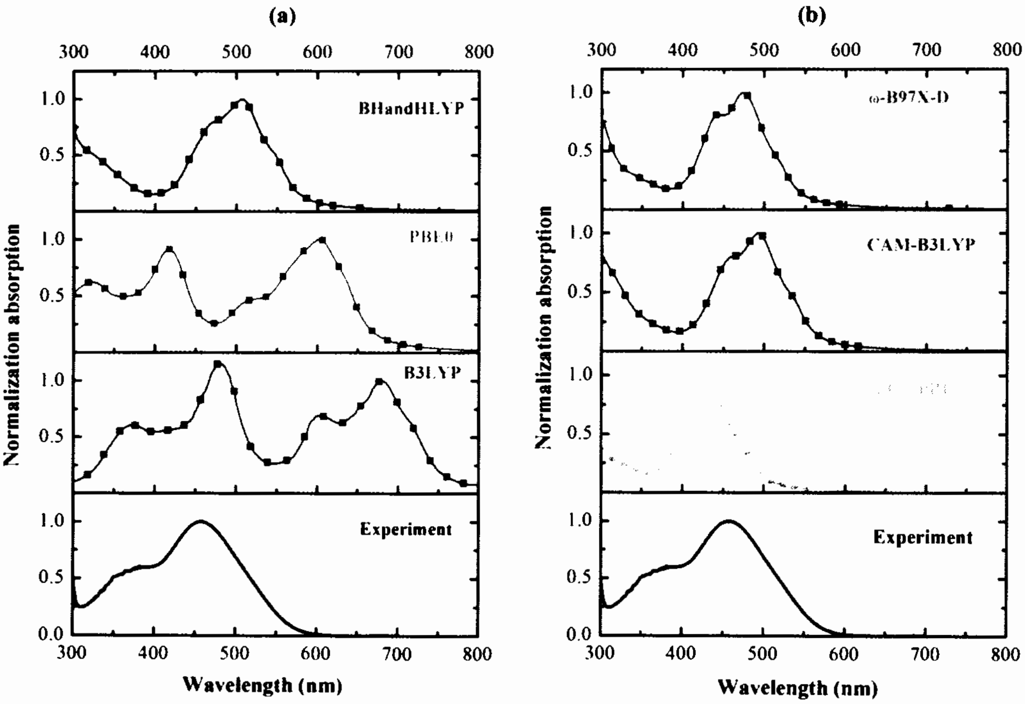

Figure 4.10 Absorption spectra of CCTA during DFTB dynamics

Figure 4.10 illustrated absorption spectra of **CCTA** during DFTB dynamics. The trajectory sampling was then performed from the available NVE trajectories, drawing independently selected sets of 20 geometries for subsequent TDDFT single point excitation energy calculations. This data suggests that 20 point-sampling produces converge UV/vis absorption spectrum. The results showed that the maximal wavelength (λ_{max}) of ICT spectra show red-shifted than long range corrected function. It is shown that functionals with an increased amount of exact exchange provide the best estimation of the optical properties. While B3LYP fails to predict the excitation energies due to its intrinsic problems in describing charge transfer (CT) states, the long-range corrected ωB97XD functionals deliver good agreement with the experimental UV/vis absorption spectrum.

4.2.3.2 Adsorption of organic sensitizers on the TiO_2 cluster

To further study the structure of the dye sensitizer-semiconductor interface and the process of electron transfer from the dye sensitizer to semiconductor surface, we modeled the **CCTA-** and **CFTA-TiO_2** adsorption complexes (**Dyes-TiO_2**) as shown in Figure 4.11. As shown, the optimized adsorbed-dye structures are positioned almost perpendicular to the TiO_2 surface, linked by two O-Ti bonds in a bidentate-bridging adsorption mode. The calculated E_{ads} values for **Dyes-TiO_2** are -20.81 kcal/mol for **CCTA-TiO_2** which is slightly stronger than -17.84 kcal/mol of **CFTA-TiO_2**. We can predict that electrons injection efficiency from **CCTA** toward **TiO_2** surface would be better than **CFTA**.

Figure 4.11 Optimized bidentate bridging mode of CCTA and CFTA on the $(TiO)_{38}$. Molecular dynamics simulation of S_0 using DFTB at 298 K, dt = 0.7254 fs with NVT and NVE ensemble

Additionally, a bulky electron-donating group in **CCTA** can suppress dye aggregation as illustrated in Figure 4.12. In view of molecular geometry, unfavorable aggregation of dyes should be prohibited to achieve high conversion efficiency. The distances between each **CFTA** on TiO_2 surface are significantly closer than that of **CCTA**. Figure 4.12 show the more possible π-π aggregation phenomena in **CFTA**-TiO_2 compared with **CCTA**-TiO_2 system resulted in self-quenching and reduction of electron injection to TiO_2. These results corresponding to experimental observation in J_{sc} value of **CFTA** (8.99 $mAcm^{-2}$) is significantly lower than **CCTA** (11.31 $mAcm^{-2}$). Furthermore, π-π aggregation leads to decrease of instability due to the formation of excited triplet states and unstable radicals [69]. Stability of dyes in its excited and ionized states is important for efficiency and durability.

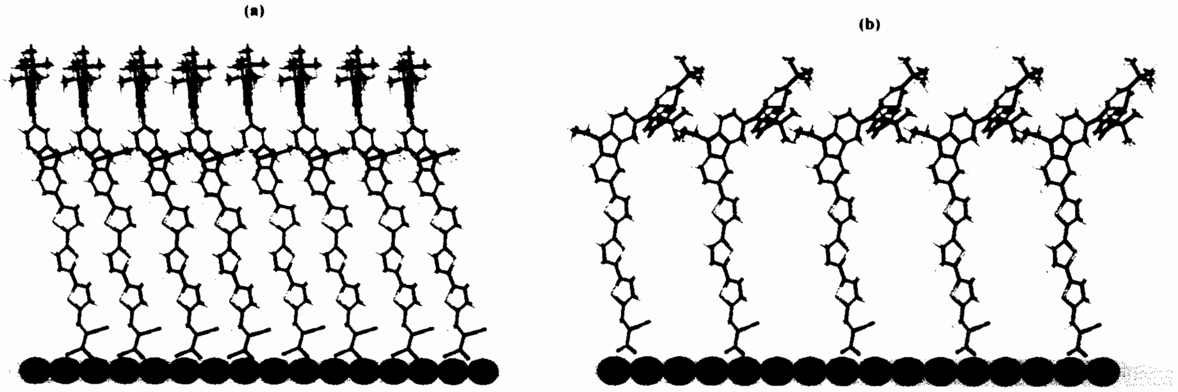

Figure 4.12 The possible π-π aggregation phenomena in CFTA-TiO_2 (a) compared with CCTA-TiO_2 (b)

Table 4.4 Photovoltaic parameters of DSCs with carbazole dye and N719 sensitizers

Dyes	J_{sc} [mA cm^{-2}]	V_{oc} [V]	FF	PCE [%]
CCTA	11.31	0.71	0.71	5.69
CFTA	8.99	0.62	0.66	3.64
N719	11.63	0.71	0.72	5.92

Typically, the recombination strongly depends on the molecular structure of the dyes molecule and their arrangement on the surface of the oxide electrodes. The geometry optimization by means of computational calculations showed that the **CCTA** dye with donor carbazole-carbazole induces a V-shape oriented dye geometry when adsorb on TiO_2 surface, while the **CFTA** dye donor carbazole-fluorene affect to a linear oriented dye geometry when adsorb on TiO_2 surface. We found that the V-shape structure of **CCTA** dye can prevent the recombination between oxidized electrolyte and injected electron on semiconductor surface, leading to increase V_{oc} value from 0.62 to 0.71 V for **CFTA** and **CCTA** respectively.

To study the electron injection mechanism of selected dyes at the interface of the dye-TiO_2 surface, the ten lowest vertical transitions are simulated using TD-ωB97XD/6-31G(d). The calculated excitation energies for the peak having the highest oscillator strength are illustrated in Figure 4.13 and Table 4.5. The results show that the strongest transition in our dyes is characterized as a linear combination of The Kohn–Sham orbitals, which are most relevant to these transitions, are shown in Figure 8(a) and (b). Both **CFTA-TiO$_2$** and **CCTA-TiO$_2$** show similar transitions, only **CCTA-TiO$_2$** system has been discussed. The highest oscillator strength of 2.6631 for **CCTA** is assigned as the linear combination of 0.44(H → L+23) - 0.34 (H-1 → L+23) - 0.16(H-4 → L+23) - 0.10(H → L+22). These orbitals, together with TDDFT functional, show that the transition with large oscillator strength characterized as the transition from the orbitals localized in the donor–π-spacer (D-π) unit to the orbitals delocalized over the acceptor (A) unit of dyes and the $(TiO_2)_{38}$ cluster. The former orbitals are similar to the HOMOs of dyes and the latter orbitals correspond to the interacting orbitals between the LUMOs of dyes and the conduction band of TiO_2. This means that the electron excitation of this system directly induces the electron injection from dye into TiO_2 surface.

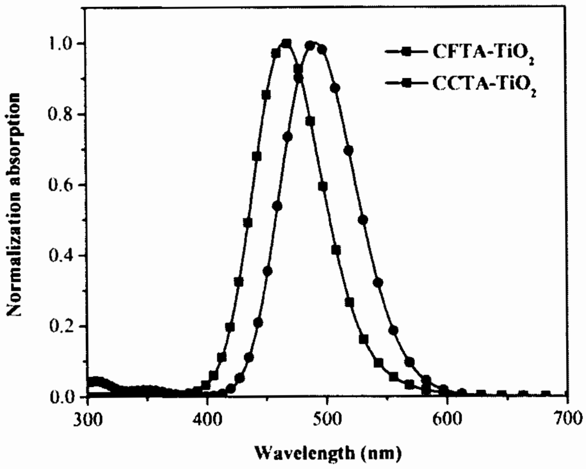

Figure 4.13 Absorption spectra of CFTATiO₂ and CCTA-TiO₂ calculated by TD-ωB97XD/6-31G(d) level in gas phase

Table 4.5 The electronic properties, absorption wavelength and oscillator strength (*f*) obtained by TD-ωB97XD/6-31G(d) on DFTB geometry

Complexes	Electronic transitions	λ_{max} (nm/eV)	*f*	Assignment; H=HOMO, L=LUMO, etc.
$CFTA-TiO_2$	$S_0 \rightarrow S_5$	466 (2.65)	2.7580	(0.36) H → L+5 (0.31) H-1 → L+5 (0.68) H-3 → L+5 (0.11) H → L+6
$CCTA-TiO_2$	$S_0 \rightarrow S_1$	491 (2.52)	2.6631	(0.44) H → L+23 (-0.34) H-1 → L+23 (-0.16) H-4 → L+23 (-0.10) H → L+22

4.2.3.3 Electronic coupling between dye and TiO_2 surface of **CCTA** and **CFTA** dyes.

The rate of electron injection from the dye to TiO_2, a critical step in the generation of photocurrent, is related to the magnitude of the dye-semiconductor electronic coupling. To determine the extent to which the dye-semiconductor electronic coupling differs between **CCTA-TiO_2** and **CFTA-TiO_2** DSCs, a series of constrained DFT configuration interaction (CDFT-CI) calculations were performed on a collection of uncorrelated snapshots from the dye-semiconductor molecular dynamics trajectories discussed in Section 4.2.3.2.

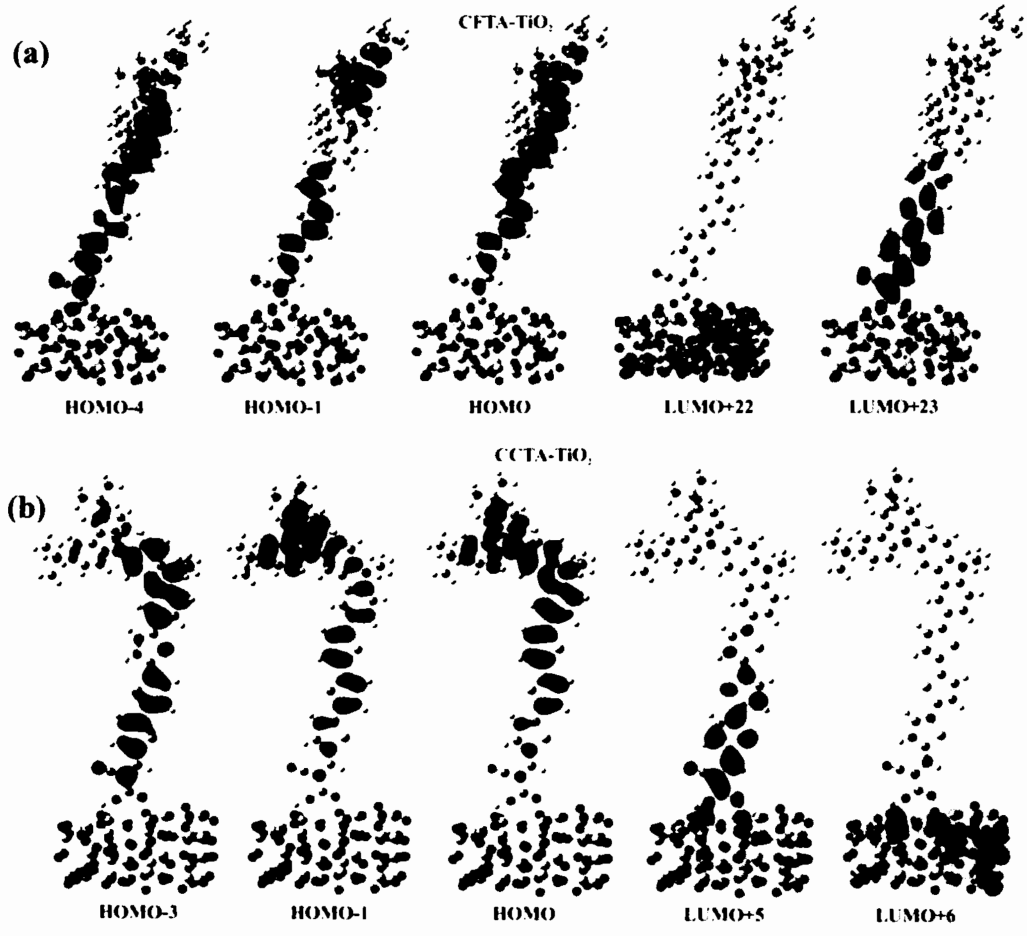

Figure 4.14 MOs relevant to the transition from S_0 to S_1 of (a) CFTA (b) CCTA organic sensitizer adsorbed on the $(TiO_2)_{38}$ in gas phase calculated by TD-ωB97XD/6-31G(d) on DFTB geometry

Two types of electronic coupling are expected to influence the overall PCE. The first is the coupling for charge separation V_{CS} between the dye-localized S_1 excited state and the lowest charge-transfer (CT) state mediating charge injection into TiO_2. The second is the coupling for charge recombination V_{CR} between the CT state and the ground state, which represents loss of the excitation energy through nonradioactive recombination. V_{CS} and V_{CR} were obtained through CDFT-CI calculations in the 3-state CI basis [72-74]. Here, the S_0 state was treated in CDFT by constraining the net charge and spin on the dye and TiO_2 fragments to zero; this procedure raises the energy slightly above that of the fully optimized ground state but yields a diabatic electronic state better suited to the CDFT electronic coupling calculation. To obtain the S_1 state, a constrained ΔSCF approach was applied using the same charge/spin constraints as the S_0 state but adding an orbital occupation constraint to capture the electronic excitation on the dye [75-76]. The CT state was obtained by constraining a net charge difference of two electrons between the dye and TiO_2, corresponding to a hole on the dye and an excess electron on the semiconductor.

CDFT-CI electronic couplings for CR and CS were computed for **CCTA-TiO$_2$** and **CFTA-TiO$_2$** geometries sampled from DFTB molecular dynamics (192 snapshots and 129 snapshots, respectively) and are collected in Figure 4.15. These couplings are not expected to be quantitatively accurate enough for rate predictions but are nevertheless valuable for comparing the relative strength of coupling for the cases of **CCTA** and **CFTA**. Interestingly, the distribution of couplings for CR is significantly more Gaussian for both DSCs than the distribution of couplings for CS. In particular, for both DSCs the coupling for CR fluctuates around a value in the hundreds of meV while the coupling for CS persists in the vicinity of 1 meV, with occasional fluctuations that strengthen the coupling by up to an order of magnitude.

The distributions in Figure 4.15 (a) and (c) demonstrate that **CCTA-TiO$_2$** achieves a smaller coupling for CR than **CFTA-TiO$_2$**, while Figure 4.15 (b) and (d) reveal that the typical coupling for CS is also smaller for **CCTA-TiO$_2$** than for **CFTA-TiO$_2$**. The smaller CR rate for **CCTA-TiO$_2$** suggests that a smaller fraction of generated electron-hole pairs will recombine before doing any useful work. This interpretation is consistent with the experimental finding that the **CCTA** device achieves a higher PCE than the **CFTA** device. While the CS rate is also smaller for **CCTA-TiO$_2$** than for **CFTA-TiO$_2$**, the difference is negligible (only a few meV) compared to the difference in CR rates (hundreds of meV). Furthermore, the couplings reported here for CR are 2-3 orders of magnitude larger than couplings for CS, suggesting that the CR rate plays the greater role in determining the overall charge separation efficiency than the CS rate.

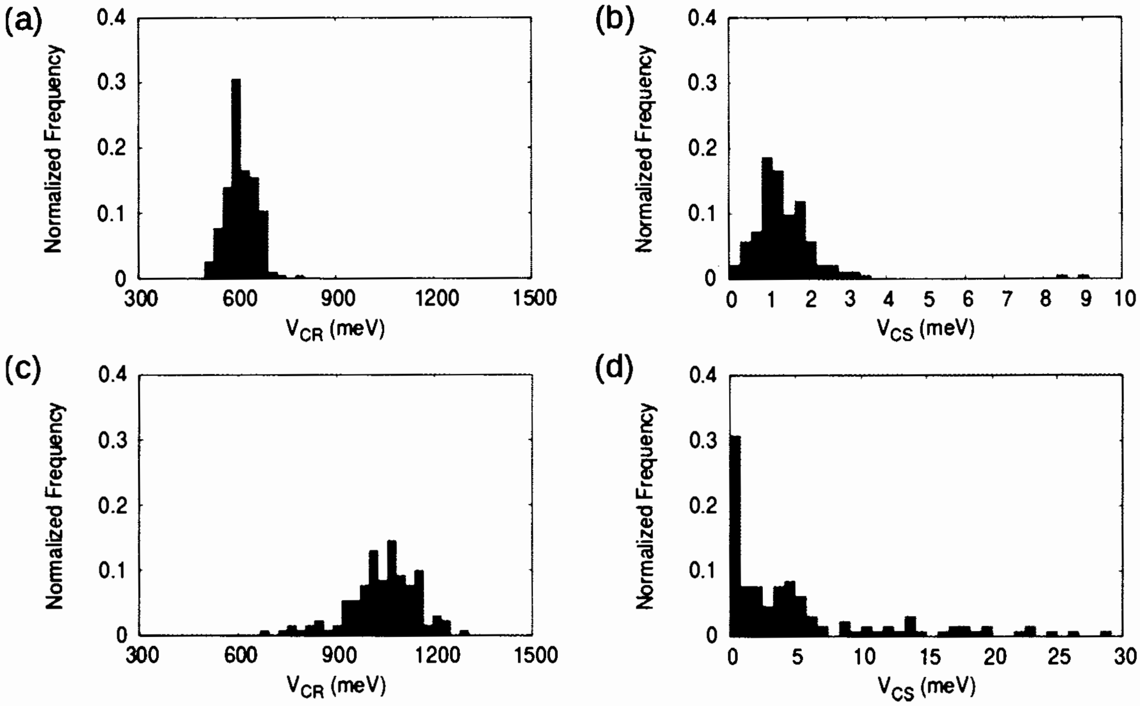

Figure 4.15 Observed distribution of electronic couplings (in meV) for charge recombination V_{CR} and charge separation V_{CS} in CCTA-TiO$_2$ (a,b) and CFTA-TiO$_2$ (c,d). Distributions are presented over geometries sample from *NVE* molecular dynamics simulations

4.3 Conclusion

For a series of different linker group on absorption properties of carbazole-fluorene and carbazole-carbazole derivatives to form D-D-π-A system, which extended conjugation linker by increase thiophene, phenyl and furan ring. The result show than **CarFT3C** and **CarCarT3C** with large conjugation length exhibits red-shifted compared to that of organic dyes in this series. In addition, we study on effect of bulky-donor to charge recombination and charge separation in **CFTA (CarFT3C)** and **CCTA (CarCarT3C)** in dye-semiconductor electronic coupling differs between **CCTA-TiO_2** and **CFTA-TiO_2** by constrained DFT configuration interaction (CDFT-CI) calculations. This interpretation is consistent with the experimental finding that the **CCTA** device achieves a higher PCE than the **CFTA** device while the CS rate is also smaller for **CCTA-TiO_2** than for **CFTA-TiO_2**, the difference is negligible compared to the difference in CR rates. Furthermore, the couplings reported here for CR are 2-3 orders of magnitude larger than couplings for CS, suggesting that the CR rate plays the greater role in determining the overall charge separation efficiency than the CS rate.

CHAPTER 5

THE EFFECT OF AUXILIARY ACCEPTOR ON DYE SENSITIZED SOLAR CELLS

Metal-free organic molecular dyes as alternative sensitizers have also attracted research attention due to a number of potential advantages ranging from the control of structure organic compounds bring, to the access to low cost materials and environmentally benign resources, high light absorptivity, and simple synthesis. Organic dyes have been evaluated as sensitizers and the highest efficiency cells have achieved comparable PCEs (> 10%) as those with metal-based dyes [77]. Arylamine-based organic dyes still present some challenges including lack of absorption in the near IR region and dye aggregation on the TiO_2 film. Further red shifted absorption spectra can be obtained by adding conjugated bridge between the donor and acceptor units to form a D-π-A-π-A framework owing to the expended conjugation [78]. However, slightly lower efficiency, metal-free organic dyes drew great attention due to their lower cost, easy purification and more flexibility in molecular design. Framework of metal-free dyes include D-π-A (D, donor; π-conjugated; A, acceptor), D-π-A′-π-A, (D)2-π-A, and D-π-(A)2. D-π-A′-π-A type sensitizers with incorporation of an additional electron-withdrawing segment A′ in the conjugated bridge, such as benzothiadiazole, benzoxadiazole, benzothiazole, quinoxaline, isoindigo, thiazole, and fluoro-substituted phenyl, received considerable studies [77]. Isoindigo has a strong electron-withdrawing property due to the two lactam rings. It has been widely used in the dye industry and can be obtained easily from various natural sources. The perfect planar π-conjugated structure and the strong-withdrawing effect make it ideal monomer for synthesis of D-A low band gap conjugated polymer for organic solar cell applications. Recently, the photovoltaic performance of isoindigo-based polymer solar cells has been reported and the best efficiency of 6.3% has been reached [27-28].

In this chapter, two of dyes containing auxiliary are discussed, TPA-dyes with/without sets isoindigo as auxiliary acceptor and indoline dyes containing different auxiliary acceptor (EDOT, BT and BTD).

5.1 Computational details

The ground-state structures of organic dye molecules are fully optimized using DFT at the B3LYP hybrid functional with 6-31G(d,p) basis set. The excitation energies and the electronic absorption spectra of organic dye molecules are investigated using TDDFT at the CAM-B3LYP functional, with the same basis set as in the ground-state calculations. The solvation effect is included by means of C-PCM. The solvent used in our calculations and experiment is CH_2Cl_2. The absorption spectra of all organic sensitizers and the contribution of molecular orbitals in the electronic transitions are simulated using the GaussSum program version 3.0. The results are compared with the experimental date. All calculations are performed using the Gaussian09 program package. The electron-injection characteristics from dye to the TiO_2 (101) anatase surface are carried out. The dye-$(TiO_2)_{38}$ systems are fully optimized by the PBE functional with the DNP basis set. The core electron is treated with DFT with DSPPs by DMol^3 code in Materials Studio 5.5. The energy convergence tolerance is set to 2×10^{-5} Hartree, the maximum force 0.004 Hartree Å^{-1}, and the maximum displacement 0.005 Å. The optical properties of the relaxed complex are then computed with the TD-CAMB3LYP/6-31G(d) method. The adsorption energies (E_{ads}) of dyes on the $(TiO_2)_{38}$ clusters can be obtained using the following expression:

$$E_{ads} = E_{dye+TiO_2} - [E_{dye} + E_{TiO_2}]$$

Where $E_{dye+TiO_2}$ is the total energy of the dye@$(TiO_2)_{38}$ system, and E_{dye} and E_{TiO_2} are the energies of the dye and $(TiO_2)_{38}$ cluster, respectively.

Theoretical studies on physical and chemical properties of dye are important to understand the relationship between the structure, properties and performance in order to design and synthesize new molecules for this purpose. In this chapter we study in D-π-A-π-A (**TIDT** and **TIDP**), and D-π-A (**TTPC** and **TT2C**) organic sensitizers. For **TIDT** and **TIDP**, TPA as the donor, thiophene as the linker, isoindigo as an auxiliary electron withdrawing unit, different linker is thiophene ring for **TIDT**, phenyl ring for **TIDP**, and a cyanoacrylic acid moiety acting as the anchoring group compared to TPA-dyes without (**TTPC** and **TT2C**) (Figure 5.1).

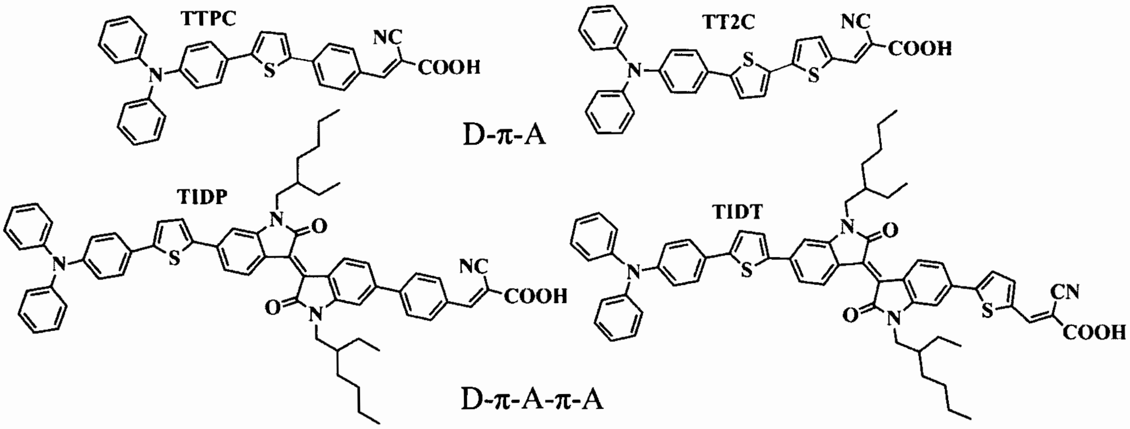

Figure 5.1 Sketch map of TPA-dyes with/without sets isoindigo as auxiliary acceptor (TTPC, TT2C, TIDP and TIDT)

5.2 Results and discussion

5.2.1 TPA-dyes with and without isoindigo as auxiliary acceptor

5.2.1.1 Ground-state geometries of organic sensitizers

The optimized geometries obtained by DFT at B3LYP/6-31G(d,p) level of organic dye molecules and selected important inter-ring distance and dihedral angle parameters shown in Table 5.1. The bond lengths of all important inter-ring bonds are in the range of 1.38 to 1.46 Å. The dihedral angles between the donor unit and the linker are in the range of 22-13° which the twisted structure in donor part of these dyes resulted in preventing dye aggregation. In the acceptor part, the dihedral angles between linker and anchoring group are coplanar in the range of 0.39° to 1.01°.

Moreover, we also found that the dihedral angles between the isoindigo auxiliary acceptor with different linker which phenyl ring for **TIDP** and thiophene ring for **TIDT** are calculated to be -34.16° and 21.81° respectively, **TIDP** show significantly larger than **TIDT**. Therefore the electron from the donor can efficiently delocalize to the acceptor moiety, as a result transferring to the conduction band (CB) of semiconductor.

Table 5.1 The selected important inter-ring distances (*r*, Å) and dihedral angles (*ϕ*, °) calculated by B3LYP/6-31G(d,p) calculations

Dyes	Dihedral angle (*ϕ*) and inter-ring distance (*r*)				
	TPA- T	**T - L**	**T-ID**	**ID-L**	**L-C**
TTPC	22.21 (1.46)	-11.52 (1.45)	-	-	0.39 (1.44)
TT2C	23.62 (1.46)	-6.02 (1.43)	-	-	0.41 (1.42)
TIDP	23.13 (1.46)	-	18.77 (1.45)	-34.16 (1.38)	0.34 (1.44)
TIDT	22.04 (1.46)	-	15.74 (1.45)	21.81 (1.46)	-1.01 (1.42)

5.2.1.2 Electronic structures of organic sensitizers

To gain insight into the electronic structures, frontier molecular orbital were obtained to examine the highest occupied molecular orbital (HOMO) and the lowest unoccupied molecular orbital (LUMO) due to the relative ordering of the HOMO and LUMO providing a reasonable qualitative indication of the excitation properties. The molecular orbital surfaces of **TTPC**, **TT2C**, **TIDP** and **TIDT** are shown in Figure 5.2 and the density of state (DOS) are presented in Table 5.2. In all dye, the electron density on HOMO is delocalized on donor group and the electron density on LUMO is delocalized on acceptor group, the HOMO to LUMO transition that corresponding mixed transition between ICT from donor group to acceptor group. Moreover, suitable energy level and location of HOMO and LUMO orbitals of the dye are required to match the I^-/I_3^- redox potential and conduction band level of the TiO_2 semiconductor. The calculated molecular orbital energies of **TTPC**, **TT2C**, **TIDP** and **TIDT** were computed by using B3LYP/6-31G(d,p) the CB of TiO_2 as shown in Figure 5.3. The results were found that the HOMO energy levels of **TTPC**, **TT2C**, **TIDP** and **TIDT** are -5.12, -5.05, -4.99, and -5.00 eV respectively; the LUMO energy levels are -2.73, -2.71, -3.09 and -3.12 eV, respectively. We found that, for isoindigo auxiliary acceptor the LUMO is lying closer to the conduction band of TiO_2 compared to that of others leading to the excited electrons are then efficiently injected into semiconductor electrode. Whereas the HOMO energy all dye are lying above the redox couple of the electrolyte which is the most suitable for donation of electrons from the I^-/I_3^- redox couple in the electrolyte solution.

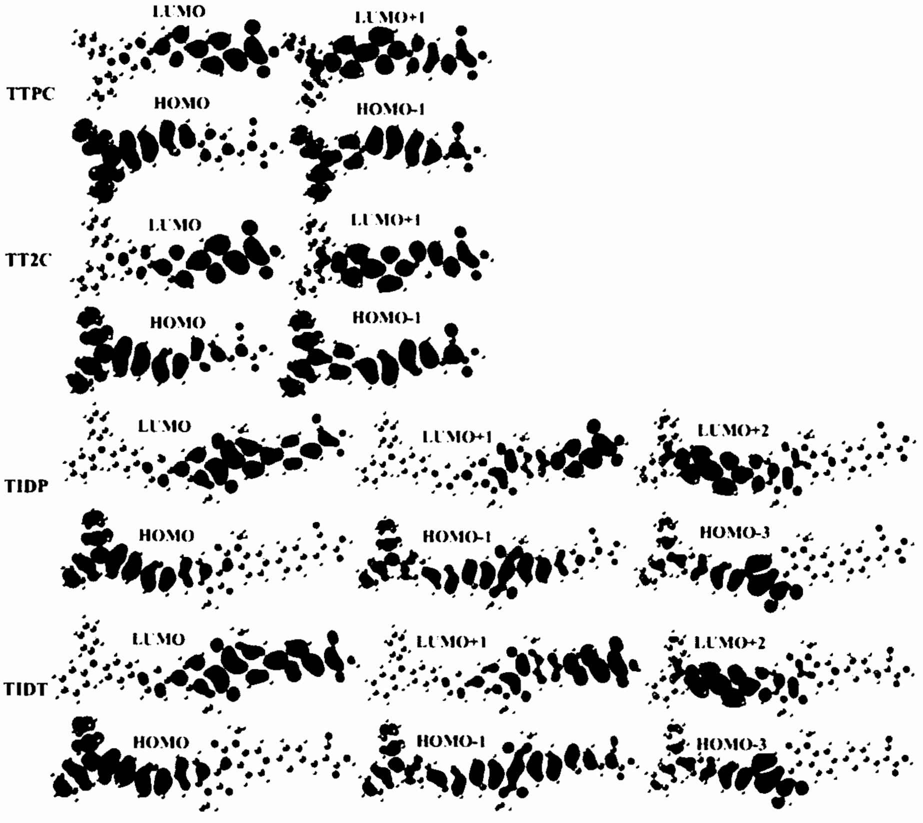

Figure 5.2 The molecular orbital surface at the ground state and first excited state when transition occurs

Table 5.2 The energies and percentage composition of frontier molecular orbitals

Dyes	Molecular orbitals	Percentage composition				
		TPA	Thiophene	Auxiliary acceptor	Linker	Acceptor
TTPC	LUMO	5	46	-	-	49
	HOMO	76	22	-	-	2
TT2C	LUMO	5	52	-	-	42
	HOMO	72	24	-	-	4
TIDP	LUMO	1	5	72	10	12
	HOMO	70	18	12	0	0
TIDT	LUMO	1	4	67	13	14
	HOMO	69	18	12	1	0

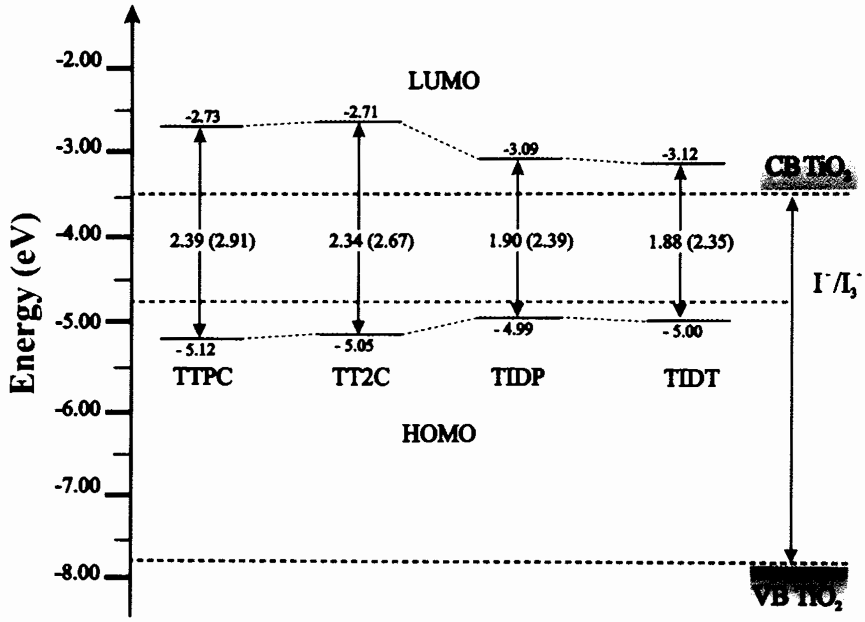

Figure 5.3 Molecular orbital energy level diagrams of the dyes, TiO_2 conduction band, and redox couple of I^-/I_3^- electrolyte

5.2.1.3 Absorption spectra of organic sensitizers

The absorption spectra of these molecules have been studied by TD-CAM-B3LYP/6-31G(d,p) level. The transition energies of electronic spectra, oscillator strength, configurations of the orbital, and the calculated values of the absorption wavelength of **TTPC**, **TT2C**, **TIDP** and **TIDT** are listed in Table 5.3. The UV/vis absorption spectra of **TTPC**, **TT2C**, **TIDP** and **TIDT** are shown in Figure 5.4. It was found that, the λ_{max} of **TTPC**, **TT2C**, **TIDP** and **TIDT** are 425, 463, 527 and 542 nm, respectively. These results indicate that **TIDP** and **TIDT** dye exhibits red-shifted compared to that of organic dyes. The absorption spectra of the auxiliary acceptors of **TIDP** and **TIDT** as D-π-A-π-A system play exactly different roles in absorption and intramolecular charge transfer compared D-π-A system. Moreover, the isoindigo-based sensitizers can result in broader spectral range near IR region and beneficial to light-harvesting for higher electricity conversion efficiency.

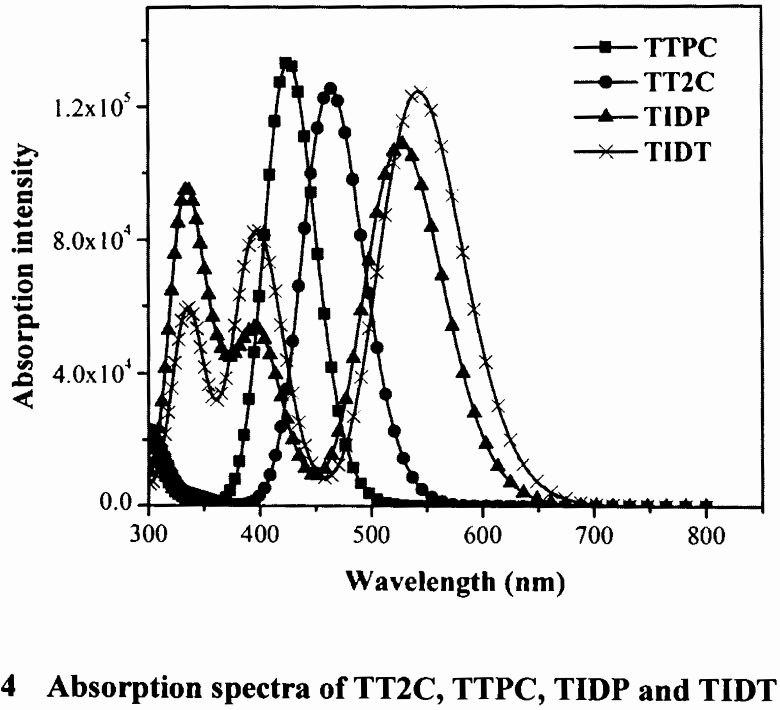

Figure 5.4 Absorption spectra of TT2C, TTPC, TIDP and TIDT calculated by TD-CAM-B3LYP /6-31G (d,p) level in CH_2Cl_2 solvent (C-PCM model)

Table 5.3 Calculated TDDFT (CAM-B3LYP) excitation energies for the lowest transition (eV, nm), oscillator strengths (*f*), composition in terms of molecular orbital contributions and experimental absorption maxima

Dyes	State	Composition	E (eV, nm)	*f*	Expt. (eV, nm)
TTPC	$S_0 \rightarrow S_1$	(0.57) H → L (-0.32) H-1 → L (0.20) H-1 → L+1	2.91, 425	1.8432	*N.A.*
TT2C	$S_0 \rightarrow S_1$	(0.57) H → L (0.36) H-1 → L (0.14) H-1 → L+1	2.67, 463	1.7298	*N.A.*
	$S_0 \rightarrow S_1$	(-0.45) H → L (0.47) H-1→ L	2.35, 527	1.4997	570
TIDP	$S_0 \rightarrow S_6$	(0.48) H → L+2 (-0.30) H→ L	3.75, 330	0.7714	
	$S_0 \rightarrow S_3$	(0.46) H-3 → L (0.33) H→ L (0.25) H-1→ L	3.11, 398	0.6803	
	$S_0 \rightarrow S_1$	(-0.43) H → L (0.48) H-1→ L (-0.13) H → L+1	2.28, 542	1.7182	584
TIDT	$S_0 \rightarrow S_3$	(0.45) H-3 → L (0.34) H→ L (0.23) H-1 → L	3.06, 404	0.6906	
	$S_0 \rightarrow S_6$	(0.43) H → L+2 (-0.26) H→ L (0.23) H → L+1	3.68, 336	0.6793	

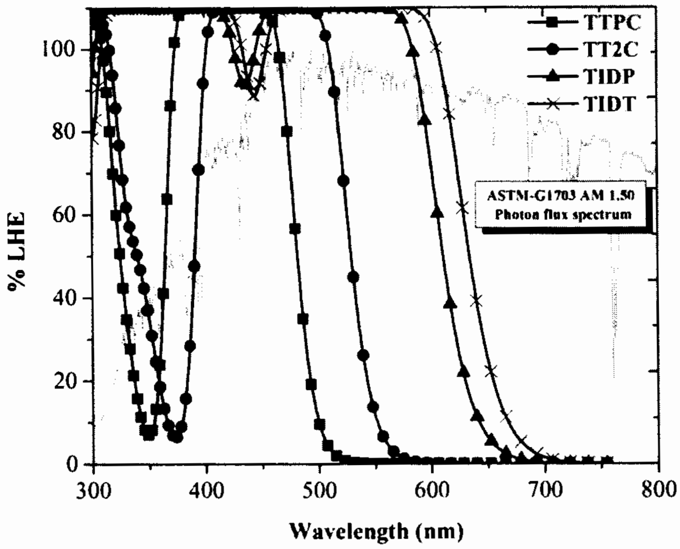

Figure 5.5 LHE of TTPC, TT2C, TIDP and TIDT calculated by TD-CAM-B3LYP /6-31G (d,p) level in CH_2Cl_2 solvent (C-PCM model)

To estimate the photocurrent performance of these dyes, the LHE needs to be as large as possible to maximize the photocurrent response. We were interested in how the auxiliary acceptor and π-spacer within the molecular structure affect J_{sc} values. To provides an approximation to J_{sc} following equation.

$$J_{sc} = \int \mathrm{LHE}(\lambda)\Phi_{\mathrm{inject}}\eta_{\mathrm{collect}}d\lambda$$

In this equation, LHE is the light-harvesting efficiency at a specific λ, Φ_{inject} is the electron injection efficiency, and $\eta_{collect}$ is the electron collection efficiency, which is constant. According to equation, to obtain a high value for J_{sc}, LHE and Φ_{inject} should both be as large as possible. The LHE can be calculated using this equation.

$$\mathrm{LHE} = 1-10^{-A} = 1-10^{-f}$$

where *A(f)* is the absorption intensity (oscillator strength) of the dye, corresponding to λ_{max}.

The LHE is the efficiency of dye in responding to light. The value of LHE of the dyes has to be as high as possible to maximize the photocurrent response. The LHE of **TTPC**, **TT2C**, **TIDP** and **TIDT** molecules are shown in Figure 5.5. The LHE of all dyes will give similar trend with absorption spectra. We can assume that the auxiliary acceptors of **TIDP** and **TIDT** as D-π-A-π-A system can improve light harvesting efficiency better than **TTPC**, **TT2C** as D-π-A system.

In general, the adsorption of a dye with carboxylic acid is possible by either physisorption or chemisorption. In the case of chemisorption, there are some possibilities in terms of bonding to the surface such as via a monodentate ester, bidentate chelating, or bidentate bridging, etc. It has been reported in many experimental studies, such as ATR-FTIR, that the terminal carboxylic acid usually adsorbs on the TiO_2 surface via bidentate bridging in the prototype system. Therefore, only chemisorption via bidentate bridging was investigated in the present study.

The electronic spectra of **TIDP** and **TIDT** on TiO_2 cluster are shown in Table 5.4. The maximum absorption peaks for **TIDP** and **TIDT** are 532 and 565 nm respectively. Compared with the solution absorption, the absorption bands of the dyes on the TiO_2 surface are slightly red-shifted by 5 and 23 nm, respectively. Generally, the sensitizers have a tendency to aggregate at solid-liquid interface when they are adsorbed onto the TiO_2 surface.

To study the electron injection mechanism of selected dyes in the interface of dye-TiO_2 surface, the ten lowest vertical transitions were simulated using TD-CAM-B3LYP/6-31G(d). The results show that the strongest transition in our dyes is characterized as the linear combination of some configurations. The Kohn-Sham orbitals, which are most relevant to these transitions, are shown in Figure 5.6. The highest oscillator strength of 1.7219 for **TIDP** is assigned as the linear combination of 0.23(H-1→L+10) + 0.24(H→L+10) + 0.21 (H-1→L+20) -0.22 (H→L+20) -0.12 (H-1→L+23) and the highest oscillator strength of 2.0546 for **TIDT** is assigned as the linear combination of -0.36(H-1→L+4) + 0.39(H→L+4) + 0.17(H-1→L+6) -0.19(H→L+6). These orbitals, together with TDDFT functional, show that the transition with large oscillator strength is characterized as the transition from the orbitals localized in the donor-π-spacer (D-π) unit to the orbitals delocalized over the acceptor (A) unit of dyes and the $(TiO_2)_{38}$ cluster. The former orbitals are similar to HOMOs of dyes and the latter orbitals correspond to the interacting orbitals between the LUMOs of dyes and the conduction band of TiO_2. This means that the electron excitation of this system directly induces the electron injection from dye into TiO_2 surface. This is the origin of the high photoelectric conversion efficiency of this system. Note that the latter orbitals are embedded in the conduction band of TiO_2 and then the injected electron is transferred to the conduction bands of TiO_2.

Table 5.4 The electronic properties, absorption wavelength and oscillator strength (f) obtained by TDDFT at the CAM-B3LYP/6-31G (d)

Complexes	Electronic transitions	λ_{max} (nm/eV)	f	Assignment; H=HOMO, L=LUMO, etc.
TIDP-TiO$_2$	$S_0 \rightarrow S_1$	532 (2.32)	1.7219	(0.23) H-1 → L+10 (0.24) H → L+10 (0.21) H-1 → L+20 (-0.22) H → L+20 (-0.12) H-1 → L+23
TIDT-TiO$_2$	$S_0 \rightarrow S_1$	565 (2.19)	2.0546	(-0.36) H-1 → L+4 (0.39) H → L+4 (0.17) H-1 → L+6 (-0.19) H → L+6

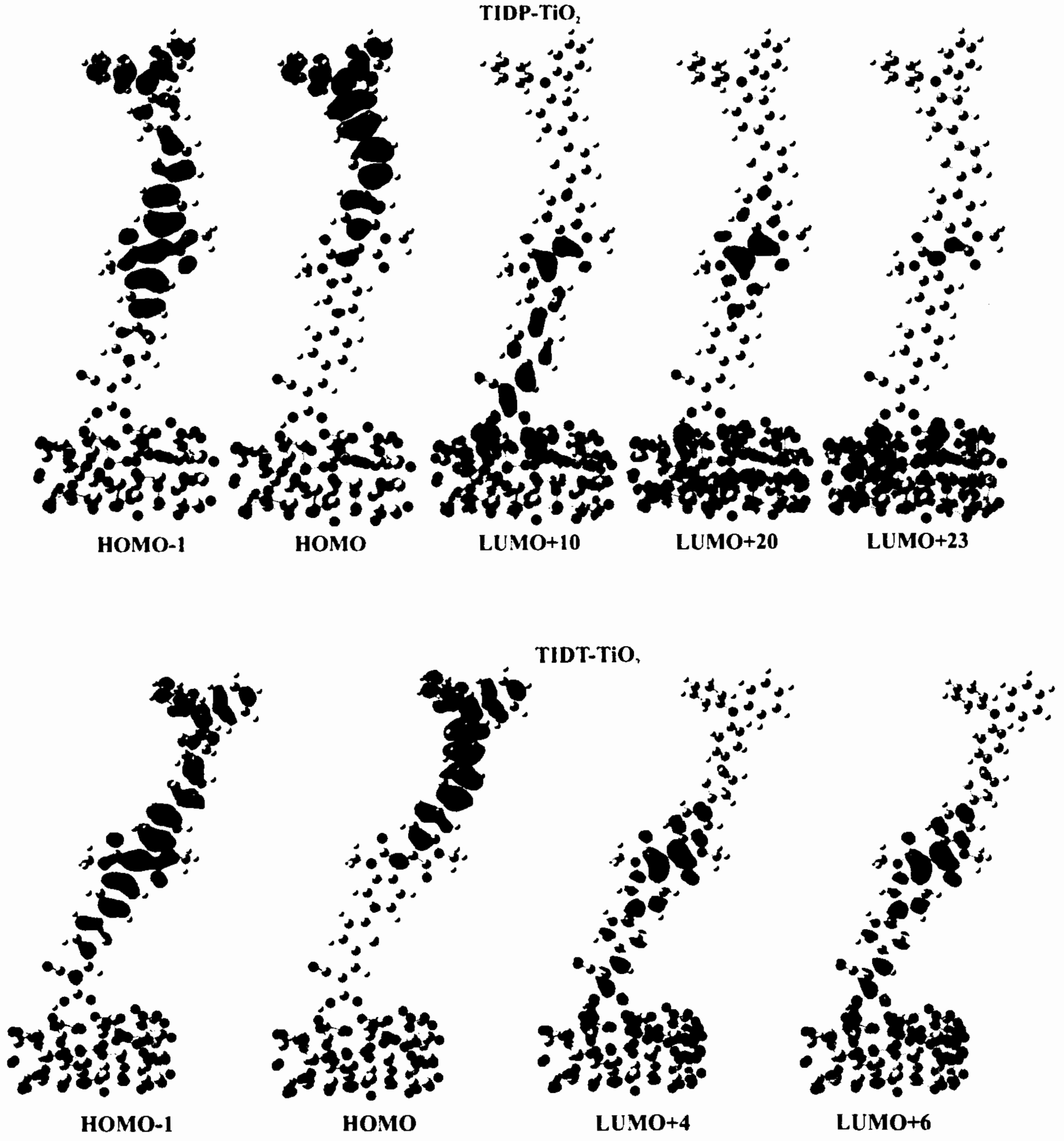

Figure 5.6 Frontier molecular orbitals of organic sensitizer adsorbed on the $(TiO_2)_{38}$ in gas phase calculated by CAM-B3LYP/6-31G(d) on DMol^3 geometry

5.2.1.4 The adsorption of D-π-A-π-A@TiO_2

The optimized structures of dye-$(TiO_2)_{38}$ adsorption complexes are shown in Figure 5.8. The intermolecular Ti-O bond distances and adsorption energies calculated by PBE/DNP are tabulated in Table 5.5. The bond distances of Ti-O and Ti-O′ of **TIDP** and **TIDT** were 2.02-2.24 Å. The adsorption energy (E_{ads}) of **TIDP-TiO$_2$** and **TIDT-TiO$_2$** were calculated to be -19.96 and -19.90 kcal/mol^{-1} respectively, indicating the strong interactions between the dyes and the TiO_2 cluster. The slightly higher adsorption energy of **TIDP** with phenyl linker resulted in the stronger electronic coupling strengths between the anchoring group of dye and the TiO_2 surface which could be corresponding to higher observed J_{sc}. However, we found that the adsorption energies were not corresponding to observed J_{sc} as expected. The J_{sc} of 8.59 mA cm^{-2} for **TIDP** was significantly higher than that of 5.80 mA cm^{-2} for **TIDT**. These results can be rationalized by dipole moment of these **TIDP-TiO$_2$** and **TIDT-TiO$_2$** (Figure 5.8). The dipole moment of these complexes were investigated, it was found that dipole moment after binding to TiO_2 surface for **TIDP-TiO$_2$** (32.02 D) is higher than that **TIDT-TiO$_2$** (14.22 D), indicating that stronger dipole moment affect to strength of change transfer properties of **TIDP-TiO$_2$** complex.

Table 5.5 The selected bond length (Å) and adsorption energy (kcal/mol) of dye-TiO$_2$ calculated by PBE/DNP in DMol^3

Complexes	Ti - O	Ti - O'	E_{ads} (kcal/mol)	J_{sc} (mA)	V_{oc} (V)	PCE (%)
TIDP-TiO$_2$	2.03	2.22	-19.96	8.59	0.702	4.37
TIDT-TiO$_2$	2.02	2.24	-19.90	5.80	0.634	2.71
N719	-	-	-	18.41	0.711	9.09

Moreover, the phenyl induces a vertically oriented **TIDP** dye geometry when it binds to TiO_2 surface, while the thiophene orients the **TIDT** dye with a tilt angle, resulting in a relatively shorter distance between the dyes donor moiety and the TiO_2

surface. The thiophene ring linker a reduced a more tilted anchoring mode of dye molecules on the surface of TiO_2. This feature of a self-assembled dye layer is well-associated with fast interfacial charge recombination and reduced photovoltage output [79].

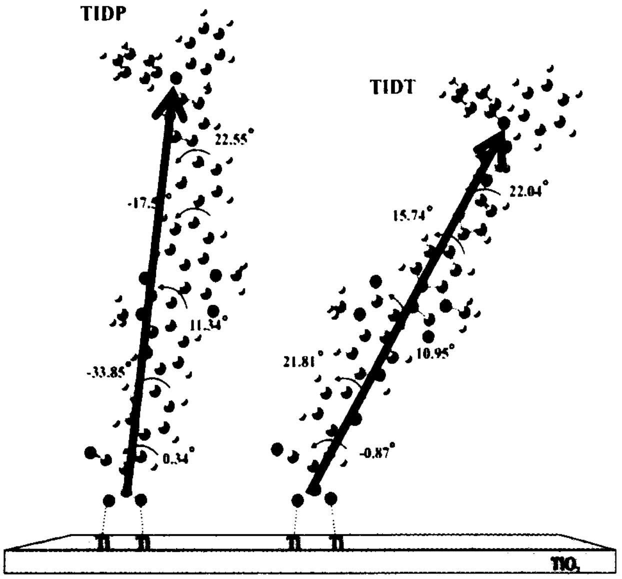

Figure 5.7 Conjugation units affect dyes orientation on the surface of TiO_2

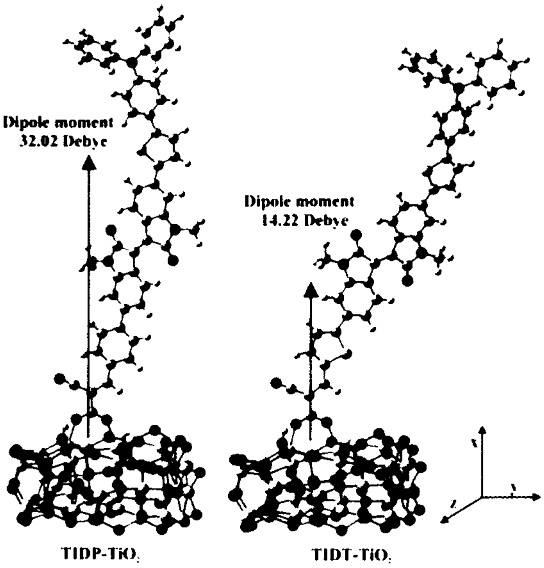

Figure 5.8 Optimization geometry dyes on the surface of TiO_2 calculated by PBE/DNP in $DMol^3$

5.2.2 Indoline series with different auxiliary acceptor

Recently, several kinds of electron-withdrawing units, benzothiadiazole, benzotriazole, quinoxaline, and diketo-pyrrolopyrrole have been systematically carried out as the auxiliary acceptor for viable D-A-π-A framework. Along with a large effort into the molecular engineering of organic D-A-π-A sensitizers, this demonstrated a significant increase in the efficiency from ~5% to greater than 10%. In a series of systematical studies, indoline derivative as the electron donor, and utilized a thiophene unit to connect the auxiliary acceptor and anchoring acceptor Interesting, the different electron-withdrawing capability of additional acceptors in the framework has a significant impact on the frontier orbital donor HOMO orbital and the acceptor LUMO orbital are largely responsible for the location of the frontier orbitals in the D-A system, which in turn light-absorption properties. Their energy band and absorption characters are mainly modulated by tuning the structure of donor and π-conjugation. In the case of the D-A-π-A motif, the additional auxiliary acceptor provides an alternative route for tuning the band energy as well as light absorption profile [80-82].

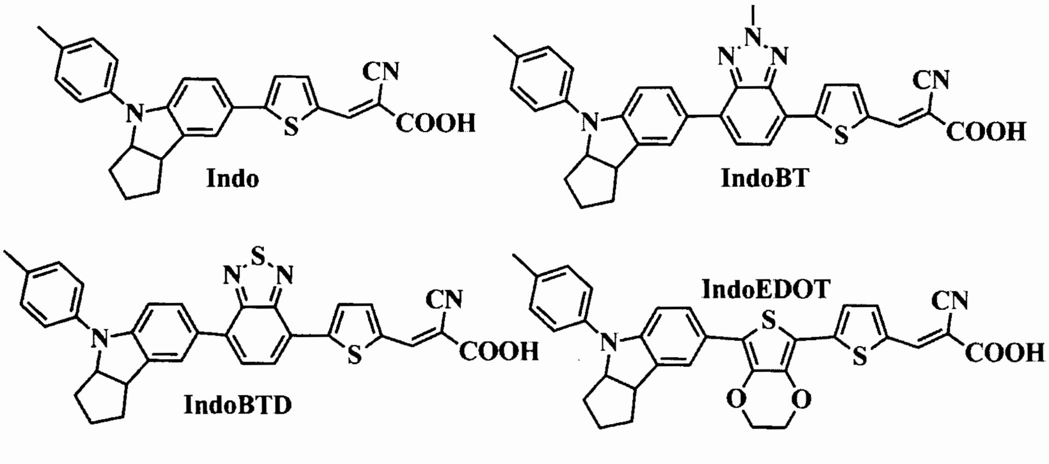

Figure 5.9 Sketch map of the indoline series (Indo, IndoEDOT, IndoBT, and IndoBTD)

5.2.2.1 Ground-state geometries of organic sensitizers

The optimized geometries obtained by density functional theory (DFT) B3LYP/6-31G(d,p) level of organic dye molecules are shown in Figure 5.10 and selected important inter-ring distance and dihedral angle parameters shown in Table 5.6. It is found that the inter-ring distance 1of all important inter-ring bonds are in the range of 1.41-1.47 Å. The dihedral angle between donor and conjugation (**Indo**) and auxiliary acceptor for EDOT, BT and BTD for **IndoEDOT**, **IndoBT** and **IndoBTD** can be computed to be 13.11°, 18.16°, 28.37° and 32.80°, respectively The dihedral angle is less twisted comparing to the **Indo** dye and the dye with auxiliary acceptor (**IndoEDOT**, **IndoBT** and **IndoBTD**). The twisted structure in donor part of these dyes resulted in preventing dye aggregation. In the acceptor part, the dihedral angles between thiophene ring and cyanoacrylic acid anchoring are coplanar in the range of 0.04° to 1.01°. Therefore the electron from the donor can efficiently delocalize to the acceptor moiety, as a result transferring to the conduction band (CB) of semiconductor.

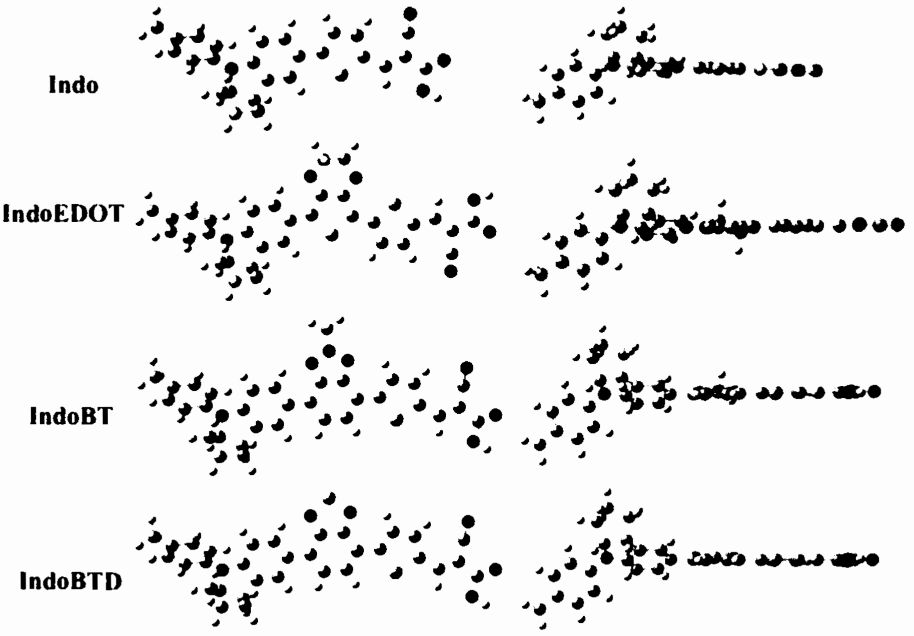

Figure 5.10 Optimized structures of Indo, IndoEDOT, IndoBT, and IndoBTD by DFT/B3LYP/6-31G(d,p)

Table 5.6 The selected important inter-ring distances (r, Å) and dihedral angles (ϕ, °) calculated by B3LYP/6-31G(d,p) calculations

Dyes	Dihedral angle (ϕ) and inter-ring distance (r)			
	Indo - Thiophene	Indo - Acceptor	Acceptor-Thiophene	Thiophene – Cyanoacrilic acid
Indo	13.11 (1.45)	-		-1.01 (1.41)
IndoEDOT	-	18.16 (1.45)	-0.16 (1.42)	-0.06 (1.41)
IndoBT	-	28.37 (1.47)	-0.32 (1.45)	0.04 (1.42)
IndoBTD	-	32.80 (1.47)	-3.33 (1.45)	0.25 (1.42)

Acceptor: BTD, and BT

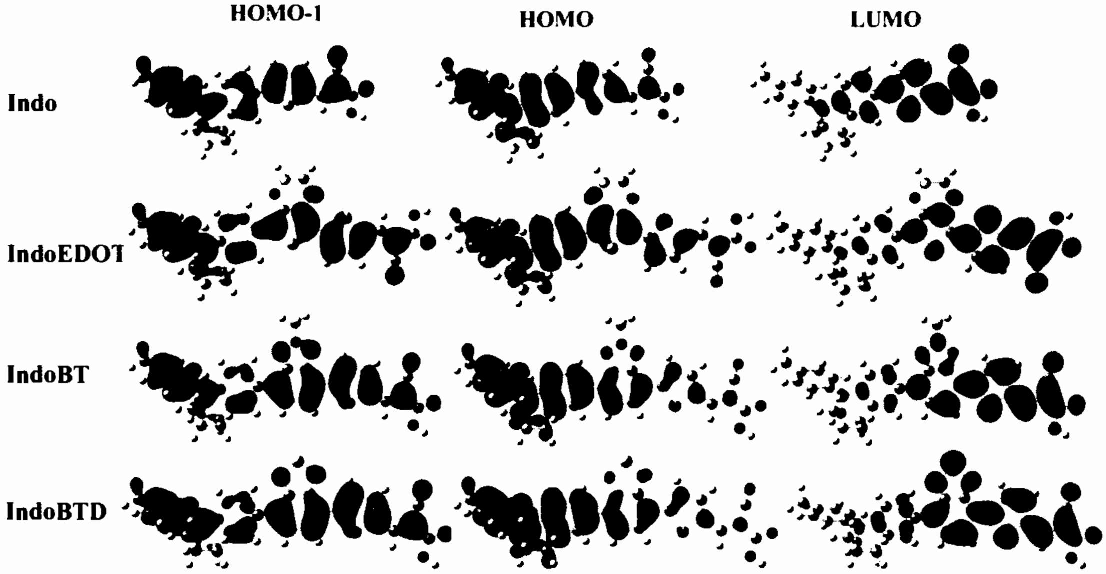

Figure 5.11 The molecular orbital surface at the ground state and first excited state when transition occurs

5.2.2.2 Electronic structures of organic sensitizers

To gain insight into the electronic structures, frontier molecular orbital were obtained to examine the highest occupied molecular orbital (HOMO) and the lowest unoccupied molecular orbital (LUMO) due to the relative ordering of the HOMO and LUMO providing a reasonable qualitative indication of the excitation properties. The molecular orbital surfaces of **Indo**, **IndoEDOT**, **IndoBT** and **IndoBTD** are shown in Figure 5.11 and the density of state (DOS) are presented in Table 5.7. In all dye, the electron density on HOMO is delocalized on donor group and the electron density on LUMO is delocalized on acceptor group, the HOMO to LUMO transition that corresponding mixed transition between intramolecular charge transfers (ICT) from donor group to acceptor group. Moreover, suitable energy level and location of HOMO and LUMO orbitals of the dye are required to match the I^-/I_3^- redox potential and conduction band level of the TiO_2 semiconductor. The calculated molecular orbital energies of **Indo**, **IndoEDOT**, **IndoBT** and **IndoBTD** were computed by using B3LYP/6-31G(d,p) the conduction band (CB) of TiO_2 as shown in Figure 5.12. The results were found that the HOMO energy levels of **Indo**, **IndoEDOT, IndoBT** and **IndoBTD** are -5.04, -4.82, -4.92, and -4.97 eV respectively; the LUMO energy levels are -2.64, -2.68, -2.85, and -3.02 eV, respectively. We found that, for **BTD** auxiliary acceptor the LUMO is lying closer to the conduction band of TiO_2 compared to that of others leading to the excited electrons are then efficiently injected into semiconductor electrode. Whereas the HOMO energy all dye are lying above the redox couple of the electrolyte which is the most suitable for donation of electrons from the I^-/I_3^- redox couple in the electrolyte solution.

Table 5.7 The energies and percentage composition of frontier molecular orbitals of dyes

Dyes	Molecular orbitals	Percentage composition			
		Indo	Acceptor	Thiophene	Cyanoacrilic acid
Indo	LUMO	15	-	37	48
	HOMO	75	-	16	9
IndoEDOT	LUMO	7	19	33	41
	HOMO	61	22	11	7
IndoBT	LUMO	6	24	32	38
	HOMO	77	14	6	3
IndoBTD	LUMO	7	51	20	22
	HOMO	80	12	5	3

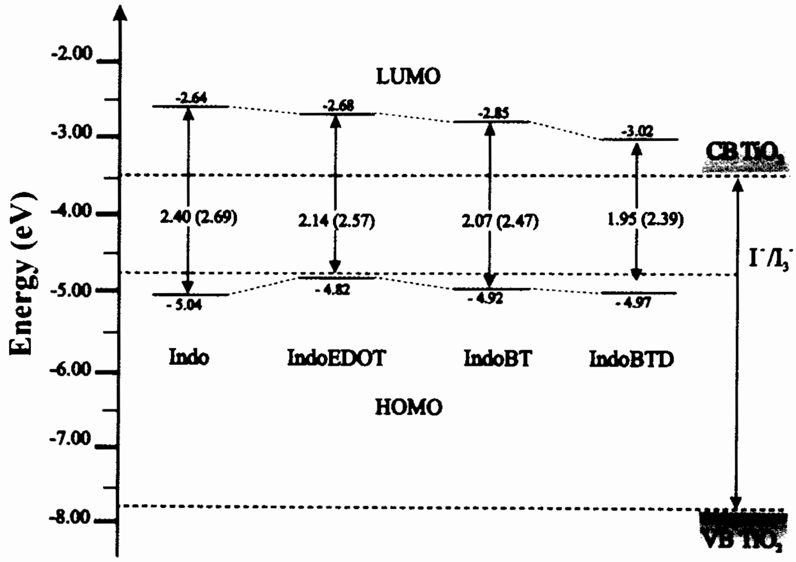

Figure 5.12 Molecular orbital energy level diagram of the dyes, TiO_2 conduction band, and redox couple of I^-/I_3^- electrolyte

5.2.2.3 Absorption spectra

The absorption spectra of these molecules have been studied by TD-CAM-B3LYP/6-31G(d,p) level. The transition energies of electronic spectra, oscillator strength, configurations of the orbital, and the calculated values of the absorption wavelength of **Indo**, **IndoEDOT**, **IndoBT** and **IndoBTD** are listed in Table 5.8. The UV/vis absorption spectra of **Indo**, **IndoEDOT**, **IndoBT** and **IndoBTD** are shown in Figure 5.13. It was found that, the λ_{max} of **Indo**, **IndoEDOT**, **IndoBT** and **IndoBTD** are 460, 510, 480, and 516 nm, respectively. This composition of the electronic transitions for **Indo**, **IndoEDOT**, **IndoBT** and **IndoBTD** dyes, as shown in Figure 5.11.These results indicate that **IndoBTD** dye exhibits red-shifted compared to that of organic dyes. The absorption spectra of the two auxiliary acceptors of **IndoBT** and **IndoBTD** play exactly different roles in absorption and intramolecular charge transfer compared **Indo** molecule.

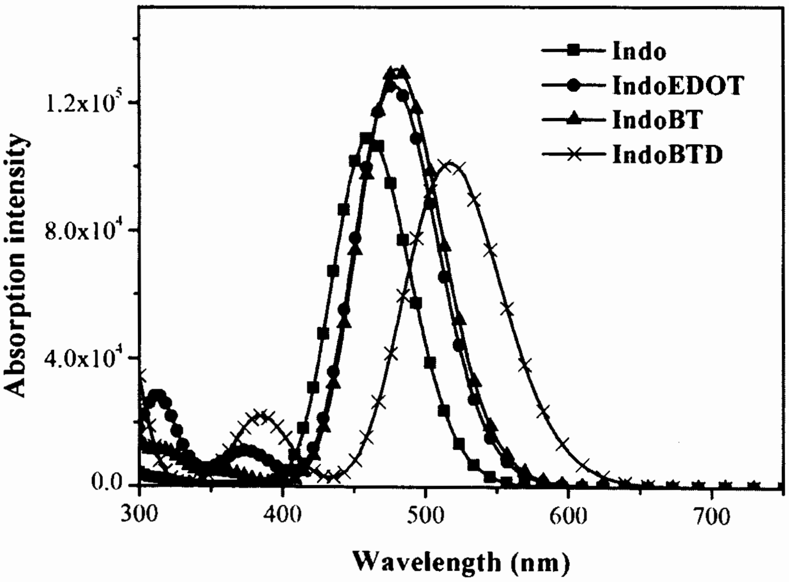

Figure 5.13 Absorption spectra of Indo, IndoEDOT, IndoBT, and IndoBTD calculated by TD-CAM-B3LYP /6-31G (d,p) level in CH_2Cl_2 solvent (C-PCM model)

Table 5.8 Calculated TDDFT (CAM-B3LYP) excitation energies for the lowest transition (eV, nm), oscillator strengths (*f*), composition in terms of molecular orbital contributions and experimental absorption maxima

Dyes	State	Composition	E (eV, nm)	*f*
Indo	$S_0 \rightarrow S_1$	0.21 (H-1→L) 0.65 (H→ L)	2.69, 460	1.5054
IndoEDOT	$S_0 \rightarrow S_1$	-0.30 (H-1→ L) 0.61 (H→ L)	2.47, 510	1.8294
IndoBT	$S_0 \rightarrow S_1$	0.33 (H-1→ L) 0.58 (H→ L)	2.57, 480	1.8182
Indo-BTD	$S_0 \rightarrow S_1$	0.28 (H-1→L) 0.61 (H→ L)	2.39, 516	1.3952

5.2.2.4 Adsorption of organic sensitizers on TiO_2 cluster

The intermolecular Ti-O bond distances and adsorption energies calculated by PBE/DNP are listed in Table 5.9. The bond distances of Ti-O and Ti-O′ of **Indo**, **IndoEDOT, IndoBT** and **IndoBTD** were 2.11-2.16 Å. The adsorption energy (E_{ads}) of **Indo-TiO$_2$**, **IndoEDOT-TiO$_2$**, **IndoBT-TiO$_2$** and **IndoBTD-TiO$_2$** were calculated to be -13.99, -15.42, -14.99 and -15.68 kcal/mol respectively, indicating the strong interactions between the dyes and the TiO_2 cluster. The higher adsorption energy of the dye with auxiliary acceptor group resulted in the stronger electronic coupling strengths between the anchoring group of dye and the TiO_2 surface which could be corresponding to the power conversion efficiency increase from 4 to 8%.

Table 5.9 The selected bond length (Å) and adsorption energy (kcal/mol) of dye-TiO_2 calculated by PBE/DNP in $DMol^3$

Dyes	Ti - O	Ti - O'	Eads (kcal/mol)	Efficiency (%)
Indo	2.169	2.153	-13.95	4.40
IndoEDOT	2.169	2.136	-15.42	6.05
IndoBT	2.166	2.160	-14.99	6.74
IndoBTD	2.115	2.169	-15.68	8.70

To study the electron injection mechanism of selected dyes at the interface of the dye-TiO_2 surface, the ten lowest vertical transitions are simulated using TDCAM-B3LYP/6-31G(d). The calculated excitation energies for the peak having the highest oscillator strength are illustrated in Table 5.10. The results show that the strongest transition in our dyes is characterized as a linear combination of The Kohn–Sham orbitals, which are most relevant to these transitions, are shown in Figure 5.14 and listed in Table 5.10. **Indo-TiO_2**, **IndoEDOT-TiO_2**, **IndoBT-TiO_2** and **IndoBTD-TiO_2** complexes show similar trend compared to isolate dyes. These orbitals, together with TDDFT functional, show that the transition with large oscillator strength characterized as the transition from the orbitals localized in the donor-liker (D-π) unit and auxiliary acceptor to the orbitals delocalized over the acceptor (A) unit of dyes and the $(TiO_2)_{38}$ cluster. The former orbitals are similar to the HOMOs of dyes and the latter orbitals correspond to the interacting orbitals between the LUMOs of dyes and the conduction band of TiO_2. This means that the electron excitation of this system directly induces the electron injection from dye into TiO_2 surface.

Indo-TiO_2

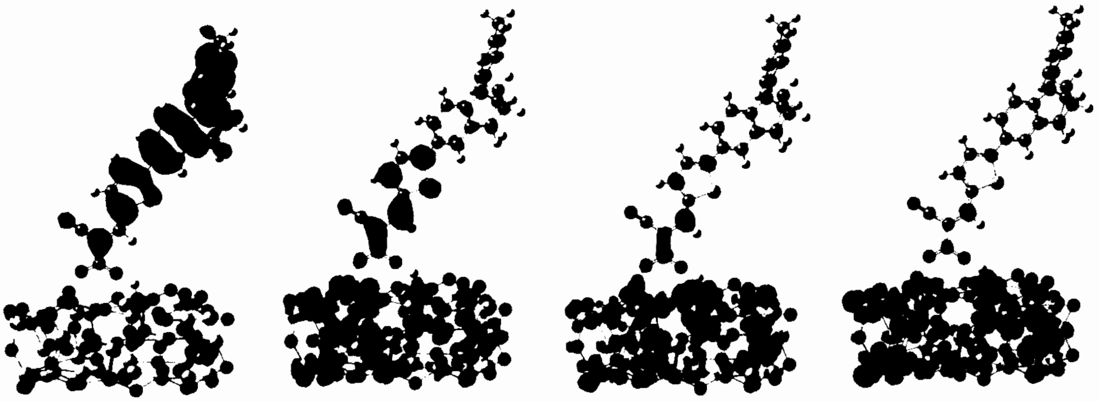

IndoEDOT-TiO_2

Figure 5.14 MOs relevant to the transition from S_0 to S_1 of organic sensitizer adsorbed on the $(TiO_2)_{38}$ in gas phase calculated by TD-CAM-B3LYP/6-31G(d) on DMol^3 geometry

IndoBT-TiO$_2$

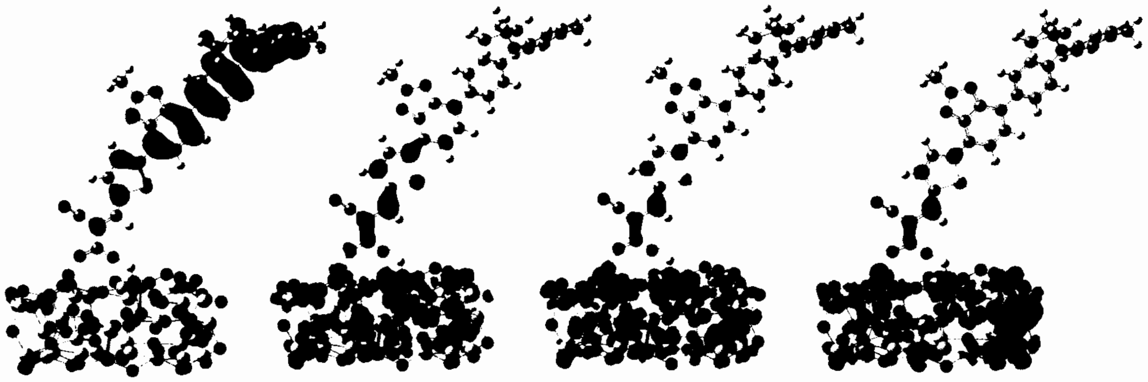

HOMO LUMO+23 LUMO+22 LUMO+21

IndoBTD-TiO$_2$

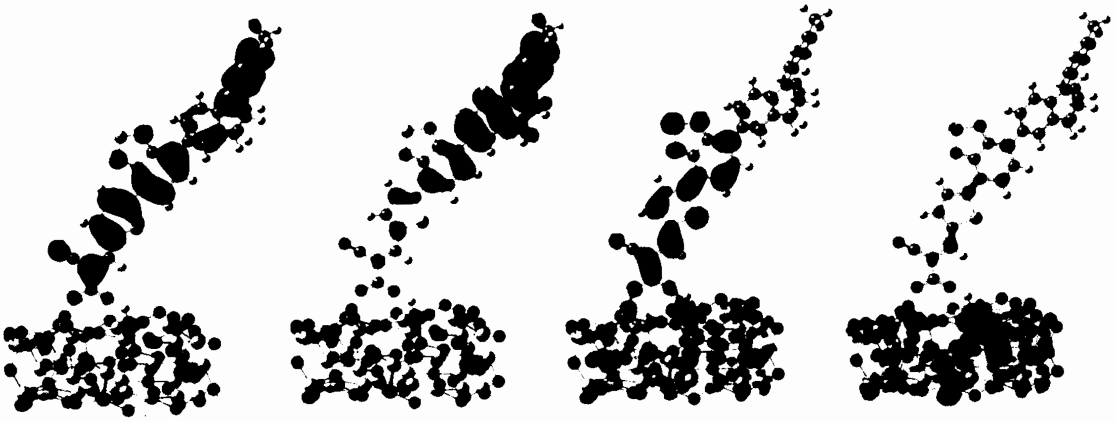

HOMO-1 HOMO LUMO+12 LUMO+14

Figure 5.14 MOs relevant to the transition from S_0 to S_1 of organic sensitizer adsorbed on the $(TiO_2)_{38}$ in gas phase calculated by TD-CAM-B3LYP/6-31G(d) on DMol^3 geometry

Table 5.10 The electronic properties of the TiO_2-dye complexes calculated by TD-CAM-B3LYP/6-31G(d,p) level of theory

Dyes	Electronic transitions	λ_{max} (nm/eV)	f	Assignment; H=HOMO, L=LUMO, etc.
Indo	$S_0 \rightarrow S_1$	448 (2.76)	1.6296	0.28(H→L+38) 0.23(H→L+25) -0.16(H→L+27)
IndoEDOT	$S_0 \rightarrow S_1$	482 (2.57)	1.9765	0.33(H→L+24) 0.18(H-1→L+24) 0.17(H→L+25)
IndoBT	$S_0 \rightarrow S_1$	485 (2.55)	1.9955	-0.26(H→L+23) -0.21(H→L+22) 0.21(H→L+21)
IndoBTD	$S_0 \rightarrow S_1$	524 (2.36)	1.5399	0.47(H→L+12) -0.21(H-1→L+12) -0.21(H→L+14)
	$S_0 \rightarrow S_6$	392(3.16)	0.1074	0.43(H→L+2) 0.25(H→L+4) -0.22(H→L+5)

5.3 Conclusion

For a series of the effect of auxiliary acceptor on sensitizer in DSCs, D-π-A-π-A organic sensitizers (**TIDT** and **TIDP**), in which TPA as the donor, thiophene as the linker, isoindigo as an auxiliary electron withdrawing unit, different linker is thiophene ring for **TIDT**, phenyl ring for **TIDP**, and a cyanoacrylic acid moiety acting as the anchoring group compared to TPA dye without (**TTPC** and **TT2C**). We found that **TIDP** and **TIDT** dyes exhibits red-shifted compared to that of **TTPC** and **TT2C** dyes. The absorption spectra of the auxiliary acceptors of **TIDP** and **TIDT** as D-π-A-π-A system play exactly different roles in absorption and intramolecular charge transfer compared D-π-A system. Different performance of DSCs based on synthesized **TIDP** and **TIDT** dyes can explain by dipole moment after binding to TiO_2 surface for **TIDP-TiO$_2$** (32.02 D) is higher than that **TIDT-TiO$_2$** (14.22 D), indicating that stronger dipole moment affect to strength of change transfer properties of **TIDP-TiO$_2$** complex.

In the case of the D-A-π-A motif, the different auxiliary acceptor by additional EDOT, BT and BTD group (**Indo**, **IndoEDOT**, **IndoBT**, and **IndoBTD)** baes on indoline as donor. The results show that **IndoBTD** dye exhibits red-shifted compared to that of organic dyes. The absorption spectra of the two auxiliary acceptors of **IndoBT** and **IndoBTD** play exactly different roles in absorption and intramolecular charge transfer compared **Indo** molecule.

CHAPTER 6

THE EFFECT OF ACCEPTOR POSITION ON INDOLE MOIETY ON ABSORPTION SPECTRA

Dye-sensitized solar cells (DSCs) have attracted great attention over the last 15 years owing to their prospect of high energy conversion efficiency and low production cost. The major advantages of these metal-free dyes are their tunable absorption and electrochemical properties through suitable molecular design. Recently, numerous organic dyes leading to the construction of DSCs with high efficiency have been reported. Such organic dyes generally consist of electron donor moieties like triarylamine, carbazole and indoline, π-conjugated groups like thiophenes, benzene, benzothiadiazole as spacer and electron withdrawing units like cyano acetic acid, rhodanine acetic acid, malonic acid and pyridine as acceptors. Indole or indoline aromatic heterocyclic compounds have been extensively used in designing new metal-free sensitizers. Assimilation of these moieties into the dye molecular framework often extends the π-conjugation (towards the red side of the visible spectra) as well as the electron-donating ability and thus helps to improve the efficiency.

One of the common tools to improve the absorption of organic dyes is the extended of the effective conjugation length, because the absorption band of π-conjugated materials originate from the degree of interaction π-orbitals. However, the degree of π-orbital interaction is also strongly affected by chain conformation, which limits the practical implication of the conjugation length in tuning the absorption properties of dyes. Another efficient way to control a dyes absorption range is by combining an electron-donating (D) and an electron-accepting (A) moiety within the same conjugated framework [83]. The D-A structure induces ICT properties, which facilitates π-orbital overlap via the quinoid resonance structure and produces consequent redshift absorption of the dye [84]

6.1 Computational details

The ground-state structures of organic dye molecules are fully optimized using DFT at the B3LYP hybrid functional with 6-31G(d,p) basis set. The excitation energies and the electronic absorption spectra of organic dye molecules are investigated using TDDFT at the CAM-B3LYP functional, with the same basis set as in the ground-state calculations. The solvation effect is included by means of C-PCM. The solvent used in our calculations and experiment is CH_2Cl_2. The absorption spectra of all organic sensitizers and the contribution of molecular orbitals in the electronic transitions are simulated using the GaussSum program version 3.0. The results are compared with the experimental date. All calculations are performed using the Gaussian09 program package. The electron-injection characteristics from dye to the TiO_2 (101) anatase surface are carried out. The dye-$(TiO_2)_{38}$ systems are fully optimized by the PBE functional with the DNP basis set. The core electron is treated with DFT with DSPPs by DMol^3 code in Materials Studio 5.5. The energy convergence tolerance is set to 2 x 10^{-5} Hartree, the maximum force 0.004 Hartree Å^{-1}, and the maximum displacement 0.005 Å. The optical properties of the relaxed complex are then computed with the TD-CAMB3LYP/6-31G(d) method. The adsorption energies (E_{ads}) of dyes on the $(TiO_2)_{38}$ clusters can be obtained using the following expression:

$$E_{ads} = E_{dye+TiO_2} - [E_{dye} + E_{TiO_2}]$$

where $E_{dye+TiO_2}$ is the total energy of the dye@$(TiO_2)_{38}$ system, and $E_{dye}$and E_{TiO_2} are the energies of the dye and $(TiO_2)_{38}$ cluster, respectively.

In this chapter we focus on the D-A framework on indole-based dyes absorption, absorption spectra of indole-based dyes with different acceptor substitution position and different π-conjugation were investigated. The D-A structure of indole-based dyes are shown in Figure 6.1.

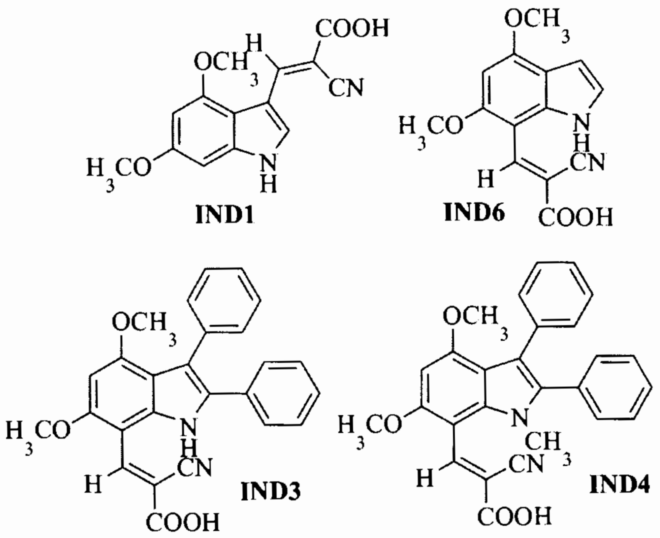

Figure 6.1 Sketch map of the synthesized IND1, IND6, IND3, and IND4 sensitizer

6.2. Results and discussion

6.2.1 Ground-state geometries

The optimized geometries obtained by DFT at B3LYP/6-31G(d,p) level of **IND1**, **IND6**, **IND3**, and **IND4** are shown in Figure 6.2, and the important inter-ring distance and dihedral angle parameters are shown in Table 6.1. The result was found that dihedral angles between donor group and acceptor group (indole-cyanoacylic acid) can be computed to be 0.00°, 17.40°, -18.14°, and 29.60°, respectively, dihedral angles between indole-phenyl ring can be computed to be in rang -36.40°-59.39°. The dihedral angles of donor group and acceptor group and indole-phenyl ring are different, the effect of different substitution position of anchoring groups on indole ring affect to co-planarity molecule between donor group and acceptor group in **IND1** and twisted molecule between donor group and acceptor group in **IND3**, **IND4**, and **IND6.** These results indicate that six-membered ring substitution position (**IND4**, **IND6** and **IND7**) can be preventing dye aggregation.

Table 6.1 Selected important inter-ring distances (Å) and dihedral angles (°) calculated by B3LYP/6-31G(d,p) calculations

Dyes	Dihedral angles in degree (Inter-ring distances in angstrom)		
	Indole-Cyanoacylic acid	Indole-Phenyl_1	Indole-Phenyl_2
IND1	0.00 (1.41)	-	-
IND6	17.40 (1.42)	-	-
IND3	18.14 (1.42)	-36.40 (1.46)	-59.39 (1.48)
IND4	29.60 (1.42)	-53.72 (1.47)	-58.97 (1.48)

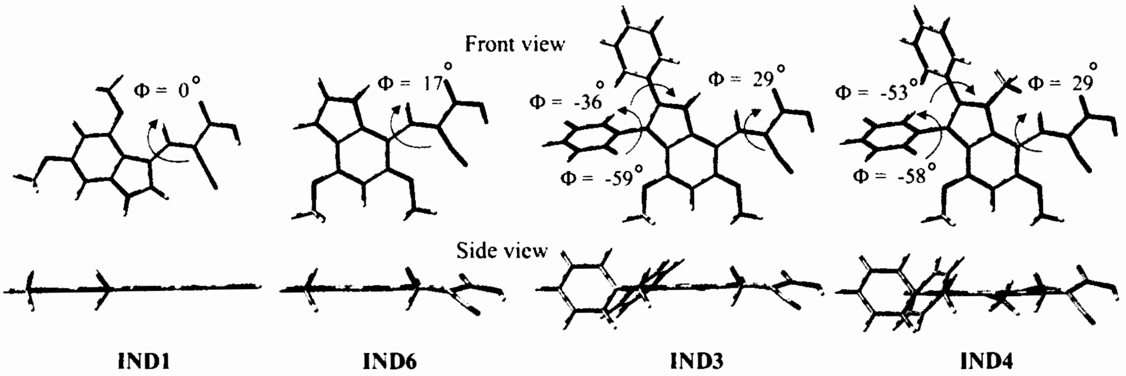

Figure 6.2 Optimized structures of IND1, IND6, IND5 and IND4 by DFT/B3LYP/6-31G(d,p)

6.2.2 Electronic structures of organic sensitizers

To gain insight into the electronic structures, frontier molecular orbital were obtained to examine the HOMO and the LUMO due to the relative ordering of the HOMO and LUMO provides a reasonable qualitative indication of the charge transfer properties. The molecular orbital surfaces of **IND1**, **IND6**, **IND3**, and **IND4** molecules are presented in Figure 6.3 and the density of state (DOS) are presented in Table 6.2.

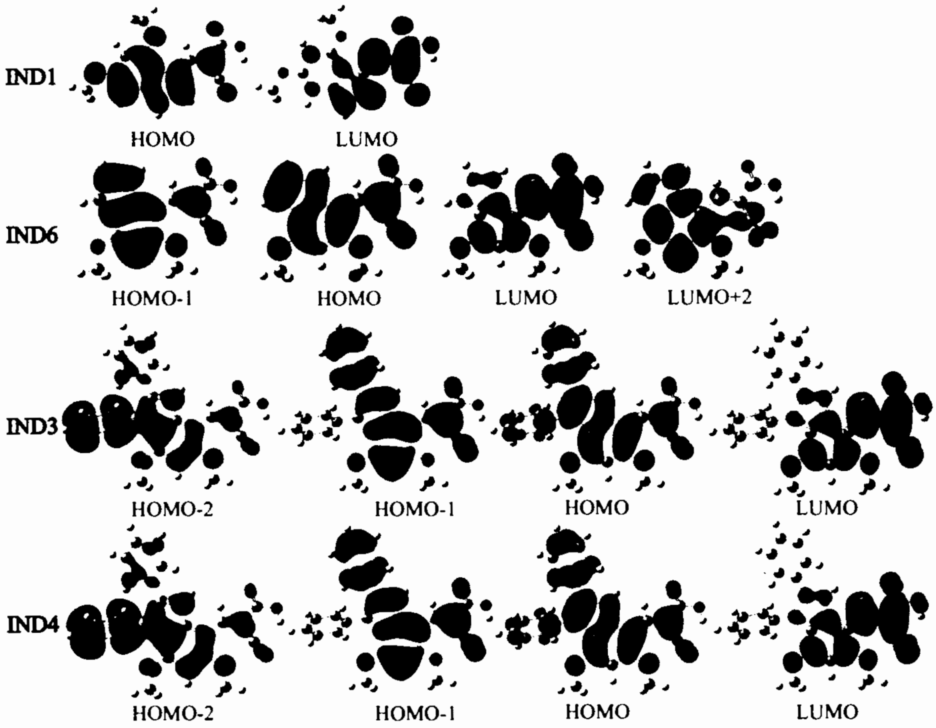

Figure 6.3 The molecular orbital surfaces of IND1, IND6, IND3, IND4 molecules

For all dyes, the HOMOs of the dyes were mainly located on the indole unit. The LUMOs of the dyes were contributed by the cyanoacrylic acid acceptor. From this it is evident that the HOMOs to LUMOs electronic excitation will result in the charge transfer from the indole unit to the cyanoacrylic acid acceptor. These electron distributions will therefore ensure efficient electron injection from dye molecule to the conduction band of TiO_2.

Table 6.2 The energies and percentage composition of frontier molecular orbitals of organic sensitizers

Dyes	Molecular orbitals	Orbitals energy (eV)	Percentage composition	
			Donor	Acceptor
IND1	LUMO	-2.43	33	67
	HOMO	-5.73	85	15
IND6	LUMO	-2.45	40	60
	HOMO	-5.69	80	20
IND3	LUMO	-2.49	42	58
	HOMO	-5.53	89	11
IND4	LUMO	-2.40	40	60
	HOMO	-5.50	83	17

Additionally, suitable energy level of HOMO and LUMO orbitals of the organic dye are required to match the I^-/I_3^- redox potential and conduction band level of the TiO_2 semiconductor. The energy levels HOMO and LUMO are depicted in Figure 6.4. It was reported that the HOMO-LUMO energy gap can be effectively decreased by substitution position of acceptor unit in the indole ring, which results in a redshift of the electronic absorption spectra. In Figure 6.5, the computed HOMO-LUMO energy gap of five-membered ring substitution position (**IND1**) is larger than six-membered ring substitution (**IND3-IND6**). The HOMO-LUMO energy level of **IND3** show the most matching the I^-/I_3^- redox potential and conduction band level of the TiO_2 semiconductor compare to other dyes. However, the HOMOs are below the redox potential of the I^-/I_3^- redox potential and that the LUMOs are energetically higher than the conduction band edge of the frequently used TiO_2 semiconductor which confirms that all dye molecules are suitable to ensure the electron injection from the excited dye to conduction band level TiO_2 semiconductor and the dye regeneration by the redox couple in DSCs.

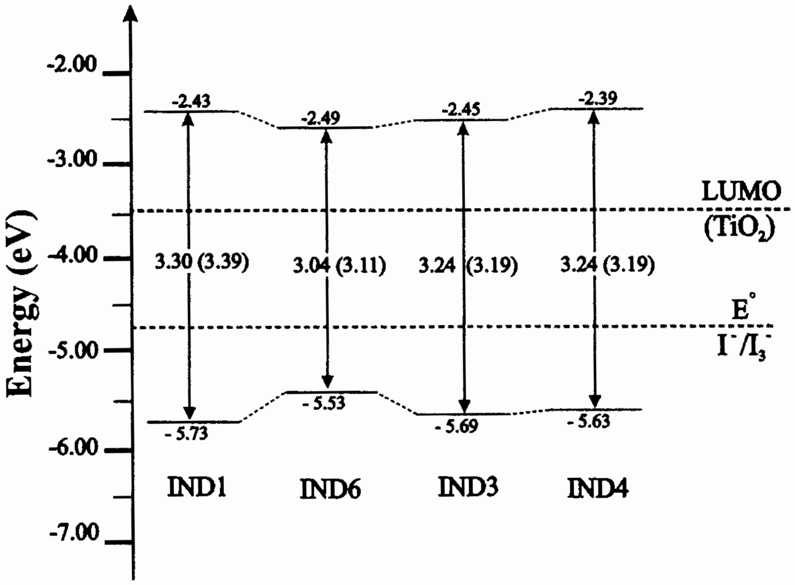

Figure 6.4 Molecular orbital energy level diagram of the dyes, TiO_2 conduction band, and redox couple of I^-/I_3^- electrolyte

6.2.3 Absorption spectra of organic sensitizers

The absorption spectra of these molecules have been studied by TD-CAM-B3LYP/6-31G(d,p) level. Comparison of the theoretically calculated wavelength with experimental data was performed. The absorption spectra of **IND1-IND6** are shown in Figure 6.5. The electronic properties, oscillator strength, configurations of the orbitals, and the calculated values of the absorption wavelength in the solvent phase of all dyes are shown in Table 6.3. The strongest absorption peak with the largest oscillator strengths arise from $S_0 \rightarrow S_1$ transition corresponding to intramolecular charge transfer transition. It is found that the λ_{max} of **IND1, IND6, IND3, and IND4**, are 365, 393 398, and 395 nm, respectively. **IND6, IND3** and **IND4** dyes exhibit two distinct absorption bands: first absorption band in the region of 314-324 nm is ascribed to the π-π* transition of the donor part; and the second band in the region of 388-398 nm, which is assigned to intramolecular charge transfer (ICT) between the electron-donating unit and the electron-accepting units. The spectra of **IND6, IND3** and **IND4** are quite similar; the maximum absorption peak of **IND3** is red-shifted compared to the other dyes due to the stronger electron donating nature of the six-membered ring substitution position than five-membered ring substitution position of indole ring.

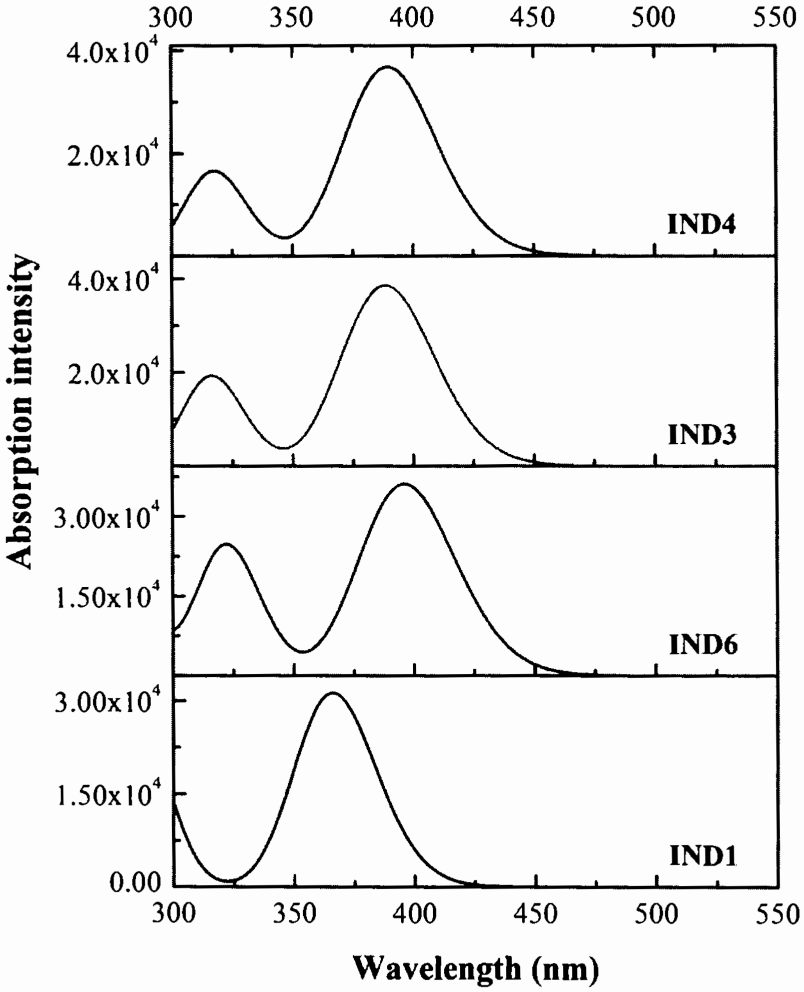

Figure 6.5 Absorption spectra of IND1, IND6, IND3, and IND4 calculated by TD-CAM-B3LYP/6-31G (d,p) level in CH_2Cl_2 solvent (C-PCM model)

Table 6.3 The electronic properties, absorption wavelength and oscillator strength (*f*) obtained by TDDFT at the CAM-B3LYP/6-31G (d,p) in CH_2Cl_2 solvent (C-PCM model)

Dyes	Electronic transitions	λ_{max} (nm/eV)	*f*	Assignment; H=HOMO, L=LUMO, etc.	Expt. λ_{max} (nm/eV)
IND1	$S_0 \rightarrow S_1$	365 (3.39)	0.4313	(0.69) H → L	401 (3.09)
IND6	$S_0 \rightarrow S_1$	388 (3.19)	0.5337	(0.69) H → L	*N.A.*
	$S_0 \rightarrow S_2$	316 (3.92)	0.2667	(0.68) H-1 → L (-0.11) H → L+2	
IND3	$S_0 \rightarrow S_1$	398 (3.11)	0.4775	(0.68) H → L	368 (3.36)
	$S_0 \rightarrow S_2$	324 (3.81)	0.4843	(-0.12) H-2 → L (0.66) H-1 → L	
IND4	$S_0 \rightarrow S_1$	395 (3.13)	0.4984	(-0.10) H-2 → L (0.68) H → L	439 (2.82)
	$S_0 \rightarrow S_2$	321 (3.85)	0.3421	(0.67) H-1 → L	

6.2.4 Adsorption of organic sensitizers on TiO_2 cluster

In general, the adsorption of a dye with carboxylic acid is possible by either physisorption or chemisorption. In the case of chemisorption, there are some possibilities in terms of bonding to the surface such as via a monodentate ester, bidentate chelating, or bidentate bridging, etc. It has been reported in many experimental studies, such as ATR-FTIR, that the terminal carboxylic acid usually adsorbs on the TiO_2 surface via bidentate bridging in the prototype system. Therefore, only chemisorption via bidentate bridging was investigated in the present study.

The adsorption dye-$(TiO_2)_{38}$ complexes was first fully optimized using the PBE functional together with the Double-Numerical with polarization performed in the $DMol^3$ program. The Ti-O bond distances and adsorption energies calculated by PBE/DNP are listed in Table 6.4. The bond distances of Ti-O and Ti′-O′ of **IND1-TiO_2**, **IND6-TiO_2**, **IND3-TiO_2**, and **IND4-TiO_2**, were 2.11–2.26 Å. The adsorption energy (E_{ads}) of **IND1-TiO_2**, **IND6-TiO_2**, **IND3-TiO_2**, and **IND4-TiO_2** complexes were calculated to be -17.65, -18.82, -20.38, and -18.87 kcal/mol respectively, indicating the strong interactions between the dyes and the TiO_2 surface. The higher adsorption energy of **IND3** with stronger electron donating group resulted in the stronger electronic coupling strengths between the anchoring group of dye and the TiO_2 surface.

Table 6.4 The selected bond length (Å) and adsorption energy (kcal/mol) of dye-TiO_2 calculated by PBE/DNP in DMol^3

Complexes	Ti - O	Ti - O′	E_{ads} (kcal/mol)	J_{SC} (mA cm^{-2})	V_{OC} (V)	FF	Dye uptake (molecule cm^{-2})	PCE (%)
IND1-TiO_2	2.04	2.14	-17.65	0.18	0.468	0.655	1.862 x 10^{14}	0.05
IND6-TiO_2	2.03	2.15	-18.82	*N.A.*				
IND3-TiO_2	2.03	2.16	-20.38	6.50	0.647	0.745	4.954 x 10^{16}	3.13
IND4-TiO_2	2.03	2.16	-18.90	7.91	0.707	0.735	1.098 x 10^{17}	4.11

6.2.5 Electron injection mechanism of dye-TiO_2 adsorption

To study the electron injection mechanism of dyes in the interface of dye-TiO_2 surface, the 10 lowest singlet transitions were simulated using TD-CAM-B3LYP/6-31G(d,p). The transition character of all dyes is included. The results of excitation energies and oscillator strengths for the 10 low-lying states are presented in Table 6.5. The molecular orbitals of dyes adsorbed on the $(TiO_2)_{38}$ that also significantly contribute to this transition are displayed in Figures 6.6 for all the dye-$(TiO_2)_{38}$ systems. The strongest absorption peak with the largest oscillator strengths arise from $S_0 \rightarrow S_2$ transition. The absorption spectra are very similar for the isolated dyes, with a slight red shift observed for the substitutes of acceptor on six-membered ring of indole.

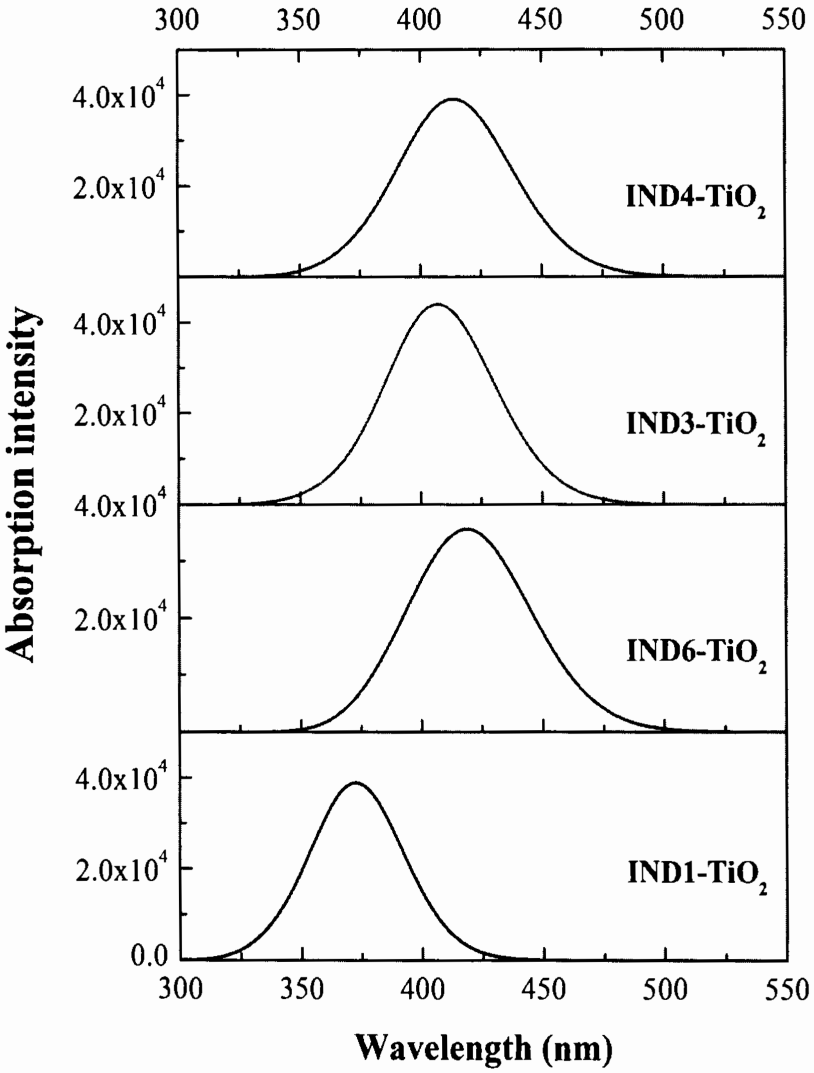

Figure 6.6 **Absorption spectra of sensitizer adsorbed on the $(TiO_2)_{38}$ in gas phase calculated by CAM-B3LYP/6-31G(d,p) on DMol^3 geometry**

Table 6.5 The electronic properties, absorption wavelength and oscillator strength (f) obtained by TDDFT at the CAM-B3LYP/6-31G (d,p) in gas phase

Complexes	Electronic transitions	λ_{max} (nm/eV)	f	Assignment; H=HOMO, L=LUMO, etc.
IND1-TiO_2	$S_0 \rightarrow S_2$	373 (3.32)	0.4236	(-0.25) H → L (+0.24) H → L+3 (+0.15) H → L+18
IND6-TiO_2	$S_0 \rightarrow S_2$	407 (3.04)	0.5377	(-0.18) H → L (-0.21) H → L+3 (+0.17) H → L+53 (+0.17) H → L+18
IND3-TiO_2	$S_0 \rightarrow S_2$	419 (2.95)	0.4772	(0.24) H → L+3 (-0.18) H → L+54 (+0.17) H → L+61
IND4-TiO_2	$S_0 \rightarrow S_2$	423 (2.92)	0.4081	(0.30) H → L+3 (+0.17) H → L+18 (-0.14) H → L+68

6.2.6 Driving force and electron injection process

For electron injection processes in DSCs, the free energy is an important parameter for characterizing the rate and efficiency of the reaction. The free energy change that occurs as a result of electron injection in a DSCs. The initial state of the reaction is the excited electron of dye adsorbed on a TiO_2 surface, and the final state corresponds to the injected electron on TiO_2 surface. The divining force can be obtained from equation below, representing the energy difference between these initial and final states, where E^{*}_{ox} representing to the photo-induced excited states of the organic dyes and E_{CB} representing to reduction potential of the TiO_2 semiconductor. The E^{*}_{ox} can be computed from equation below, where E_{ox} is the redox potential of the dye-TiO_2 in the ground state and labs is the absorption energy.

$$\text{Driving force} = E^{*}_{ox} - E_{CB}$$

$$E^{*}_{ox} = E_{ox} - \lambda_{abs}$$

Figure 6.7 displays alignment the calculated energy levels of the ground and excited state energy levels for the dye-TiO_2 complexes and the frontier molecular orbital of dyes adsorbed on the $(TiO_2)_{38}$. The energy alignment is the combination of the occupied energy level and the TD-DFT calculation. The excited state energy level is accordingly calculated to be at 3.32, 3.04, 2.95 and 2.92 eV for the lower-energy transitions of the **IND1-TiO$_2$**, **IND6-TiO$_2$**, **IND3-TiO$_2$** and **IND4-TiO$_2$**, respectively. Therefore, the driving forces for electron injection are 0.62, 0.90, 0.99 and 1.02 eV for the **IND1-TiO$_2$**, **IND6-TiO$_2$**, **IND3-TiO$_2$** and **IND4-TiO$_2$**, respectively (relative to the energy level of the experimental conduction band of TiO_2. The calculated results also indicated that all complexes have sufficient driving force for the electron injection. In addition, the **IND4-TiO$_2$** largest driving force (1.02 eV) compared to other complexes in the series, indicating that the electron injection rate is larger in the **IND4-TiO$_2$** than other complexes in the series.

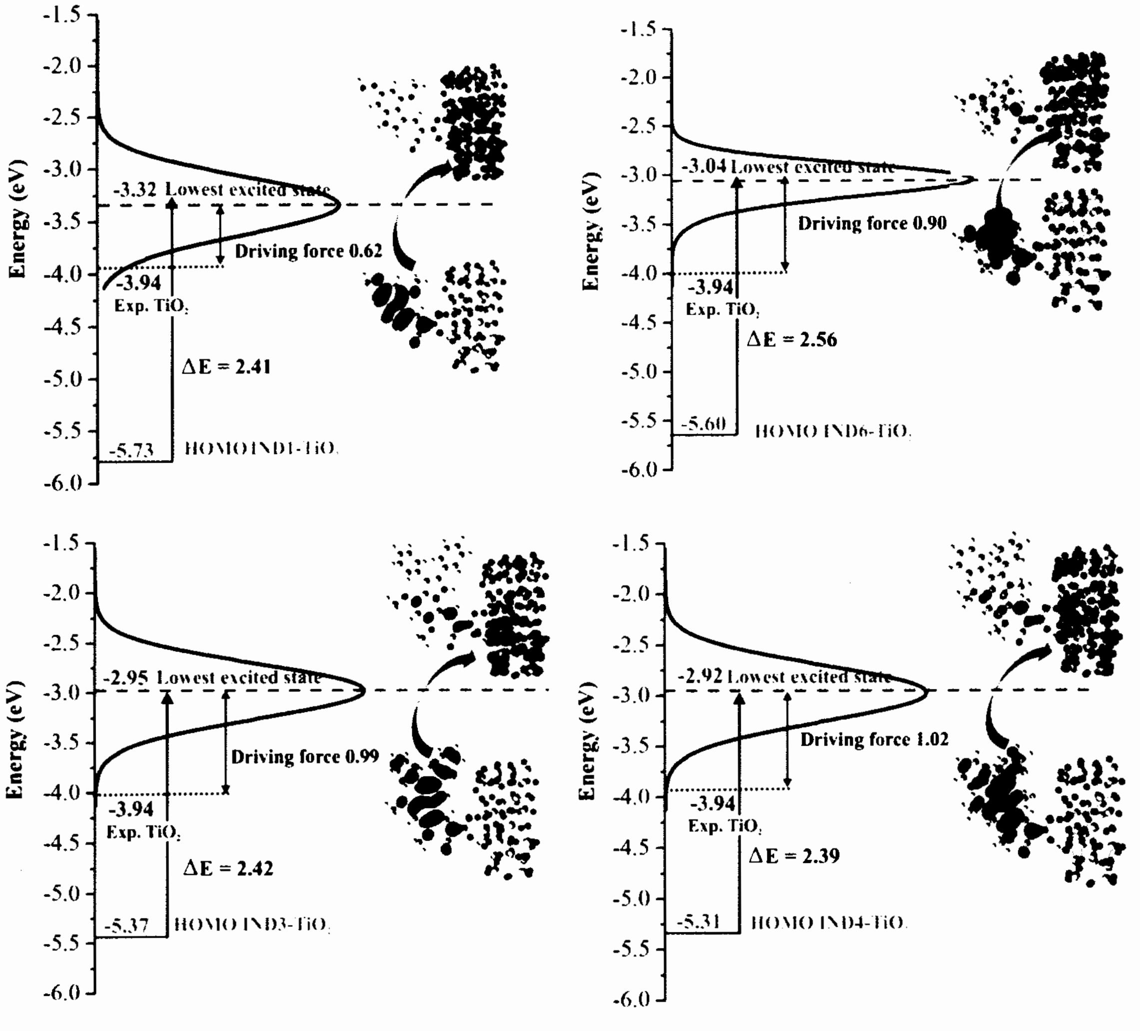

Figure 6.7 Alignment of the ground and excited state energy levels for the dye-TiO_2 complexes and the frontier molecular orbital of dyes adsorbed on the $(TiO_2)_{38}$. Purple dashed and light blue dashed lines indicate the edge of the experimental conduction band of TiO_2 and the calculated HOMO energy levels of the dye-TiO_2

6.3 Conclusion

For on the D-A framework on indole-based dyes absorption, absorption spectra of indole-based dyes with different acceptor substitution position were investigated. We found that absorption spectra of dye molecule with six-membered ring substitution position **(IND6, IND3, and IND4,)** dyes exhibit two distinct absorption bands: first absorption band in the region of 314-324 nm is ascribed to the π-π* transition of the donor part; and the second band in the region of 388-398 nm, which is assigned to intramolecular charge transfer (ICT) between the electron-donating unit and the electron-accepting units. Whereas five-membered ring substitution position (**IND1**) show one absorption peak (365 and 369 nm) in UV region. The maximum absorption peak of **IND3** is red-shifted compared to the other dyes due to the stronger electron donating nature of the six-membered ring substitution position than five-membered ring substitution position of indole ring. For adsorption dye-$(TiO_2)_{38}$ complexes of these series were investigated. We also found that the E_{ads} of the six-membered ring substitution position higher than five-membered ring substitution position and the absorption spectra show similar trend with isolate dyes.

CHAPTER 7
CONCLUSION

The theoretical studies of the structure and energetic properties of sensitizer for dye-sensitized solar cells were successfully investigated by DFT, TDDFT calculation and the adsorptions of dyes on the TiO_2 anatase (101) surface were carried out by mean of the periodic calculation.

For a series of organic dyes containing N-Substituted carbazole, diarylamine naphthalene and diarylamine-fluorene donor for **D1TC**, **D2TC**, and **D3TC**, respectively and cyanoacrylic acid acceptors bridged by thiophene fragment for DSCs applications were successfully investigated by DFT and TDDFT. We found that **D3TC** with strongest electron donating ability shows the most red shifted in UV absorption spectra and the highest performance charge transfer. Moreover, the calculated adsorption energy for **D3TC@$(TiO_2)_{38}$** complex higher than **D2TC@$(TiO_2)_{38}$** indicates the strongest interactions between the dyes and the TiO_2 surface, therefore **D3TC** has been expected to be the most potential sensitizers. Nevertheless, **D2TC** has shown the best photovoltaic performance. This controversial issue have been solved by performing the molecular volume, projected area on the TiO_2 surface and molecular width to investigate the effect of N-substituted donors on the number density of the adsorbed dye on TiO_2 surface. It has been found that more bulky of the donor moiety in **D3TC** could reduce the number density of the adsorbed dye on the TiO_2 surface. The photovoltaic performance shows poorer energy conversion efficiency of 3.91% in **D3TC** compared to the significantly better performance of 5.45% in **D2TC**.

For a series of different linker group on absorption properties of carbazole-fluorene and carbazole-carbazole derivatives to form D-D-π-A system, which extended conjugation linker by increase thiophene, phenyl and furan ring. The result show than **CarFT3C** and **CarCarT3C** with large conjugation length exhibits red-shifted compared to that of organic dyes in this series. In addition, we study on effect of bulky-donor to charge recombination and charge separation in **CFTA (CarFT3C)** and **CCTA (CarCarT3C)** in dye-semiconductor electronic coupling differs between **CCTA-TiO$_2$** and **CFTA-TiO$_2$** by constrained DFT configuration interaction (CDFT-CI) calculations. This interpretation is consistent with the experimental finding that the **CCTA** device achieves a higher PCE than the **CFTA** device while the CS rate is also smaller for **CCTA-TiO$_2$** than for **CFTA-TiO$_2$**, the difference is negligible compared to the difference in CR rates. Furthermore, the couplings reported here for CR are 2-3 orders of magnitude larger than couplings for CS, suggesting that the CR rate plays the greater role in determining the overall charge separation efficiency than the CS rate.

For a series of the effect of auxiliary acceptor on sensitizer in DSCs, D-π-A-π-A organic sensitizers (**TIDT** and **TIDP**), in which triphenylamine as the donor, thiophene as the linker, isoindigo as an auxiliary electron withdrawing unit, different linker is thiophene ring for **TIDT**, phenyl ring for **TIDP**, and a cyanoacrylic acid moiety acting as the anchoring group compared to TPA dye without (**TTPC** and **TT2C**). We found that **TIDP** and **TIDT** dyes exhibits red-shifted compared to that of **TTPC** and **TT2C** dyes. The absorption spectra of the auxiliary acceptors of **TIDP** and **TIDT** as D-π-A-π-A system play exactly different roles in absorption and intramolecular charge transfer compared D-π-A system. Different performance of DSCs based on synthesized **TIDP** and **TIDT** dyes can explain by dipole moment after binding to TiO$_2$ surface for **TIDP-TiO$_2$** (32.02 D) is higher than that **TIDT-TiO$_2$** (14.22 D), indicating that stronger dipole moment affect to strength of change transfer properties of **TIDP-TiO$_2$** complex.

In the case of the D-A-π-A motif, the different auxiliary acceptor by additional EDOT, BT and BTD group (**Indo, IndoEDOT, IndoBT,** and **IndoBTD)** baes on indoline as donor. The results show that **IndoBTD** dye exhibits red-shifted compared to that of organic dyes. The absorption spectra of the two auxiliary acceptors of **IndoBT** and **IndoBTD** play exactly different roles in absorption and intramolecular charge transfer compared **Indo** molecule.

For on the D-A framework on indole-based dyes absorption, absorption spectra of indole-based dyes with different acceptor substitution position were investigated. We found that absorption spectra of dye molecule with six-membered ring substitution position **(IND6**, **IND3**, and **IND4)** dyes exhibit two distinct absorption bands: first absorption band in the region of 314-324 nm is ascribed to the π-π* transition of the donor part; and the second band in the region of 388-398 nm, which is assigned to intramolecular charge transfer (ICT) between the electron-donating unit and the electron-accepting units. Whereas five-membered ring substitution position **(IND1)** show one absorption peak (365 and 369 nm) in UV region. The maximum absorption peak of **IND3** is red-shifted compared to the other dyes due to the stronger electron donating nature of the six-membered ring substitution position than five-membered ring substitution position of indole ring. For adsorption dye-$(TiO_2)_{38}$ complexes of these series were investigated. We also found that the E_{ads} of the six-membered ring substitution position higher than five-membered ring substitution position and the absorption spectra show similar trend with isolate dyes. In conclusion, it has been shown that these computational tools described above can provide the detailed characterizations which are in agreement with experimental efficiency. Therefore, it can be of valuable help in further design of novel organic sensitizer for higher efficiency of photovoltaic device.

REFERENCES

REFERENCES

[1] O'Regan, B., Gratzel, Michael. “A low-cost, high-efficiency solar cell based on dye-sensitized colloidal TiO_2 films”, **Nature.** 353:737-740.; October, 1991.

[2] Grätzel, M. “Dye-sensitized solar cells”, **Journal of Photochemistry and Photobiology C: Photochemistry Reviews**. 4(2): 145-153; October, 2003.

[3] Hagfeldt, A. and et al. “Dye-Sensitized Solar Cells”, **Chemical Reviews**. 110(11): 6595-6663; November, 2010.

[4] R. M. Siverstein, G. C. B. a. T. C. M. **Spectrometric Identification of Organic Compounds**. 5th ed. New York: John Wiley & Sons, 1991.

[5] Lakowicz., J. R. **Principles of Fluorescence Spectroscopy**. 2nd ed. New York: Plenum Publishers, 1999.

[6] Nau, W. “Modern Molecular Photochemistry of Organic Molecules. by N. J. Turro, V. Ramamurthy, J. C. Scaiano”, **a European journal of chemical physics and physical chemistry**. 12(13): 2496-2497; June, 2011.

[7] Standard, J. M. a. C., B. K. “The Franck-Condon Principle and Condon Parabolas in a Physical Chemistry or Quantum Physics Course”, **Journal of Chemical Education**. 76(10): 1363-1366; May, 1999.

[8] He, R. and et al. “Quantum chemical study on excited states and charge transfer of oxazolo[4,5-b]-pyridine derivatives”, **Science China Chemistry**. 55(10): 2186-2196; October, 2012.

[9] T. H. Dunning, a. P. J. H. **Modern Theoretical Chemistry; Schefer III: Gaussian basis sets for molecular calculations**. New York: H.F. Ed. Plenum, 1997.

[10] Yang, R. G. P. a. W. **Density Functional Theory of Atoms and Molecules**. Oxford: Oxford University Press, 1998.

[11] Rappoport, D.; Furche, F. “**In Time-Dependent Density Functional Theory**” Marques, M. A. L., Ullrich, C. A., Nogueira, F., Rubio, A., Burke, K., Gross, E. U. K., Eds.; Springer Berlin Heidelberg: Berlin, Heidelberg, 2006.

REFERENCES (CONTINUED)

[12] Elliott, P. and et al. **In Reviews in Computational Chemistry**. John Wiley & Sons, Inc: 2009.

[13] Shen, L. and et al. "A TD-DFT study on photo-physicochemical properties of hypocrellin A and its implications for elucidating the photosensitizing mechanisms of the pigment", **Journal of Photochemistry and Photobiology A: Chemistry**. 180(1-2): 65-68; May, 2006.

[14] Fadda, E. and et al. "Time-dependent density functional theory as a foundation for a firmer understanding of sum-over-states density functional perturbation theory: "Loc.3" approximation ", **International Journal of Quantum Chemistry**. 91(2): 67-83; November, 2003.

[15] Dreuw, A.; Head-Gordon, M. "Single-Reference ab Initio Methods for the Calculation of Excited States of Large Molecules", **Chemical Reviews**. 105(11): 4009-4037; October, 2005.

[16] Kim, S. and et al. "Molecular Engineering of Organic Sensitizers for Solar Cell Applications", **Journal of the American Chemical Society**. 128(51): 16701-16707; December, 2006.

[17] Horiuchi, T. and et al. "High Efficiency of Dye-Sensitized Solar Cells Based on Metal-Free Indoline Dyes", **Journal of the American Chemical Society**. 126(39): 12218-12219; October, 2004.

[18] Kim, D. and et al. "Molecular engineering of organic dyes containing N-aryl carbazole moiety for solar cell", **Tetrahedron**. 63(9): 1913-1922; February, 2007.

[19] Wang, Z.-S. and et al. "Hexylthiophene-Functionalized Carbazole Dyes for Efficient Molecular Photovoltaics: Tuning of Solar-Cell Performance by Structural Modification ", **Chemistry of Materials**. 20(12): 3993-4003; May, 2008.

[20] Zhang, C.-R. and et al. "DFT and TD-DFT study on structure and properties of organic dye sensitizer TA-St-CA", **Current Applied Physics**. 10(1): 77-83; January, 2010.

REFERENCES (CONTINUTED)

[21] Jungsuttiwong, S. and et al. “The effect of conjugated spacer on novel carbazole derivatives for dye-sensitized solar cells: Density functional theory/time-dependent density functional theory study”, **Journal of Computational Chemistry**. 33(17): 1517-1523; April, 2012.

[22] Lee, E. and et al. “Synthesis of Alkyl-functionalized Organic Dyes and Their Application to Dye Sensitized Solar Cells (DSSCs)”, **Notes**. 33(1): 293; November, 2012.

[23] Chang, Y. J.; Chow, T. J. “Dye-sensitized solar cell utilizing organic dyads containing triarylene conjugates”, **Tetrahedron**. 65(24): 4726-4734; June, 2009.

[24] Namuangruk, S. and et al. “D–D–π–A-Type Organic Dyes for Dye-Sensitized Solar Cells with a Potential for Direct Electron Injection and a High Extinction Coefficient: Synthesis, Characterization, and Theoretical Investigation”, **The Journal of Physical Chemistry C**. 116(49): 25653-25663; November, 2012.

[25] Li, W. and et al. “Organic sensitizers incorporating 3,4-ethylenedioxythiophene as the conjugated bridge: Joint photophysical and electrochemical analysis of photovoltaic performance”, **Dyes and Pigments**. 99(1): 176-184; October, 2013.

[26] Zhu, W. and et al. “Organic D-A-π-A Solar Cell Sensitizers with Improved Stability and Spectral Response”, **Advanced Functional Materials**. 21(4): 756-763; December, 2011.

[27] Wang, D. and et al. “Near-infrared absorbing isoindigo sensitizers: Synthesis and performance for dye-sensitized solar cells”, **Dyes and Pigments**. 112(327-334; January, 2015.

REFERENCES (CONTINUTED)

[28] Ying, W. and et al. "Series of New D-A-π-A Organic Broadly Absorbing Sensitizers Containing Isoindigo Unit for Highly Efficient Dye-Sensitized Solar Cells", **ACS Applied Materials & Interfaces**. 4(8): 4215-4224; July, 2012.

[29] Venkateswararao, A. and et al. "Organic dyes containing indolo[2,3-b]quinoxaline as a donor: synthesis, optical and photovoltaic properties", **Tetrahedron**. 70(36): 6318-6327; September, 2014.

[30] Babu, D. D. and et al. "New D-π-A type indole based chromogens for DSSC: Design, synthesis and performance studies", **Dyes and Pigments**. 112 183-191; January, 2015.

[31] Peña, B. and et al. "Cytotoxicity Studies of Cyclometallated Ruthenium(II) Compounds: New Applications for Ruthenium Dyes", **Organometallics**. 33(5): 1100-1103; March, 2014.

[32] Campbell, W. M. and et al. "Highly Efficient Porphyrin Sensitizers for Dye-Sensitized Solar Cells", **The Journal of Physical Chemistry C**. 111(32): 11760-11762; July, 2007.

[33] Hart, A. S. and et al. "Porphyrin-Sensitized Solar Cells: Effect of Carboxyl Anchor Group Orientation on the Cell Performance", **ACS Applied Materials & Interfaces**. 5(11): 5314-5323; June, 2013.

[34] Namuangruk, S. and et al. "Theoretical investigation of the charge-transfer properties in different meso-linked zinc porphyrins for highly efficient dye-sensitized solar cells", **Dalton Transactions**. 43(24): 9166-9176; March, 2014.

[35] Karthikeyan, S.; Lee, J. Y. "Zinc-Porphyrin Based Dyes for Dye-Sensitized Solar Cells", **The Journal of Physical Chemistry A**. 117(42): 10973-10979; October, 2013.

REFERENCES (CONTINUTED)

[36] Ripolles-Sanchis, T. and et al. "Design and characterization of alkoxy-wrapped push-pull porphyrins for dye-sensitized solar cells", **Chemical Communications**. 48(36): 4368-4370; March, 2012.

[37] Tarsang, R. and et al. "Tuning the electron donating ability in the triphenylamine-based D-π-A architecture for highly efficient dye-sensitized solar cells", **Journal of Photochemistry and Photobiology A: Chemistry**. 273: 8-16; January, 2014.

[38] Namuangruk, S. and et al. "Organic sensitizers with modified di(thiophen-2-yl)phenylamine donor units for dye-sensitized solar cells: a computational study", **Theoretical Chemistry Accounts**. 133(9): 1-15; July, 2014.

[39] Thongkasee, P. and et al. "Carbazole-Dendrimer-Based Donor–π–Acceptor Type Organic Dyes for Dye-Sensitized Solar Cells: Effect of the Size of the Carbazole Dendritic Donor", **ACS Applied Materials & Interfaces**. 6(11): 8212-8222; June, 2014.

[40] Tarsang, R. and et al. "Modification of D–A–π–A Configuration toward a High-Performance Triphenylamine-Based Sensitizer for Dye-Sensitized Solar Cells: A Theoretical Investigation", **a European journal of chemical physics and physical chemistry**. 15(17): 3809-3818; October, 2014.

[41] Tang, J. and et al. "New starburst sensitizer with carbazole antennas for efficient and stable dye-sensitized solar cells", **Energy & Environmental Science**. 3(11): 1736-1745; July, 2010.

[42] Ning, Z.; Tian, H. "Triarylamine: a promising core unit for efficient photovoltaic materials", **Chemical Communications**. 37: 5483-5495; June, 2009.

[43] Tian, H. and et al. "Effect of Different Dye Baths and Dye-Structures on the Performance of Dye-Sensitized Solar Cells Based on Triphenylamine Dyes", **The Journal of Physical Chemistry** C. 112(29): 11023-11033; July, 2008.

REFERENCES (CONTINUED)

[44] Liang, M. and et al. "New Triphenylamine-Based Organic Dyes for Efficient Dye-Sensitized Solar Cells", **The Journal of Physical Chemistry C**. 111(11): 4465-4472; March, 2007.

[45] Hara, K. and et al. "Molecular Design of Coumarin Dyes for Efficient Dye-Sensitized Solar Cells", **The Journal of Physical Chemistry B**. 107(2): 597-606; December, 2002.

[46] Wang, Z. S. and et al. "A High-Light-Harvesting-Efficiency Coumarin Dye for Stable Dye-Sensitized Solar Cells", **Advanced Materials**. 19(8): 1138-1141; March, 2007.

[47] Chen, Z. and et al. "Organic D-π-A;-A Dyes for Dye-Sensitized Solar Cell", **Current Organic Chemistry**. 11(14): 1241-1258; September, 2007.

[48] Surawatanawong, P. and et al. "Density functional study of mono-branched and di-branched di-anchoring triphenylamine cyanoacrylic dyes for dye-sensitized solar cells", **Journal of Photochemistry and Photobiology A: Chemistry**. 253: 62-71; February, 2013.

[49] Wan, Z. and et al. "Influence of different arylamine electron donors in organic sensitizers for dye-sensitized solar cells", **Dyes and Pigments**. 95(1): 41-46; October, 2012.

[50] Becke, A. D. "A new mixing of Hartree–Fock and local density-functional theories", **The Journal of Chemical Physics**. 98(2): 1372-1377; September, 1993.

[51] Francl, M. M. and et al. "Self-consistent molecular orbital methods. XXIII. A polarization-type basis set for second-row elements", **The Journal of Chemical Physics**. 77(7): 3654-3665; May, 1982.

[52] Yanai, T. and et al. "A new hybrid exchange–correlation functional using the Coulomb-attenuating method (CAM-B3LYP)", **Chemical Physics Letters**. 393(1–3): 51-57; July, 2004.

REFERENCES (CONTINUTED)

[53] O'boyle NM, T. A. and Langner KM. “A library for package-independent computational chemistry algorithms”, **Journal of Computational Chemistry**. 29(5): 839-845; July, 2007.

[54] Kritsada Ronyhut. **Fabrication and characterization of dye sensited solar cell based (Z)-2-cyano-3-(5-(4-(naphthalene-2-ylamino)phenyl)thiophen-2-yl)acrylic acid** Bachelor's degree: Ubon Ratchathani University, 2013.

[55] Frisch, M. J. T.and et al. **Gaussian 09, Revision C.01**, Gaussian, Inc., Wallingford CT, 2009.

[56] Namuangruk, S. and et al. “D–D–π–A-Type Organic Dyes for Dye-Sensitized Solar Cells with a Potential for Direct Electron Injection and a High Extinction Coefficient: Synthesis, Characterization, and Theoretical Investigation”, **The Journal of Physical Chemistry C**. 116(49): 25653-25663; December, 2012.

[57] Chen, X. and et al. “Theoretical investigation of phenothiazine–triphenylamine-based organic dyes with different π spacers for dye-sensitized solar cells ”, **Spectrochimica Acta Part A: Molecular and Biomolecular Spectroscopy**. 123: 282-289; April, 2014.

[58] Jia, C. and et al. “Theoretical study of carbazole–triphenylamine-based dyes for dye-sensitized solar cells”, **Spectrochimica Acta Part A: Molecular and Biomolecular Spectroscopy**. 86: 387-391; February, 2012.

[59] Nazeeruddin, M. K. and et al. “Investigation of Sensitizer Adsorption and the Influence of Protons on Current and Voltage of a Dye-Sensitized Nanocrystalline TiO_2 Solar Cell”, **The Journal of Physical Chemistry B**. 107(34): 8981-8987; August, 2003.

REFERENCES (CONTINUED)

[60] Liang, M.; Chen, J. "Arylamine organic dyes for dye-sensitized solar cells", **Chemical Society Reviews**. 42(8): 3453-3488; February 2013.

[61] Kim, B.-G. and et al. "Molecular Design Principle of All-organic Dyes for Dye-Sensitized Solar Cells", **Chemistry – A European Journal**. 19(17): 5220-5230; March, 2013.

[62] Chou, C.-P. and et al. "Automatized Parameterization of DFTB Using Particle Swarm Optimization", **Journal of Chemical Theory and Computation**. 12(1): 53-64; January, 2016.

[63] Zheng, G. and et al. "Performance of the DFTB method in comparison to DFT and semiempirical methods for geometries and energies of C20-C86 fullerene isomers", **Chemical Physics Letters**. 412: 210-216; July, 2015.

[64] He, H. and et al. "A Theoretical Study of CO_2 Anions on Anatase (101) Surface", **The Journal of Physical Chemistry C**. 114(49): 21474-21481; December, 2010.

[65] Yakhanthip, T. and et al. "Theoretical investigation of novel carbazole-fluorene based D-π-A conjugated organic dyes as dye-sensitizer in dye-sensitized solar cells (DSCs)", **Journal of Computational Chemistry**. 32(8): 1568-1576; February, 2011.

[66] Sobuś, J. and et al. "Carbazole Dye-Sensitized Solar Cells Studied from Femtoseconds to Seconds-Effect of Additives in Cobalt- and Iodide-Based Electrolytes", **Chemistry & Sustainable Chemistry**. 8(18): 3118-3128; August, 2015.

[67] Keerthi, A. and et al. "Architectural influence of carbazole push–pull–pull dyes on dye sensitized solar cells", **Dyes and Pigments**. 99(3): 787-797; December, 2013.

[68] Venkateswararao, A. and et al. "Organic Dyes Containing Carbazole as Donor and π-Linker: Optical, Electrochemical, and Photovoltaic Properties", **ACS Applied Materials & Interfaces**. 6(4): 2528-2539; February, 2014.

REFERENCES (CONTINUTED)

[69] Jungsuttiwong, S. and et al. "Theoretical study on novel double donor-based dyes used in high efficient dye-sensitized solar cells: The application of TDDFT study to the electron injection process", **Organic Electronics**. 14(3): 711-722; March, 2013.

[70] Sudyoadsuk, T. and et al. "An organic dye using N-dodecyl-3-(3,6-di-tert-butylcarbazol-N-yl)carbazol-6-yl as a donor moiety for efficient dye-sensitized solar cells", **Tetrahedron Letters**. 54(36): 4903-4907; September, 2013.

[71] Promarak, V. and et al. "Synthesis of electrochemically and thermally stable amorphous hole-transporting carbazole dendronized fluorene", **Synthetic Metals**. 157(1): 17-22; January, 2007.

[72] Shao, Y. G.and et al. "Advances in molecular quantum chemistry contained in the Q-Chem 4 program package" **Molecular Physics.** 113: 184-215; January, 2015.

[73] Kaduk, B. and et al. "Constrained Density Functional Theory", **Chemical Reviews**. 112(1): 321-370; January, 2012.

[74] Wu, Q. and et al. "Configuration interaction based on constrained density functional theory: A multireference method", **The Journal of Chemical Physics**. 127(16): 164119; October, 2007.

[75] Kowalczyk, T. and et al. "Assessment of the ΔSCF density functional theory approach for electronic excitations in organic dyes", **The Journal of Chemical Physics**. 134(5): 054128; February, 2011.

[76] Yost, S. R. and et al. "A transferable model for singlet-fission kinetics", **Nature Chemistry**. 6(6): 492-497; May, 2014.

[77] Ni, J.-S. and et al. "Organic Dyes Incorporating the Dithieno[3′,2′:3,4;2″,3″:5,6]benzo[1,2-c]furazan Moiety for Dye-Sensitized Solar Cells", **ACS Applied Materials & Interfaces**. 6(24): 22612-22621; December, 2014.

REFERENCES (CONTINUTED)

[78] Stalder, R. and et al. "Panchromatic Donor–Acceptor–Donor Conjugated Oligomers for Dye-Sensitized Solar Cell Applications", **ACS Applied Materials & Interfaces**. 6(11): 8715-8722; June, 2014

[79] Yan, C. and et al. "Efficient Triarylamine–Perylene Dye-Sensitized Solar Cells: Influence of Triple-Bond Insertion on Charge Recombination", **ACS Applied Materials & Interfaces**. 7(1): 801-809; January, 2015.

[80] Zhu, W. and et al. "Organic D-A-π-A Solar Cell Sensitizers with Improved Stability and Spectral Response", **Advanced Functional Materials**. 21(4): 756-763; February, 2011.

[81] Wu, Y. and et al. "Insight into D–A–π–A Structured Sensitizers: A Promising Route to Highly Efficient and Stable Dye-Sensitized Solar Cells", **ACS Applied Materials & Interfaces**. 7(18): 9307-9318; May, 2015.

[82] Cui, Y. and et al. "Incorporating Benzotriazole Moiety to Construct D–A–π–A Organic Sensitizers for Solar Cells: Significant Enhancement of Open-Circuit Photovoltage with Long Alkyl Group", **Chemistry of Materials**. 23(19): 4394-4401; October, 2011.

[83] Kim, B.-G. and et al. "Molecular Design Principle of All-organic Dyes for Dye-Sensitized Solar Cells", **Chemistry – A European Journal**. 19(17): 5220-5230; April, 2013.

[84] Kleinhenz, N. and et al. "Low-Band-Gap Polymers That Utilize Quinoid Resonance Structure Stabilization by Thienothiophene: Fine-Tuning of HOMO Level", **Macromolecules**. 44(4): 872-877; February, 2011.

CURRICULUM VITAE

Name	Miss Yaowarat Surakhot
Date of Birth	29th October 1986
Birth Place	Si-Sa-Ket, Thailand
Education	B.Sc. (Chemistry), Ubon Ratchathani University, Ubon Ratchathani, Thailand (2009) M.Sc. (Chemistry), Ubon Ratchathani University, Ubon Ratchathani, Thailand (2011)
Address	39 Moo. 7, Tambon Doo, Amphor Rasri-Sa-Lai, Si-Sa-Ket, Thailand, 33160
Scholarship	Thailand Graduate Institute of Science and Technology (TGIST), National science and technology development agency Thailand (NSTDA)